FINITE ELEMENT SIMULATION OF MACHINING A NICKEL-BASED SUPERALLOY - INCONEL 718

By

DHANANJAY JOSHI

Bachelor of Engineering

University of Pune

Pune, India

(June, 2000)

Submitted to the Faculty of the
Graduate College of the
Oklahoma State University
in partial fulfillment of
the requirements for
the Degree of
MASTER OF SCIENCE
December, 2004

FINITE ELEMENT SIMULATION OF MACHINING A NICKEL-BASED SUPERALLOY - INCONEL 718

Thesis approved:

Dr. Ranga Komanduri

Thesis Adviser

Dr. Hong Bing Lu

Dr. Samit Roy

Dr. Gordon Emslie

Dean of the Graduate College

ACKNOWLEDGEMENTS

I wish to express my gratitude to my parents for their confidence in me. I would like to thank them for their consistent encouragement and love. I would like to extend my gratitude to my brother and sister for their inspiration, support and love. My special thanks are due to my roommates in Nandanvan for their motivation and support during my studies.

I would like to express my sincere thanks to my adviser, Dr. Ranga Komanduri for his supervision, constructive guidance, financial support and inspiration throughout the study. I would like to thank him for providing me with sophisticated and friendly work environment. My master's studies under him was a wonderful experience. I would also like to extend my sincere appreciation to Dr. Samit Roy and Dr. Hong Bing Lu for providing invaluable guidance and encouragement throughout this study. I would like to thank Dr. Zen Bing Hou and Dr. Bo Wang for their guidance in the field of material model, material properties and finite element analysis in this study.

This project has been funded by a grant from the Division of Design, Manufacturing and Industrial Innovation (DMII) of the National Science Foundation (NSF). I would like to thank Dr. George Hezelrigg of NSF for his interest and support of this work.

I wish to express my sincere gratitude to Mr. Parag Konde and Mr. Syed Kareem for their co-operation, discussions and friendship throughout this study. I would like to

acknowledge their contribution in deriving equations for Recht's catastrophic shear failure criterion to apply in FEM software code for this study. I wish to extend my gratitude to Mr. Nitin Daphalapurkar for discussions on plasticity and material model during this study.

I would like to thank Dr. Troy Marusich and Mr. Christopher Brand of the Third Wave Systems for their technical support in using and applying AdvantEdge software for machining simulations.

Finally, I would like to thank the Department of Mechanical and Aerospace Engineering for providing me with the opportunity to pursue M.S. at Oklahoma State University.

TABLE OF CONTENTS

Chapter **Page**

LIST OF TABLES

Table **Page**

LIST OF FIGURES

Figure **Page**

NOMENCLATURE

τ	Shear stress (Pa)
ε	Shear strain
τ_y	Initial shear yield strength (Pa)
ε_y	Initial yield strain
θ	Temperature (°C)
κ	Thermal conductivity (W/m.K)
ρ	Density (N/m^3)
c	Specific heat (J/Kg.K)
W	Work equivalent of heat (J)
ν	Poisson's ratio
E	Elastic modulus (Pa)

CHAPTER 1

INTRODUCTION

1.1 Applications of nickel-based superalloys

Nickel-based superalloy development for aerospace applications began in the 1930s. Need for more creep resistant material than the then available austenitic stainless steel propelled research to develop new superalloys. The principal characteristics of nickel as an alloy-base are high phase stability of face-centered cubic (fcc) nickel matrix and outstanding strength retention up to 0.7 T_m (melting point). These characteristics encourage use of nickel based superalloys in vast number of applications subjected to high temperatures [1]. Commercially available nickel-base superalloys include Inconel, Nimonic, Rene, Udimet, and Pyromet. Inconel 718 is the most frequently used of the nickel-base superalloys; hence this study is focused on an investigation into the mechanics of machining Inconel 718.

Some of the applications of nickel-based superalloys are in aircraft gas turbines (eg. disks, combustion chambers, casings, shafts, exhaust systems, blades, vanes, burner

cans, stack gas reheaters), reciprocating engines (eg. turbochargers, exhaust valves, hot plugs, valve seat inserts), metal processing (eg. hot work tools and dies), space vehicles (eg. aerodynamically heated skins, rocket engine parts) heat treating equipments (eg. trays, fixtures, conveyor belts, baskets, fans, furnace mufflers), nuclear power plants, chemical and petrochemical industries, and heat exchangers.

1.2 Metallurgy of nickel-based superalloys

Nickel-based superalloys are complex alloys as they incorporate 10 to 12 elements as indicated in Table 1.1. Major phases present in nickel-based superalloys are gamma phase (γ), gamma prime phase (γ'), and gamma double prime phase (γ'') phase. γ phase is a continuous matrix of an fcc nickel-based non-magnetic phase. In the γ' phase there is an addition of aluminum and titanium in amounts required to precipitate fcc γ' Ni_3 (Al, Ti) phase coherent with austenitic γ phase. This phase is required for high-temperature strength and creep resistance.

Table 1.1 Nominal chemical composition of Inconel 718 (% wt) [1].

Ni	Fe	Cr	Mo	Nb	Ti	Al	C	Mn	Si
52.5	18.5	19	3.0	5.1	0.9	0.5	0.04	0.2	0.2

In γ'' phase, nickel and niobium combine in the presence of iron, as a catalyst, to form body centered tetragonal (bct) Ni_3Nb, which is coherent with γ phase. This phase provides high strength at low and intermediate temperatures but is unstable above 650° C.

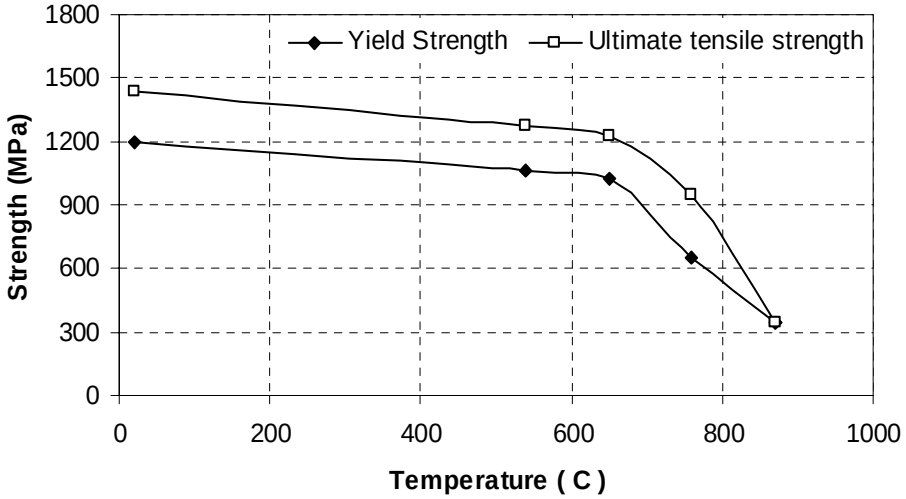

Fig. 1.1 Temperature dependent ultimate tensile strength and yield strength of Inconel 718 [1]

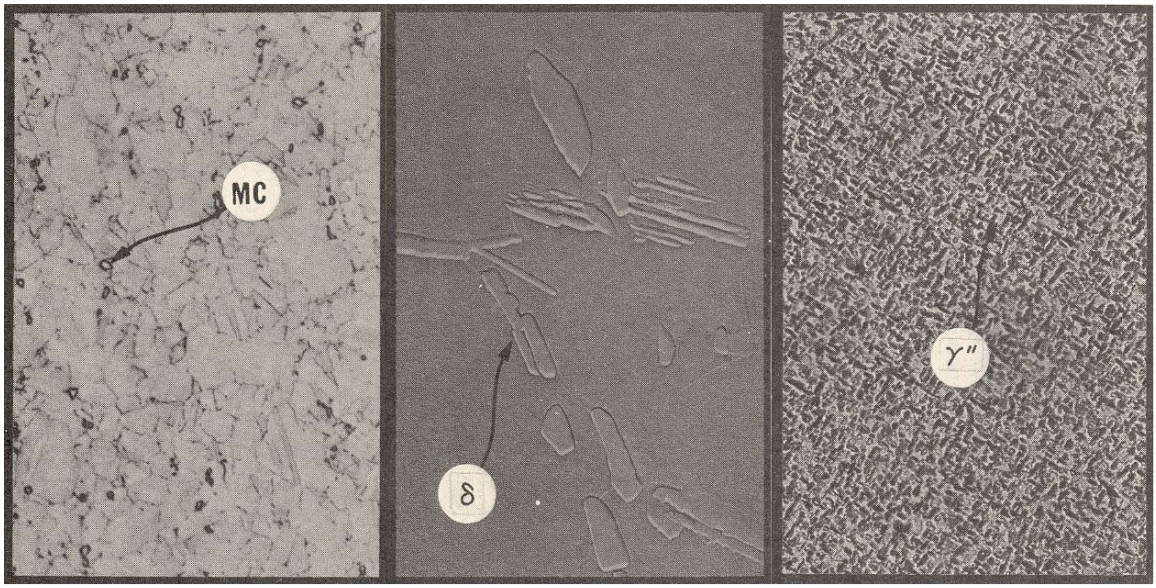

(a) (b) (c)

Fig.1.2 Microstructure of Inconel 718 with different phases in the alloy at different magnification (a) Light micrograph (100X) (b) Replica electron micrograph (7700X) (c) Extraction electron micrograph (34,000X) [3]

Inconel 718 is strengthened by coherent bct phase γ'' (Ni_3Nb). Inconel 718 contains 5.1% niobium and smaller quantities of aluminum and titanium, which leads to

the formation of γ' Ni_3 (Al, Ti) phase [1]. Along with these two phases, there is a possibility of formation of stable orthorhombic delta (δ) phase, which is the result of improper heat treatment. Delta phase is used to pin the grain boundaries and inhibit grain growth during solution heat treatment. Inconel 718 is also capable of forming intragranular platelets. Optical examination of wrought Inconel 718 shows uniform distribution of fine size γ'' and γ' phases in the austenite matrix with δ platelets at the grain boundaries along with isolated MC carbides [2].

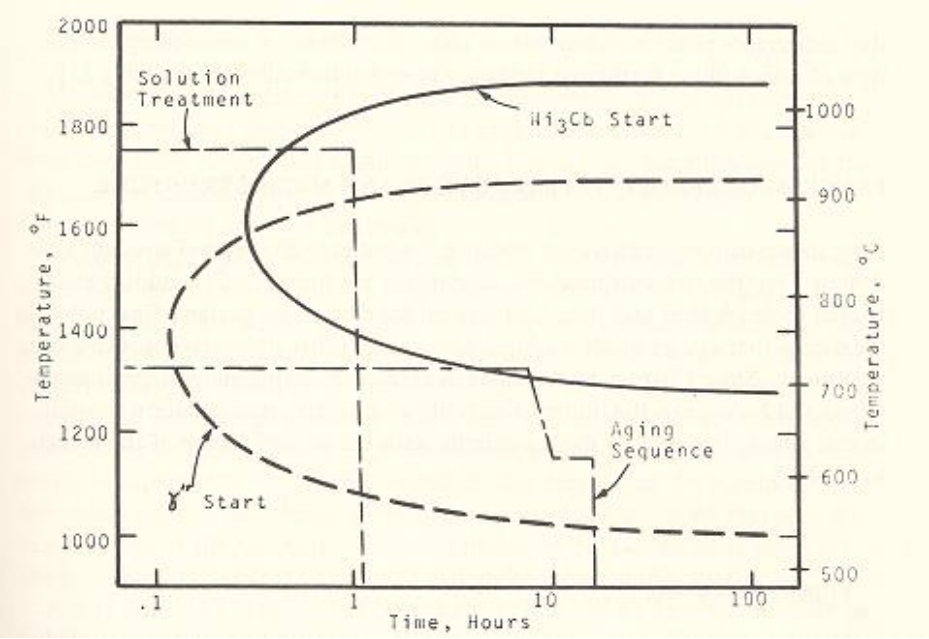

Fig. 1.3 Time-temperature transformation diagram for Inconel 718 [3].

Inconel 718 gains strength by age hardening due to the presence of fine and uniformly distributed γ'' metaphase in the matrix. Coherency strains associated with γ'' particles are considerably greater than for γ'. This attributes to high strength of the alloy at low and moderate temperatures. At high temperatures (above 650°C) strength of the alloy decreases significantly due to rapid coarsening of γ'' phase, some solutioning of γ''

phase and due to the formation of orthorhombic δ phase. Traces of boron are also added to produce borides by reacting with matrix elements. Borides are hard refractory particles which are located at grain boundaries of the alloy. They retard nucleation of cells and minimize tearing of cell boundaries under rupture loading. Carbides are inclusions formed at grain boundaries. They improve rupture strength of alloy at elevated temperatures. Minor phases, such as б, μ, Laves, collectively called as topologically close-packed (TCP) phases, may also be formed. These phases lower rupture strength and ductility of the material.

Proper heat treatment as shown in Fig. 1.2 is essential for these alloys. Lowering the carbon content can result in better properties than those of standard Inconel 718. Also, increase in Al and Nb content and Al/Ti ratio in Inconel 718 improves mechanical properties of the alloy by producing more stable γ' phase [1].

1.3 Machining of nickel-based superalloys

Nickel-based alloys work-harden rapidly. Work hardening results in strengthening of the material. Plastic deformation during machining leads to heat generation. High temperature gradients are localized in narrow bands along shear plane due to poor thermal properties of Inconel 718, leading to weakening the material in the deformation zone. When the rate of thermal softening is greater than that of strain hardening, material deforms locally, termed as adiabatic shear failure. The type of chips formed under these conditions is termed as shear localized chips. Oscillations in cutting forces and high temperatures on the rake face in the contact area can cause rapid tool wear. High pressures developed during segmented chip formation retards further machining and

increase power requirements of the process [4]. The method of minimizing work hardening during machining is to use sharp tools with a positive rake angle, control feed rate and depth of cut to avoid burnishing [4]. To achieve maximum dimensional stability under difficult machining conditions, a given part is first rough machined close to size; age hardened to relieve machining stresses and then finished to exact size. Almost any cutting fluid or none can be used in machining nickel based superalloys. Water-base fluids are preferred in high-speed turning, milling, and grinding because of their greater cooling effect. For slower operations, such as drilling, boring, tapping, and broaching heavy lubricants, and very rich mixtures of chemical solutions are needed. Tool geometry and machining parameters play important role in evaluating machining efficiency in machining Inconel 718. Single point cutting tools with positive rake angles (0° for roughing and 8° for finishing) are recommended in turning so that metal is cut instead of ploughed [4]. Inconel 718 is very much difficult to machine; not many cutting tools can cut this material easily. Ceramic tools and cubic boron nitride tools are recommended for high speed turning (60-200 m/min). Typical feed rates used are 0.15 to 0.3 mm/rev and typical depth of cuts are 1.0 mm to 2.5 mm.

Ezugwu *et al.* [5] summarized the properties of nickel-based superalloys, contributing to poor machinability as:

1. Major part of the strength is maintained during machining due to their high temperature strength properties.
2. Work hardening occurs rapidly during machining, contributing to notch wear at the tool nose and/or depth-of-cut-line (DCL).

3. Cutting tools suffer from high abrasive wear due to the presence of hard abrasive constituents in the superalloy.
4. Chemical reaction occurs at high cutting temperatures when machining with commercially available carbide or cubic boron nitride tools, leading to a high diffusion wear rate.
5. Welding/adhesion of nickel-based superalloys onto the cutting tool occurs frequently during machining with ceramic tools, causing severe notching as well as spalling on the tool rake face due to consequent pull-out of the tool material.
6. Production of a tough and a continuous chip, which is difficult to control during machining, enhances degradation of the cutting tool by seizure and cratering.
7. Poor thermal diffusivity of nickel-based alloys often generates high temperature at the tool tip as well as high thermal gradients in the cutting tool.

1.4 Contribution of FEM towards analysis of metal cutting process

Metal cutting is a highly nonlinear and coupled thermo-mechanical process. The mechanical work is converted into heat through plastic deformation involved during the chip formation process in the primary shear zone. Friction between chip-tool and workpiece-tool interface is another source of heat. Depending on the machine tool dynamics, there are variations in machining forces on tool and residual stresses in the finished workpiece. Tool geometry (back and side rake angle, clearance angle, nose radius) and process parameters (feed, cutting speed) are important factors affecting thermal aspects, residual stresses, and cutting forces in the metal cutting process. The experimental approach to study the effect of all these parameters on metal cutting

processes is expensive and time consuming. There are other tools available in the form of mathematical simulations where numerical methods are applied. Amongst the numerical procedures, finite-element method (FEM) is the most frequently used.

In metal cutting process, various disciplines, such as metallurgy, solid mechanics (elasticity, plasticity), heat transfer, tribology (contact problems), fracture mechanics, and lubrication are involved. The goal of finite-element analysis is to derive reliable computational models predicting the deformations, stresses and strains in the workpiece, as well as the loads on the tool working under specific cutting parameters. Most metal cutting processes are oblique cutting processes but orthogonal cutting process is easier to simulate and understand the basic mechanics of the process. Material and geometrical non-linear analysis, tool wear modelling, element separation criteria, residual stress prediction, adaptive remeshing are some of the techniques researchers have been working on to improve the reliability of the results of FEM. In many cases the FEM simulations have been validated by comparison with the results of experimental investigations.

The main advantage of using FEM compared to other empirical models is its ability to represent workpiece material properties as a function of temperature, stress, and strain rate. A large number of technical papers are published [6] dealing with constitutive models stress-strain relationship. Similarly, the tool/chip interface can be idealized with sticking and sliding friction conditions. Continuous heat generation and elevated temperatures cause reduced wear resistance of tool material and change in tool geometry and tool size. This results in increased cutting forces with larger deflections in workpiece resulting in chatter. Models are being developed for simulation to study the effect of friction temperature on tools and tool coatings. The major problem encountered when

modeling the effect of tool coating on tool performance is acquiring realistic mechanical property data. Coating properties, such as adhesion strength and coefficient of friction obtained from scratch tests must be treated with caution. This is because such parameters are dependent on the sliding speed, critical load and temperature used during the experiment. In addition, the grade of the substrate onto which the coating is deposited influences the mechanical properties. Consequently, little published work on FEM with coated tools is available.

Advances in computation accessories, such as faster processors and larger memory have encouraged researchers to use Lagrangian formulation for metal cutting simulation. The principal advantages of this approach are (1) the tool can be simulated from some initial state to steady state cutting and (2) the chip geometry together with workpiece residual stress can be predicted. The elements are attached to the workpiece material and chip separation criteria are used to allow the chip to separate from the workpiece. Various researchers have proposed different chip separation criteria for FEM simulation in machining, which are either classified as physical or geometric criteria. The physical criteria include strain energy density, effective plastic strain and stress, while geometric criteria relate to the distance between the overlapping nodes and the tool tip. Simulations are also conducted to predict chip flow and chip breaking phenomenon. Movement and control of chip along contact length with the tool are important factors for tool wear models. Deformation of workmaterial, contact properties, friction, large plastic strains, strain-hardening, and thermal softening effects play major role in chip formation mechanism. Simulations for optimum design of machine tools and tool geometry are carried out to provide some practical solutions to improve the process output.

Until the mid-1990s, most of the researchers used in-house finite element code; however, the use of commercial packages has increased recently. General-purpose FEM codes capable of modeling the machining process include NIKE2D, ABAQUS/Standard, ABAQUS/Explicit, MARC, ALGOR, FLUENT, LS DYNA etc. Unfortunately the majority of general-purpose FEM codes are only applicable for continuous chip formation. There are specially developed FEM codes, such as DEFORM 2D, FORGE2D, AdvantEdge, which are capable of simulating segmented and discontinuous chip formation.

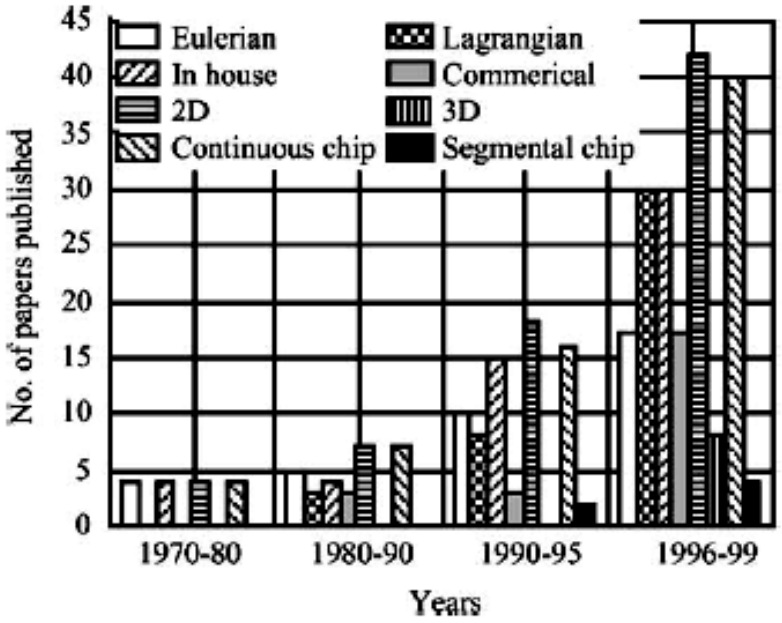

Fig. 1.4 Number of technical publications from 1970 to 1999 on modelling of the metal cutting process which shows only a handful of papers on segmental chip formation. [7]

Childs *et al.* [8] summarized the development and testing of finite element techniques for chip formation process since 1970s. Limited availability of material properties depending on temperature and strain rate, lack of reliable friction

characteristics and realistic failure criteria during evolving days of finite element theories for metal cutting is reported.

Future ways of finite element modeling of chip formation were proposed as:

1. Iterative convergence method for steady state processes could be attributed to its computing efficiency.
2. Lagrangian adaptive mesh refining methods for unsteady processes with elastic-plastic or perfectly plastic materials.
3. Lagrangian fixed mesh methods with chip separation criteria to support the studies of unsteady processes in time effective manner.

1.5 Overview

This study concentrates on the application of thermoplastic shear instability theory as chip segmentation criterion in simulating turning operation of Inconel 718. Finite element method is selected as the simulation tool. Simulations are run using the commercial software 'AdvantEdge' developed by the Third Wave Systems, Minneapolis, USA. User subroutine is incorporated with the main code to apply thermoplastic shear instability criterion originally developed by Recht [16]. Effects of various machining parameters on chip formation process, cutting and thrust forces, temperature distribution, and stress-strain distribution (in chip, tool and workpiece) are studied.

In Chapter 2, machinability aspects of Inconel 718, earlier experimental studies, clarifications on chip segmentation phenomenon, results, and analyses reported in the literature on the topic are presented. Literature on finite element analysis of machining of

difficult-to-machine materials to the extent pertinent to the present investigation is reviewed and discussed. Chip separation criterion, constitutive material model, material properties for these models, friction model are some of the important issues in the FEM simulation of metal cutting. Work reported in the literature addressing these issues is presented. Current work in FEM analysis of machining Inconel 718 is discussed.

In Chapter 3 (Problem Statement), need for this investigation and objectives of this study are discussed.

In Chapter 4, mechanics of shear localization and thermoplastic shear instability theory are discussed. Causes of chip segmentation and effects of cutting parameters are presented and discussed.

In Chapter 5, principle of finite element theory for analysis of machining is presented. Various material models for machining simulation reported in the literature are discussed. Adaptive mesh control, thermo- mechanical coupling, equations of motion are presented. Plasticity theory for updating stress in each time step is discussed. Formulation of thermoplastic shear instability theory and its implementation in the finite element code reported is discussed.

In Chapter 6, finite element simulation approach, material properties, and results of this study are presented. Effects of rake angle on cutting forces, stress-strain distribution, temperature distribution, and chip segmentation is studied and discussed. Simulations were run for a range of speeds and are compared with the experimental results of Komanduri and Schoeder [2].

In Chapter 7, simulation approach, material model and failure criterion applied in this study are mentioned in brief. Conclusions are drawn from the obtained results and future work is suggested here.

CHAPTER 2

LITERATURE REVIEW

2.1 Machining Inconel 718 – Experimental work

Machinability index of a workmaterial is accessed in terms of four factors: tool life, cutting forces, power requirements, and surface finish. Machinability index of Inconel 718 is 35 as compared to 100 for the free machining low carbon steel [9]. This means that machining Inconel 718 is about 3 times more difficult than free machining low carbon steel. Komanduri and Schroeder [2] conducted machining tests on Inconel 718 (solution treated and age hardened) alloy at various cutting speeds ranging from 15.25 m/min to 213.5 m/min. Mechanically continuous and highly coiled chips were found with inhomogeneous deformations at lower speeds (< 30 m/min). Shear localized chips were formed at speeds above 61 m/min. Metallurgical examination of the longitudinal midsections of chips showed large inhomogeneous deformations with shear localization between any two chip segments and relatively low deformation in any individual chip segment. With increase in cutting speed, extent of contact between chip

segments decreased. Intense shear localization was observed at about 100 m/min cutting speed. At about 152.5 m/min, short chips with few segments joined together were found. For higher speeds, isolated chip segments were formed.

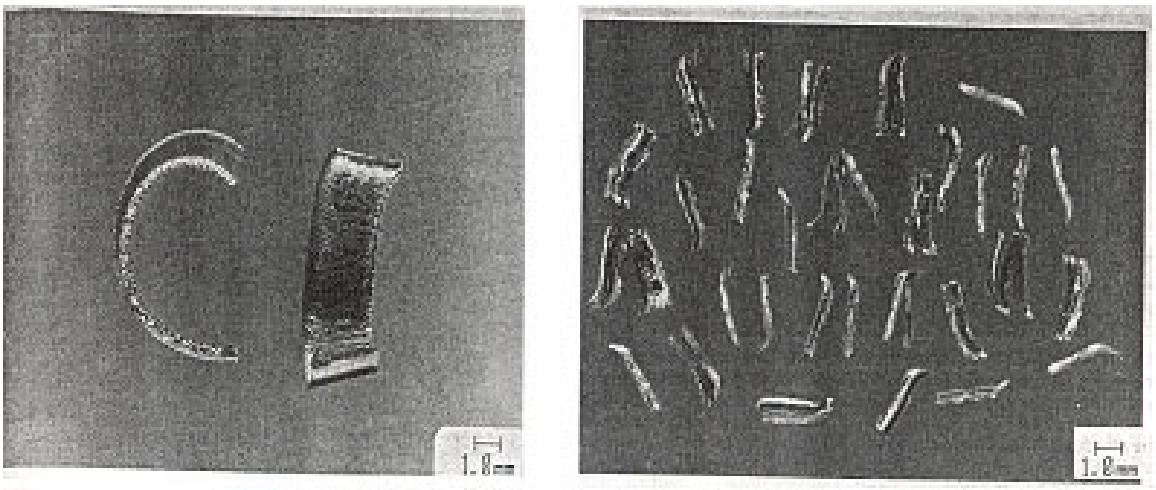

(a) (b)

Fig. 2.1 Optical micrographs of Inconel 718 chips showing (a) continuous shear localized chip at lower cutting speeds (<30.5 m/min); (b) chip segments completely separated due to intense relative shear between the chip segments at higher cutting speeds (> 152 m/min) [2]

Komanduri and Schroeder [2] explained the causes of tool wear in machining Inconel 718. In machining, shear localized chip surfaces are extremely hot and are prevented from interaction with atmosphere before contacting tool face. The contact length between the bottom of the chip segment and tool face increases with progress in upsetting. There is no relative motion between the freshly generated, hot bottom of chip segment and tool face until the end of upsetting stage of the chip segmentation process. These conditions are conducive for chemical reactions between tool and shear localized chip segment which can lead to rapid tool wear. This is the primary reason for poor tool life and limitations on cutting speeds. Komanduri *et al.* [10] summarized machining

limits as baseline reference for research. For cemented carbide grades, such as C-2 or C-3, the speeds in rough and semi rough turning of Inconel 718 are reported in the range of 21-30 m/min. For finishing and semifinishing cuts with ceramic tools, SiAlONs and cubic boron nitride, speed range reported is 183-213 m/min.

Ezugwu *et al.* [5, 11] presented the problems of short tool life and damage to workpiece as a result of metallurgical composition of nickel-based alloys. Depth-of-cut line (DCL) notching, flank and nose wear, chipping, and diffusion-attrition are common modes of tool failure in machining nickel-based superalloys. Although these alloys are not exceptionally hard (250-350 HV), their outstanding high temperature strength (up to about 650° C) and extreme toughness are the reasons behind the difficulty in machining these alloys at high cutting speeds. High hot hardness and adequate chemical stability at high temperatures are the most important requirements of a tool to machine nickel-based superalloys.

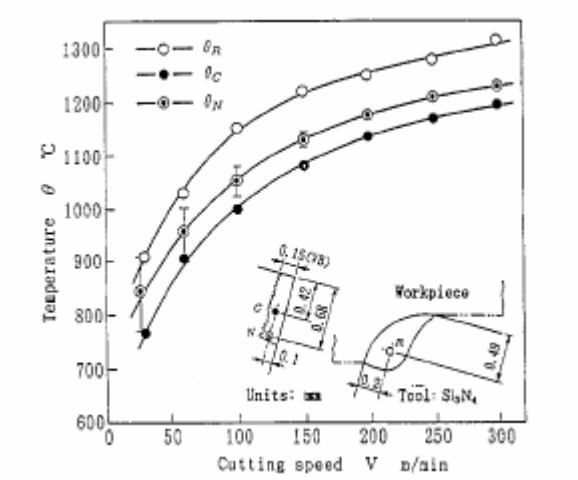

Fig. 2.2 Local tool temperature dependence on the cutting speed in machining Inconel 718. (θ_R: rake face temperature at point R; θ_C: flank face temperature at point C; θ_N: flank face temperature at point N) [12]

Flank and nose wear are reported as predominant failure modes of carbide tools in machining nickel-based alloys. Tungsten carbide tools can be used at low cutting speeds

(about 30 m/min) in high feed rate cutting and interrupted cutting. Erosion of coating layer exposes carbide substrate to high temperatures as shown in Fig. 2.2 at the tool tip. Speed range is limited to 10-30 m/min with 0.5 mm/rev feed rate in machining nickel-based superalloys with carbide tools. Ceramic tools can better withstand severe cutting conditions as they have high hot-hardness and better chemical stability at high temperatures. Tool wear for ceramic tools is dominated by abrasion mechanism. This is because of work hardening of material and presence of hard carbide phases, which may get sandwiched at tool-workpiece interface. Increase in cutting edge temperature at higher speed causes workpiece material to pressure weld on to the tool, which leads to removal of aggregates of tool particles while randomly plucking welded material. Thermal softening of workmaterial may also lead to adhesion of workpiece material to tool.

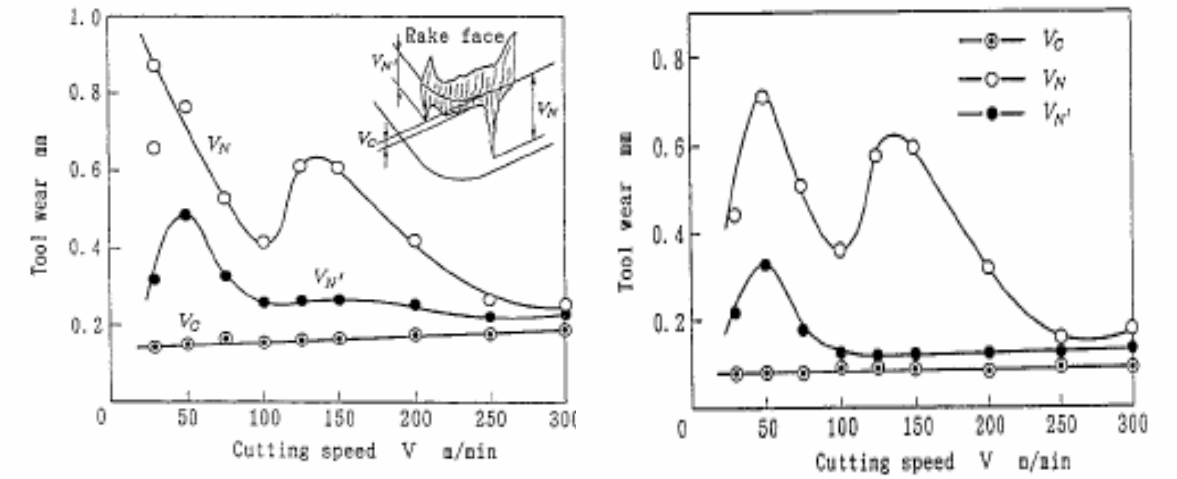

(a) (b)

Fig. 2.3 Dependence of tool wear of (a) Si_3N_4 and (b) Al_2O_3 + TiC tool on cutting speed in machining Inconel 718 at a cut distance of 50 m [12] (V_c : flank wear width, V_N : major edge notch wear, $V_{N'}$: minor edge notch wear)

Ezugwu *et al.* [5] reported some observations on limitations on cutting speed in machining Inconel 718 while milling nickel-based superalloy with different tool materials. Low fracture toughness (4.3- 4.5 MPa /√m) and low thermal shock resistance of alumina-TiC tools limit cutting speeds to 120-240 m/min [5]. SiC whisker reinforced alumina ceramic tools with higher fracture toughness (8 MPa/√m) and better thermal shock resistance can be used for cutting in the range of speeds at 200 – 750 m/min [5]. Superior mechanical and thermal properties of Si_3N_4 allows cutting at even higher speeds. Better hardness of cubic boron nitride (CBN) tools makes them better option to cut nickel-based alloys of hardness of 340 HV or more. But poor chemical resistance limits the cutting speed range to 300-600 m/min [5]. Typical modes of wear of CBN tools when machining nickel based alloys are flank wear, nose wear, and crater wear.

Chaudhury and El-Baradie [13] reported development of V-shaped groove or notch at the depth-of-cut line (DCL) as the common problem in machining nickel-based alloys. Depth-of-cut notching observed in carbide and ceramic tools governs tool life. Notching has been attributed to fatigue loading on tool, work hardened layer, adherence of workmaterial on tool and subsequent dislodgement and diffusion-attrition wear mechanism [12].

Ezugwu *et al.* [11] summarized the effect of tool geometry on tool life and surface finish. Rhomboid shape inserts enhance chip segmentation while square and round shaped inserts gave longer tool life and better surface finish. Notching failure can be suppressed by taper turning technique. Where in the depth-of-cut line (DCL) is constantly shifted along the cutting edge thus concentration of expected notch wear is distributed. Komanduri *et al.* [10] reported advantages of using rotary cutting tool system in

machining difficult to machine materials. These tools can be lubricated and cooled easily than a stationary inserts, temperature during cutting can be distributed broadly and metal build up on tool can be removed externally. Tool life improvements on the order of 20 times were reported in machining Inconel 718. Predicted potential productivity increase was 200-300 % and reduction in cost by about 50% using rotary cutting tool system.

Hot machining techniques, such as plasma enhanced machining [14] and laser assisted machining [10] were proposed to enhance machining performance. Localized heating (above 700° C) of the workmaterial near the tool tip reduces cutting forces and improves surface finish with higher material removal rates. Increase in the flank wear of CBN and carbide tools is also reported in this case. To overcome poor machinability of nickel-based superalloys, non-traditional machining techniques, such as chemical machining, electrical discharge machining, electrochemical machining and laser beam machining may be employed.

2.2 Chip segmentation mechanism

Aerospace structural superalloys, such as Inconel 718, Ti-6Al-4V, AISI 4340 are extremely difficult to machine at moderate to high speeds because of rapid tool wear. These materials produce segmented chips when cut in certain speed ranges. The research work done to understand the mechanics of chip segmentation dates back to 1950s.

Recht [16] reported observation of adiabatic shear in the shear zone in machining leading to catastrophic failure. Strain hardening during plastic deformation strengthens the weak shear zones in the material. Also, heat is generated due to plastic deformation and temperature gradients are established. Increasing temperatures, localized in a

particular zone due to poor thermal properties of particular materials, weaken the material. If the rate of material weakening, termed as thermal softening, exceeds that of strain hardening, material continues to deform locally. Criteria for the onset of catastrophic shear failure are presented and discussed further in Chapter 4.

Researchers concluded that chip segmentation is due to poor thermal properties of particular materials and adiabatic shear failure resulting from thermal softening in shear plane [17]. Ability of these materials to deform plastically varies with temperature due to phase transformation and subsequent metallurgical changes. Chip segmentation is a result of plastic instability in the primary shear zone which leads to catastrophic shear failure in cutting at high speed. Thin, highly strained shear bands are formed by upsetting and thermal energy is concentrated in these bands. Chip segmentation is reported to be dependent on the cutting conditions (cutting speed and feed rate) and composition and microstructure of workmaterial. Some of the researchers considered chip segmentation as self-excited vibrations and cyclic variation of shear angle as its root cause [18]. Others considered it as a result of forced vibration and proposed influence of tool system on chip segmentation [19].

Rice and coworkers [20, 21] photographed the chip segmentation process at various stages and formulated the mechanics of chip segmentation. Compression of workmaterial ahead of tool and bulging until sudden failure was observed and the concept of maximum shear strain for chip segmentation was developed. According to that concept, chip transforms from continuous to segmental when nominal shear strain reaches a critical value. Influence of material properties on chip segmentation was introduced.

Komanduri and coworkers [2, 22-27] worked on machining aerospace structural materials, such as titanium and nickel-iron based superalloys and hardened alloy steels (AISI 4340). They proposed the root cause of chip segmentation to be adiabatic shear failure at high temperature and intense shear localization in the narrow band along the shear plane. Process of chip segmentation was investigated using high-speed photographic techniques and explosive quick stop device [22]. Observations of the process revealed oscillations of shear angle in the primary shear zone and friction in the secondary shear zone. This was attributed to the ability of certain materials to deform up to large strains. Periodic adhesion of the chip to the tool face causing stick-slip friction was observed on the rake face. They concluded that crystal structure was not the only criterion for chip segmentation. In the case of Inconel 718, γ'' phase limited the deformation within the chip segment up to elevated temperature, leading to shear localization of chips [2]. High temperature generation in narrow shear bands was observed in machining titanium alloys. Adiabatic shear was found as a result of intense shear concentration in the band and poor heat dissipation from band due to poor thermal properties of workmaterial in machining titanium alloys [25]. Continuous contact of high temperature, freshly generated chip segment with tool face led to rapid flank wear as titanium is highly reactive with most tool materials. Shear localized chips were observed at all cutting speeds above 275 m/min in machining AISI 4340 [17]. At cutting speeds more than 1000 m/min chip segments were observed to be separated due to extensive shear between them. Analytical model of machining for analysis of thermoplastic shear instability was developed [26, 27]. Effect of various heat sources (such as primary, preheating and image) on temperature gradients in the shear band was studied. Shear

stress in the shear band was calculated at the shear band temperature. It was compared with the shear strength of the bulk material at the preheating temperature to predict the onset of shear localization. Effect of depth of cut and cutting speed on onset of shear localization in orthogonal machining was studied. Shear localization was expected at all speeds above a critical speed. For titanium alloys, critical speed found for varying depths of cut, was very low (maximum was 4.28 m/min for depth of cut of 0.02 mm), indicating shear localization at all practical speeds. For AISI 4340, critical cutting speed was found to be 52 m/min. This was in close accord with experimental observations [23]. Komanduri and Schroeder [2] investigated the effect of cutting speed on shear instability in machining nickel-iron based superalloy (Inconel 718). Turning experiments from 15.25 to 213.5 m/min cutting speed were conducted with 0.2 mm/rev feed rate. Continuous chip was formed at low speeds (up to 30.5 m/min) and transition of continuous chip to shear localized chip was observed at 61 m/min speed. Considerable amount of twinning was observed at all speeds. Various observations and clarifications on chip segmentation mechanism were noted [24 - 27] which are discussed further in Chapter 4.

Nakayama [28] suggested a theory of saw-tooth chip formation in the machining, contrasting to the then proposed theories. The theory proposed shear crack initiation at the free surface of workpiece as the root cause of saw-tooth chip formation. Theory states that the crack initiates at free surface of chip and propagates towards tool tip along the shear plane. As the tool advances, chip glides outwards along cracked surface till the next crack is formed.

Shaw and Vyas [29] continued their arguments on saw-tooth chip formation along the same lines as Nakayama [28] and state that saw-tooth chips formed at extremely low cutting speeds and low temperatures are caused by periodic fracture and not adiabatic shear. Opposing effects of increase in strain rate and decrease in thermal softening were observed on saw-tooth chip formation at higher cutting speeds. Adiabatic shear may only be observed if temperatures rise higher at higher cutting speed causing phase transformation. Two types of cracks observed in saw-tooth chip formation were - gross cracks running continuously across chip width and microcracks. Gross cracks cause material to move outward without any plastic deformation. Material in microcrack may lead to saw-tooth chip formation by adiabatic shear only if temperature raises high enough to cause phase transformation.

2.3 Finite element analysis of shear-localization in machining

The finite element method has been the main tool for simulation of the metal cutting processes. Pioneering work in finite element simulation of metal cutting process was done by Usui and Shirakashi [30], Iwata et al. [31], and Strenkowski and Carroll [32]. Since then many researchers have contributed significantly in developing computational models for the machining process, studying geometric effects, process parameters, thermal aspects, residual stresses, and friction effects in machining. Work has been conducted in studying dynamic effects of machine tool on machining process. Chip formation mechanism has been the major topic addressed through finite element analysis. Recently researchers have tried to study chip segmentation mechanism using FEM [6, 33].

Maekawa *et al.* [34] and Shirakashi and Obikawa [35] concluded that iterative convergence method, which is suitable for simulation of continuous chip formation cannot be applied for simulation of non-steady or serrated chip formation. Need for material separation (at pre-defined depth of cut throughout the process) and macroscopic fracture criterion were advocated. Failure of material was proposed through crack propagation. Geometrical criterion was used to dictate fracture at the tool tip. The node would be separated if it approaches within a specified distance from the tool tip. This distance depends on the element size. Nodal forces were released in steps. Critical strain criterion was introduced for separation of nodes within the chip. The constants involved in the equation for the critical strain criterion were determined empirically to simulate the chip. This was inverse analysis and a practical way to overcome non-availability of proven criterion. Discontinuous chip was formed in simulating β-brass at low cutting speed of 13 mm/min. Crack was observed to be initiated at the tool tip and propagated towards free surface. Crack was formed at highest value of horizontal force component and propagated through the chip with sharp drop in forces. This phenomenon was in accordance with the experimental observations.

The same technique was applied for simulation of machining Ti-6Al-4V alloy at 30 m/min. The fracture was observed only in chip surface and not on the tool side. High temperatures in chip were attributed to high flow stress of alloy and lower density. Localized temperature rise in the chip was attributed to low thermal conductivity of the alloy. Maximum temperature rise was observed inside the chip and not on rake face which is practical in normal case. These results, however, were reported to be in accordance with some of the experimental results. They concluded that serrations were

caused by small fracture strain of alloy, propagation of crack and localization of deformation. Adiabatic shear theory, advocating thermal softening of alloy as root cause of serrations, was denied. While this may be true at low cutting speeds, it is far from experimental observations at higher cutting speed.

It is to be remembered that the failure criterion used for initiation of crack in these simulations was empirical and was considered a compromise for non-available failure criterion as stated by researchers. A need for reliable material characteristics is expressed in the concluding remarks.

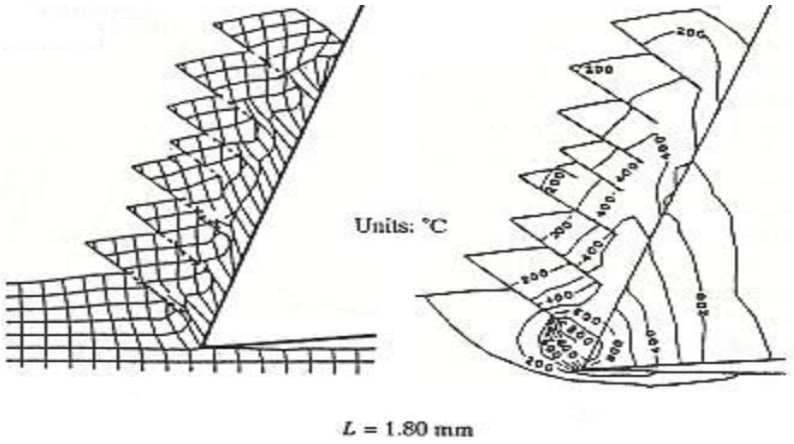

Fig. 2.4 Predicted serrated chip shape and isotherms near cutting tip in machining titanium alloy; v = 30 m/min, feed rate = 0.25 mm/rev, depth of cut = 1 mm, rake angle = 20° [34].

Baker *et al.* [36-39] simulated chip segmentation using ABAQUS/Standard (an implicit code) with the assumption of adiabatic shearing and thermal softening as the root causes for chip segmentation. High mesh density was applied in the shear zone. Fine element size on the order of one micrometer was used to ensure accuracy of stress and strain gradients. A pre-processor algorithm was written in C++ to automatically remesh

distorted zone in the shear band. Shear zone position was determined using geometric criterion and the mesh was refined. Fully integrated quadrilateral first order elements were used for simulations for better convergence. Remeshing was done in case of strong deformation of elements or tool advancement by predefined distance. Critical stress or damage model were considered to be representative of real machining process but unavailability of such criteria forced the researchers to use geometry based criteria for node separation. This technique introduced errors in the force calculations and line of material separation was predefined. To correct the force calculation errors, another technique of material removal from the deformation zone was introduced. For implementation of this technique, metal cutting process was considered as a pure deformation process (as in forging). The overlapping workmaterial on advancing tool was removed in the remeshing step.

Simulations were run by Baker *et al.* [36] for machining Ti-6Al-4V alloy at 50 m/s (=3000 m/min) and feed rate of 40 μ/rev with a rigid tool of 10° rake angle. About 5000 elements and 7000 nodes were used at the beginning of simulation which went on to 10000 and 12000 towards the end due to remeshing. The results with geometry based node separation criteria and those with pure deformation considerations were compared and were found to be in close accord with each other. It is to be noted that neither of these two approaches, are close to physical reality of metal cutting. Moreover, the cutting speed used for the simulation was far too high than the practical machining speed (15 – 300 m/min). Lower degree of chip segmentation was observed with smaller distance between the shear bands in the simulation as compared to experimental results. Shear and temperature localization was observed in narrow bands with less deformation in between

two bands. Split shear bands were found similar to those in experimental investigations but with opposite curving directions. Absolute values of force were found to be too low (by factor of 2) as compared to experimental results [36]. For the sake of parametric study, the elastic modulus [36] and thermal conductivity [37] were changed. Higher degree of chip segmentation was observed for lower elastic modulus and lower thermal conductivity. Oscillations in the cutting force due to simulation were reduced with increasing thermal conductivity.

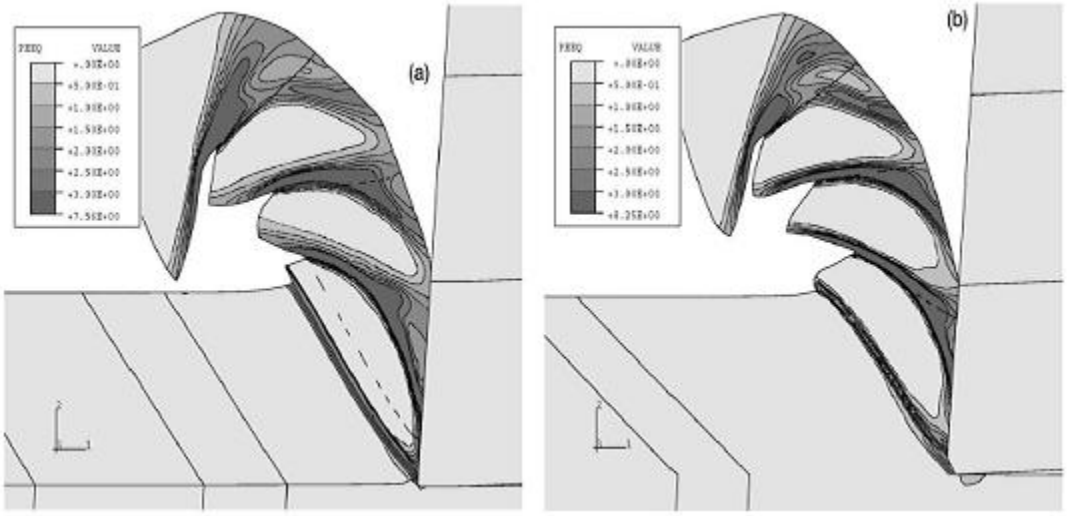

(a) (b)

Fig. 2.5 Simulations of machining Ti-6Al-4V alloy at 50 m/s with two different separation techniques: (a) node separation method; (b) pure deformation method [36].

They concluded that lack of reliable failure criterion and reliable material characteristics held researchers from expecting quantitatively accurate results from finite element simulations of shear localization process [38]. Influence of thermal softening and the hardening exponent on the chip formation of a titanium alloy was under consideration to study the effect of flow stress on chip segmentation [39]. Isotropic flow stress law used for the simulations was considered to be not realistic at high strains and strain rates in the

shear bands. Researchers concluded that simulations could not authoritatively prove that segmented chips formed during experiments were formed due to adiabatic shearing. Possibility of dominant role of damage and crack formation process in the formation of segmented chip was suggested.

Marusich and Ortiz [40] developed Lagrangian FEM code with adaptive remeshing technique for machining simulation. Dynamic effects, heat conduction, surface contact and friction, thermo-mechanical coupling were taken into account. Constitutive material model was applied to consider temperature, strain and strain rate effects on flow stress and fracture model was implemented for crack initiation and propagation.

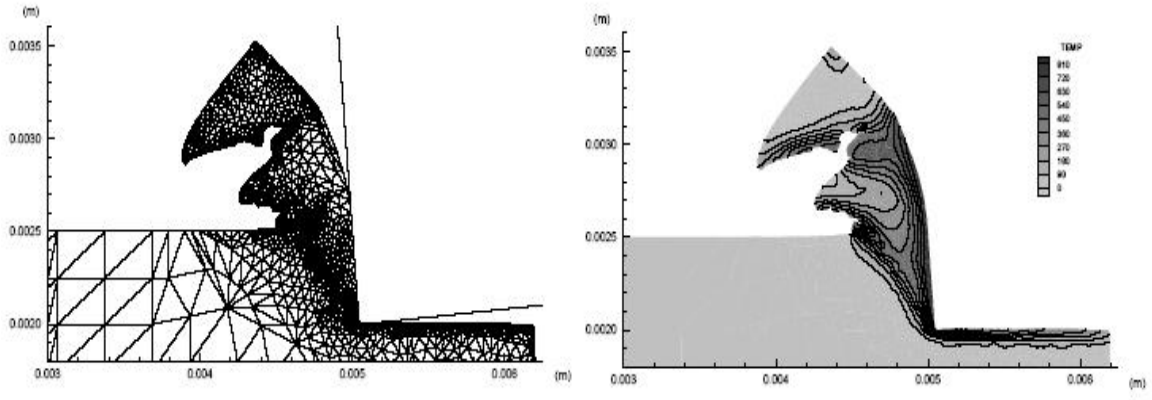

(a) (b)

Fig. 2.6 Shear localized chip in machining AISI 4340 at 10 m/s with -5^0 rake angle and 0.5 mm per rev. feed rate. (a) mesh (b) temperature gradient [40].

Simulations were run for AISI 4340 at cutting speeds of 10, 20 and 30 m/s with a feed rate of 0.5 mm/rev. Shear localization and thermal softening were observed along the shear bands. Ductile crack was observed to be initiated at the chip surface, which propagated down towards the tool tip but was arrested half way through the chip thickness. High strain values were observed along the tool face. Shear localized chip with completely detached chip segments was observed at cutting speed of 20 m/s.

Shivpuri *et al.* [41, 42] developed an implicit, Lagrangian, non-isothermal, rigid visco-plastic finite element code to simulate machining Ti-6Al-4V alloy. Dynamic flow stress model was used to represent material behavior dependent on strain, strain rate and temperature. Ductile fracture criteria were applied for crack initiation in the chip segmentation process. Variation of cutting speed affecting crack initiation and propagation was proposed as primary reason for chip segmentation. Simulations were run for 1.2, 120 and 600 m/min cutting speed and at feed rate of 0.127 mm/rev.

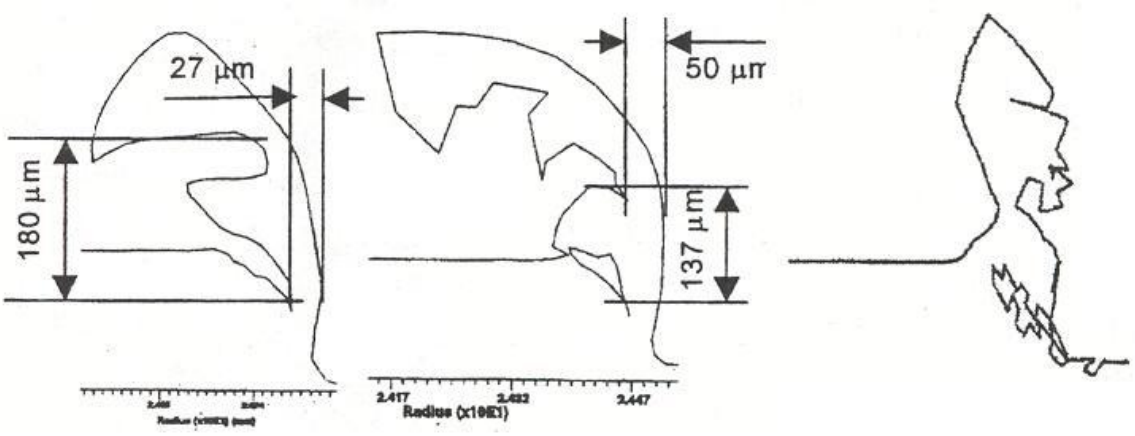

(a) (b) (c)

Fig. 2.7 Chip morphology in machining Ti-6Al-4V at a feed rate of 0.127 mm/rev and a cutting speed of (a) 600 m/min (b) 120 m/min (c) 1.2 m/min [41].

Discontinuous chip was formed at lower speed of 1.2 m/min. Crack was initiated near the tool tip and propagated upwards. This type of chip cannot be qualified for comparison with segmented chip observed in the experimental studies. Segmented chip was formed at 120 m/min and 600 m/min. Crack was initiated in the primary deformation zone, which propagated towards the free chip surface. Crack initiation was considered as the root cause of chip segmentation. Cracks were initiated in the primary shear zone and propagated towards free chip surface or tool tip depending on the cutting speed. Location

of maximum damage value shifted form a region near the tool tip to a region near the free chip surface with increase in cutting speed.

Ng and Aspinwall [43] used ABAQUS/Explicit to simulate segmented chip formation in machining tool steel (AISI H13). Workpiece was considered as incompressible, elastic-plastic material. Johnson–Cook plasticity model [47] and shear failure model [48] were applied to represent material behavior and failure criterion, respectively for the machining simulation. Adaptive remeshing and element deletion module in ABAQUS/Explicit were applied for the simulation of the chip formation process. Conditional link elements of thickness of 1 μm were located along the surface parallel to the workpiece length, separating uncut chip area and workpiece stock area. These elements were deleted when damage parameter reached unity for these elements and tool was allowed to advance towards the next link element. Sticking and sliding fiction conditions were applied between chip and tool rake face.

Machining simulations were run for AISI H13 (49 HRC) at a cutting speed of 200 m/min, feed rate of 0.25 mm /rev., and a depth of cut of 2.0 mm. Total machining time was 0.4 ms and 1.3 mm length of cut was simulated. 4000 elements were used at the beginning of simulation. Crack nucleation module was applied for prediction of onset of chip segmentation. Localization of deformation and temperature (~600°-700° C) was observed along narrow shear bands while still higher temperatures were observed along the rake face. Application of failure criterion has fecilitated in predicting machining process. The results were found in close accord with experimental observations.

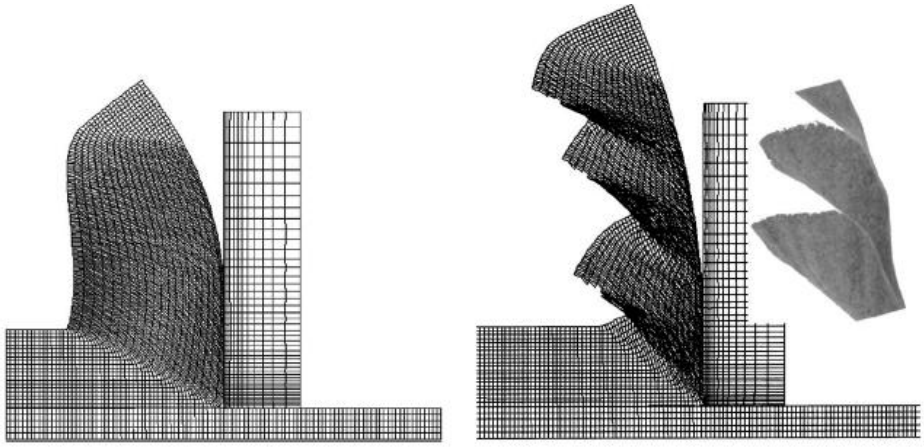

(a) (b)

Fig. 2.8 Finite element mesh in simulation of machining AISI H13 at a cutting speed of 200 m/min and a feed rate of 0.25 mm/rev. (a) continuous chip formed without applying crack nucleation module (b) segmented chip formed by applying crack nucleation module [43].

Ng *et al.* [44] conducted simulation of high-speed machining. The need for a study on the dependence of chip formation on material behavior at different cutting conditions was addressed. 3-D simulations were run for AISI 4340 at a cutting sped of 400 m/min. Johnson-Cook material model [47] and Johnson-Cook failure criterion [48] were applied to predict material behavior and failure criterion for chip separation, respectively. Recht's catastrophic shear criterion [16] was applied to predict occurrence of the chip segmentation. Chip segmentation was allowed to occur when thermal softening rate was greater than strain hardening rate. Cutting force prediction was close to experimental observation. Plastic strain and temperature distribution were close to those in actual machining.

2.4 Finite element analysis of machining Inconel 718

Sadat *et al.* [45] used general purpose finite element code (NIKE2D) for simulation of machining Inconel 718. Workpiece was modeled with 656 elements. Linear

elastic and linear strain hardening material model was assumed neglecting the effects of strain rate and temperature on the flow stress. Critical strain was used as the chip separation criterion. Simulations were run for cutting speeds ranging from 0.2 m/s to 1.6 m/s at a feed rate of 0.028 mm/rev. Cutting forces predicted by FEM simulation were reported to agree with the experimental results. Residual stresses derived were tensile in nature and reduced beneath the machined surface with increasing depth. Residual stresses and strains were concluded to be influenced by frictional condition at the tool-workpiece interface. Need for a reliable chip separation criterion and a friction model was expressed for realistic simulation of cutting Inconel 718.

Soo *et al.* [46] conducted 3-D finite element simulation of turning of Inconel 718 using ABAQUS/Explicit code. Workpiece was meshed using 8-noded, 3D solid elements. Variable mesh density was applied to ensure accuracy in large deformation region near the tool tip. At the beginning, 9072 nodes and 8120 elements were used in the simulation. Boundary conditions were applied to constrain the movement of the bottom, front and left faces of the workpiece. The workpiece was modeled as elastic–plastic material, with isotropic hardening and the flow stress was assumed to be a function of strain, strain rate, and temperature. The cutting tool was considered as a stiff elastic material. Johnson-Cook shear failure criterion [48] was applied for chip formation. Adaptive meshing was applied to avoid severe distortion of the elements. Adiabatic boundary conditions were assumed. Friction coefficient was determined using Merchant's circle and measured force components. Simulations were run at cutting speeds in the range of 50-80 m/min and at a feed rate of 0.2 mm/rev. Results obtained

after simulating the machining process for a length of 1.7 mm presented smooth continuous chip at 50 m/min and 80 m/min. The results were found to be far from reality.

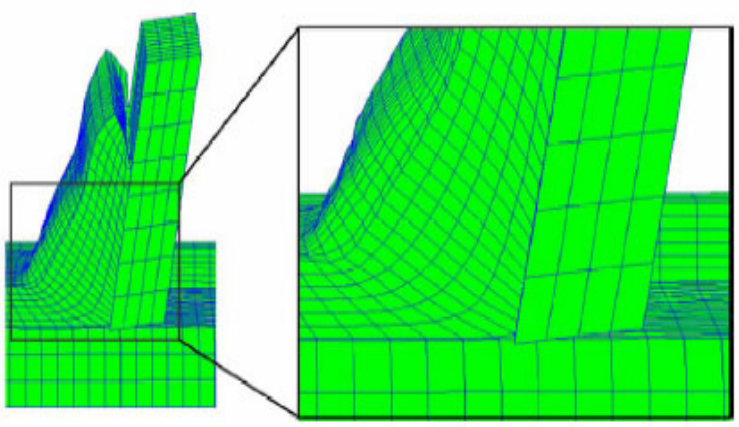

Fig. 2.9 Mesh deformation in the simulation of machining Inconel 718 at cutting speed of 50 m/min and a feed rate of 0.2 mm/rev [46].

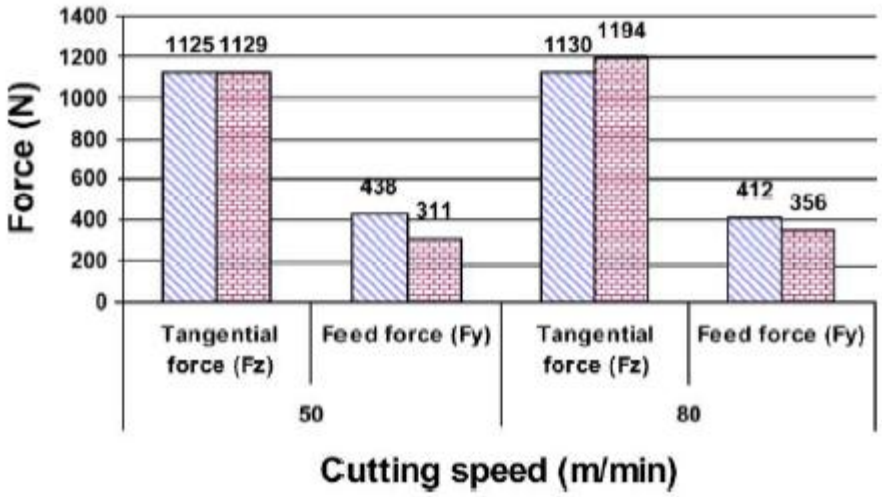

Fig. 2.10 Predicted and measured forces in the cutting and feed directions in machining Inconel 718 at cutting speed of 50 and 80 m/min and a feed rate of 0.2 mm/rev [46].

Discrepancies in the results were attributed to non-availability of finite element software code, which could predict the onset of chip segmentation, simplification of friction model, and lack of appropriate material property data. Inadequacies in the

material behavior algorithm to represent flow stress at high temperature and high strain rate conditions were addressed. Inability of shear failure criterion to predict chip formation process in machining difficult-to-machine materials was highlighted.

CHAPTER 3

PROBLEM STATEMENT

Inconel 718 has vast applications in high temperature structural regime. Metallurgical advancements and presence of γ" phase, which is stable at high temperature (up to 650° C) have made the metal stronger at high temperatures. But high temperature characteristics of this metal translate directly to machining challenges. The combination of high cutting force and high temperature when machining Inconel 718 leads to tool chipping or deformation. In addition, a hardened surface created during machining may result in depth-of-cut-line (DCL) notching of the tool and may also compromise the fatigue strength and geometric accuracy of the part. These difficulties limit the cutting speed for the alloy to the range of 15-30 m/min. Researchers have been attempting to provide solutions to improve machinability of the alloy through experimentation, analytical modelling and simulations (finite element modeling). Explanation of cause and effect of the chip segmentation process in machining Inconel 718 has been sought by researchers over the years.

There are conflicting opinions regarding the root cause of chip segmentation amongst researchers. Some of the experimental studies and computational simulations propose adiabatic shear failure as reason of instability [16, 22-27, 43, 44]. Others suggest

crack initiation and propagation in deformation zone as basis of chip segmentation [28, 29, 34, 35, 41, 42]. Focus of this investigation is to present some evidence for chip segmentation procedure based on FEM simulation.

Finite element method provides means for the study of complex machining process in a shorter time and at a lower cost as compared to experimental study. The primary concern in computational study is realistic representation of material model and reliable failure criterion. Literature review for this study has underlined lack of reliable material properties and failure criterion to explain chip formation mechanism. An attempt is made to alleviate this problem in this study.

The objectives of proposed investigation are as follows,

1. To conduct finite element simulations of machining Inconel 718 and observe chip formation mechanism.
2. To apply a material model to represent strain, strain rate and temperature dependence of flow stress in the workmaterial under machining conditions. Johnson-Cook constitutive material model is formulated in the user subroutine.
3. To apply realistic failure criterion. Recht's criterion for catastrophic shear failure is formulated and adiabatic shear is considered to be the reason for chip segmentation.
4. To validate the results of finite element simulations by comparing the cutting force, temperature on the rake face and the chip shape with experimental data reported in the literature. To compare chip formation process with experimental observations and clarifications given by Komanduri [2].

5. To simulate orthogonal machining Inconel 718 at different cutting speeds (from 30 to 180 m/min), different rake angles (-30° to 45°), and different feed rates (0.25 to 1.0 mm/rev) to study the effects on chip segmentation.
6. To predict the cutting speed for the onset of chip segmentation.
7. To study the effect of different machining conditions on the cutting and thrust forces, power consumption, shear zone temperature and rake face temperature, and equivalent plastic strain.

AdvantEdge, a commercial finite element software code is used to run the simulations. User subroutine is developed to incorporate Johnson-Cook material model and Recht's failure criterion in the main code.

CHAPTER 4

CHIP SEGMENTATION IN MACHINING

4.1 Thermoplastic shear instability

Thermoplastic instability of the workmaterial is considered as the primary reason for shear localization and a major contributor to chip segmentation. Physics based material properties, such as flow stress depends on strain, strain rate, and temperature of workmaterial. During complex process of metal cutting these parameters change rapidly. Materials get strain hardened due to plastic deformation during machining. Degree of hardening depends on metallurgy of a particular material. Similarly, material gets weakened due to rise in temperature, termed as thermal softening. These phenomena are governed by strain hardening exponent and thermal softening coefficient of the material. In case of nickel-based superalloys, it is known that γ" phase gives high strength to material up to 650° C but destabilizes due to coarsening at higher temperatures. Due to this phenomenon, material looses its strength at higher temperatures rapidly.

At low rate of deformation (low cutting speed), machining process is isothermal. Thermal energy produced due to plastic deformation of workmaterial gets distributed

within the system. Plastic shear strain has its effect on weak shear zones in the material. Material in these zones derives its strength by strain hardening. At high rate of deformation, temperature gradients are established in the workmaterial as no time is permitted for energy transfer. This effect is enhanced by poor thermal properties of certain difficult-to-cut materials, such as titanium alloys, nickel-based superalloys, and hardened steels. These temperature gradients are formed locally leading to weakening of material in that zone. This process is termed as adiabatic shear localization. If the rate of thermal softening exceeds rate of strain hardening, material continues to deform locally in that particular zone leading to catastrophic failure of shear localized band. This causes instability in the cutting process, which is known as thermoplastic shear instability.

4.2 Mechanism of adiabatic shear localization and the chip segmentation process

Adiabatic shear localization has been observed in various processes, including, ballistic impact fragmentation of cylindrical shells, blanking, high-speed metal forming, and machining of some materials. The formation of adiabatic shear band is influenced by the thermo-physical properties. Some of the properties, to mention, are specific heat, thermal conductivity and thermal diffusivity, strain hardening exponent, temperature dependence of flow stress, and density. Yield surface curvature, which depends on strain hardening and thermal softening of material, plays an important role in shear localization process. In machining titanium alloys, nickel-based superalloys, and hardened steels at particular speeds, significant amount of thermal energy is localized within the highly strained bands. Heat is generated in the deformation zone due to plastic deformation.

High temperature and high strain bands are formed due to poor thermal properties of the workmaterial and very short period of deformation. Thus, thermo-mechanical shear instability plays an important role along with machining conditions in shear localization process.

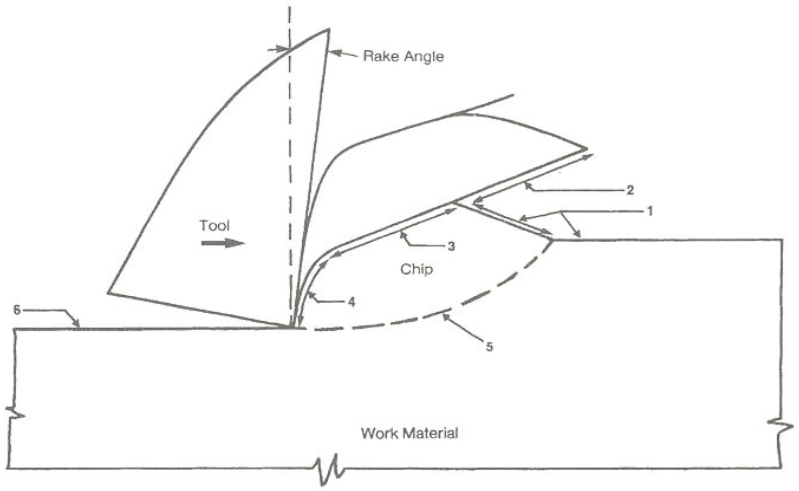

1. Undeformed surfaces
2. Part of the catastrophically shear failed surface separated from the following segment due tointense shear
3. Intense shear band formed due to catastrophic shear during upsetting stage of the segment being formed
4. Intensely sheared surface of a segment in contact with the tool and subsequent sliding on the tool face
5. Intense localized deformation in the primary shear zone
6. Machined surface

Fig. 4.1 Schematic showing the sequence of events leading to shear localized chip formation process [26].

Komanduri [25] provided some clarifications on the mechanics of chip formation when machining titanium alloys. According to him, the chip segmentation in machining some of the difficult-to-machine materials can be divided in two steps, with the first one being plastic instability and second being the upsetting process. As the tool advances, it causes plastic deformation along the shear surface in the workmaterial. Surface 5 in Fig. 4.1 represents shear surface with intense strain localization. This surface originates from

the tool tip and moves parallel to the cutting speed direction. It gradually curves with concave surface upwards until it meets the free chip surface (surface 1 in Fig. 4.1), which is undeformed. Gradual flattening of the softer half wedge occurs in the second step. This step involves very low deformation. Build up of the chip segment starts with this step. Initial contact length in this step is very short and increases as flattening progresses. No relative motion was observed between the bottom of chip segment being formed and the tool rake face until the end of the flattening step.

Bulging, also known as upsetting of the workmaterial, can be observed in the second step. Due to this, chip segment being formed is pushed upwards slowly. The stresses begin to build up in the primary shear zone as bulging progresses. The contact between the previous chip segment and the new chip segment being formed reduces as flattening progresses. It causes intense shear in the narrow band between the two chip segments. Once the shear is initiated in bulging workmaterial, it progresses rapidly. At the same time chip segment is pushed up on rake face. Periodic development of concentrated shear band with very large strain followed by catastrophic shear failure is known as adiabatic shear failure. Temperature rise in the newly forming shear band is moderate during most of the time in chip segment formation, but it increases rapidly once the large shear strains are produced in the shear band.

4.3 Effect of chip segmentation

Chip segmentation process has influence on the dynamics of the metal cutting process. Principal cutting force increases with progress of upsetting step of chip segment formation and drops down sharply as catastrophic shear failure occurs. This process is

repeated and can lead to vibrations in the machine tool system. With increasing cutting speed, the intense shear takes place very rapidly leading to very small contact between any two chip segments and separation of chip segments eventually. This influences fatigue loading on the tool and affects tool life adversely.

There is neither sticking of the chip on the rake face nor shear between the rake face and the chip, unlike in continuous chip formation. The concept of secondary shear can be neglected in the case of segmented chip formation. The chip thickness of segmented chip formed is less than the continuous chip formed under similar machining conditions for easy-to-machine materials. This is due to non-uniform deformation in machining titanium and nickel-based superalloys. Very less deformation is observed in bulk of chip being formed while major deformation takes place along narrow shear bands. Shear angle is calculated based on chip thickness and machinability of the material is predicted based on shear angle. Larger the shear angle, better the machinability. In case of segmented chip formation, machinability cannot be predicted based on shear angle as chip thickness ratio is not a true representative of machining efficiency. Freshly formed surface of segmented chip at high temperatures is in contact with the tool face for a long time as the chip segment moves slowly in the upsetting phase.

4.4 Criterion for catastrophic shear failure

Recht [16] developed a model of thermoplastic shear instability in metals under dynamic conditions. Shear strength (τ) is considered as a function of strain (ε) and temperature (θ) and the governing differential equation is

$$\frac{d\tau}{d\varepsilon} = \frac{\partial \tau}{\partial \varepsilon} + \frac{\partial \tau}{\partial \theta}\frac{d\theta}{d\varepsilon} \tag{4.1}$$

The model proposes catastrophic shear to take place at plastically deforming locations within a material when the slope of true stress-true strain ($\frac{d\tau}{d\varepsilon}$) function becomes zero.

$$\frac{\partial \tau}{\partial \varepsilon} = -\frac{\partial \tau}{\partial \theta}\frac{d\theta}{d\varepsilon} \tag{4.2}$$

The criterion for catastrophic thermoplastic shear failure was proposed as

$$0 \le \frac{\dfrac{\partial \tau}{\partial \varepsilon}}{-\dfrac{\partial \tau}{\partial \theta}\dfrac{d\theta}{d\varepsilon}} \le 1.0 \tag{4.3}$$

If the ratio is equal to one, catastrophic failure is considered to be imminent. Catastrophic shear can be expected when the ratio lies between one and zero, this indicates predominance of thermal softening over strain hardening. High positive values of this ratio (above one) indicate predominance of strain hardening and no shear localization will take place. Negative values of the ratio indicate that material gets stronger with increase in temperature and shear localization will not take place in this case either. Experimental confirmation was provided to support the model. Equation 4.3 is considered as basis for the formulation of chip segmentation in the present study.

The criterion for catastrophic failure was further simplified and written in terms of critical strain rate as

$$\dot{\varepsilon_c} = 4\Pi k \rho c (\varepsilon - \varepsilon_y)\left(\frac{\partial \tau / \partial \varepsilon}{\partial \tau / \partial \theta}\right)^2 \frac{W^2}{{\tau_y}^2 L^2} \tag{4.4}$$

Samiatin and Rao [49] developed another model to predict the onset of shear localization. This model considers heat transfer and material properties, such as strain hardening rate, temperature dependence of flow stress and strain rate sensitivity of flow stress to predict shear localization.

$$\beta = \frac{\sqrt{3}}{\dot{\bar{\gamma}}} \frac{d\dot{\bar{\gamma}}}{d\bar{\gamma}} \tag{4.5}$$

Shear localization is found to be imminent when the parameter β is equal to or greater than 5. Strain rate sensitivity has major role in this model.

Komanduri and Hou [26] applied Recht's criterion to predict the cutting speed for the onset of chip segmentation. Depending on the thermo-plastic properties of the workmaterial and the machining conditions used, this speed may vary for different materials. Temperatures generated in the shear band by various primary heat sources and preheating effects are calculated. True stress in the shear band is estimated based on shear band temperature and shear strain. This is compared with the true yield stress of the material at the preheating temperature. When true stress in the shear band at the shear band temperature is greater than or equal to the true yield stress of the workmaterial, no shear localization takes place; instead strain hardening is evident. When true stress in the shear band at the shear band temperature is less than or equal to true yield stress of the workmaterial, shear localization is imminent. The analytical predictions of cutting speed with this criterion were found to be in close accord with the experimental results for an alloy steel (AISI 4340) and a titanium alloy (Ti-6Al-4V) and a nickel-based superalloy (Inconel 718) [26, 27].

CHAPTER 5

FINITE ELEMENT ANALYSIS (FEA) OF MACHINING

5.1 FEA: Theory and Assumptions

The finite element method provides a systematic procedure for the derivation of the approximation functions for motion, force, deformation, and temperature calculations. The approximation functions are derived and expressed by a linear combination of polynomials, normally in a weighted integral form over each element. Discretization of the geometry is the first step in the finite element analysis and in this step the geometry is divided into a number of finite elements. Solutions are determined by mapping problem domain on the contour of specified points called nodes on each element and applying the calculated finite solutions to the entire geometry. Degrees of freedom are applied on nodal points. The element properties are defined in which different types of elements, such as bricks, triangular, or shell elements are used depending on the requirements of the analysis. The stiffness matrix is derived using the element properties, which describes the force–displacement relationship of the element under loading. The loading conditions, such as pressure, forces, and velocities are defined along with the boundary conditions at

specified nodes. Finally, the element descriptions, applied loads, and boundary conditions are assembled as a set of equations in matrix form. The set of equations is then solved numerically for the unknown values. Stresses, strains, and other parameters are calculated based on the resulting nodal displacements.

It may be noted that Mr. Parag Konde and Mr. Sayed Kareem contributed actively in understanding the Recht's failure criterion and deriving the equations to apply that criterion in FEM software code.

Certain assumptions are to be made to simulate complex procedure of metal cutting with FEM. These assumptions are used to define the problem to be solved as well as to apply the boundary and loading conditions. The following assumptions were made in regard to this model:

1. The cutting speed is constant.
2. The width of cut is much larger than the feed (plane strain condition), and both are constant.
3. The cutting velocity vector is normal to the cutting edge.
4. The workpiece material is a homogeneous polycrystalline, isotropic, and incompressible solid.
5. The workpiece is at a reference temperature (20° C) at the beginning of simulation.
6. Cutting is performed in air and no liquid coolants are used. Adiabatic temperature boundary conditions are assumed.
7. The machine tool is perfectly rigid and no influence of machine tool dynamics on machining is considered.

8. Constant friction at tool-chip interaction and tool-workpiece interaction.

AdvantEdge^{TM}**,** an explicit code**,** is used for the finite element simulation and analysis of machining Inconel 718 under various machining conditions. It is a commercial finite element software with 2-dimensional explicit code and Lagrangian formulation. The central difference time integration scheme is applied for each time step in explicit method. The Newmark family of temporal integrators is used to solve algorithmic approximations for the solution vector of displacement, velocity, and acceleration. The time step is related to corresponding eigen value of the element. Accuracy in computation of the system eigen value plays a major role in the success of simulation algorithm. Care should be exercised in the computation of eigen value of an element when mesh geometry is constantly changing and continuous remeshing of the geometry is taking place to avoid severe distortion of mesh in deformation zone. Critical time step for the mesh is computed from eigen value for largest element. Lumped mass matrix method is used to incorporate inertial effects.

Governing equations for mechanical computations are as follows

$$\left[M^{(e)} \right] \left\{ \ddot{\Delta}^{(e)} \right\} + \left[K^{(e)} \right] \left\{ \Delta^{(e)} \right\} = \left\{ F^{(B)} \right\} + \left\{ F^{(S)} \right\} \tag{5.1}$$

where,

$$M_{ab} = \int_B \rho N_a N_b dV_0, \qquad F_a^B = \int_B f_B N_a dV_0, \qquad F_a^S = \int_S f_S N_a d\Omega$$

Here $M^{(e)}$ is consistent mass matrix for an element, $K^{(e)}$ is elemental stiffness matrix and $F^{(B)}$ and $F^{(S)}$ are body force and traction force matrices, respectively for the corresponding element. In Equation 5.1, N is shape function array and f_b and f_s are body

force and traction force at individual nodes. Equation 5.1 is solved for $\Delta^{(e)}$ which is the solution vector for nodal displacement. Explicit time integration scheme is applied for the solution of equations.

Substantial amount of heat is generated in machining due to plastic deformation of the workmaterial and friction at the tool-chip interface and tool-workpiece interface. The temperatures generated have considerable influence on the mechanical response of the workmaterial. First law of thermodynamics is applied for temperature and heat transfer calculations.

Governing equations for temperature and heat transfer calculations are as follows

$$T_{n+1} = T_n + \Delta t \dot{T}_n \tag{5.2}$$

$$\left[C^{(e)} \right] \left\{ \dot{\mathrm{T}} \right\} + \left[K^{(e)} \right] \left\{ \mathrm{T} \right\} = \left\{ \mathrm{Q}^{(e)} \right\} \tag{5.3}$$

where,

$$C_{ab} = \int_{Bt} c\rho N_a N_b dV_0, \qquad K_{ab} = \int_{B0} D_{ij} N_{a,i} N_{b,j} dV, \qquad \dot{W}^p = \bar{\sigma} \dot{\varepsilon}^p$$

$$Q_{ab} = \int_{Bt} s N_a dV_0 + \int_{Bt} h N_a dS, \qquad h = \sqrt{\kappa \rho c}, \qquad s = 0.9 \dot{W}^p$$

Here $C^{(e)}$ is heat capacity matrix for an element, $K^{(e)}$ is elemental conductivity matrix, and $Q^{(e)}$ is heat source array. Heat supply, *h*, is computed from thermal conductivity, mass density and specific heat. Rate of heat generation, *s*, is computed from work done in plastic deformation. *T* is the array of nodal temperatures and *n* is time step.

Geometrically identical meshes are used for thermal and mechanical solution computations. Mechanical solution step is carried out at constant temperatures and heat

generation is considered as constant during the thermal step. A mechanical step is taken first based on the current distribution of temperatures, and the heat generated is computed from plastic work and frictional heat generation. The heat thus computed is transferred to the thermal mesh and the temperatures are recomputed. The resulting temperatures are transferred to the mechanical mesh and are incorporated into further computations in that step cycle.

Time step is restricted in explicit method for stability of the solution. Still it is an attractive option for finite element simulation of complex procedures, such as metal cutting, which involves complicated contact situations [40]. Contact algorithms available for explicit method are more robust and straightforward than those for implicit method. Machining involves contact between deformable bodies, such as the workpiece-tool interface and tool-chip interface. The bodies in contact may be considered as deformable or rigid. Contacting rigid surfaces are considered as master surface and deformable surfaces are treated as slave surface. Nodal accelerations from the out-of-balance forces are calculated and nodal positions, velocities, and accelerations are predicted by predictor algorithm assuming that no contact has occurred. A resulting predictor configuration shows penetration of master surface into slave surface. The contact conditions are designated by an auxiliary consecutive numbering of the nodes on the contacting surfaces. The penetration distances for all nodes on the slave surface are then calculated. The contact force required to prevent penetration is equal to force required to keep master surface stationary on predictor configuration as shown in Fig 5.1.

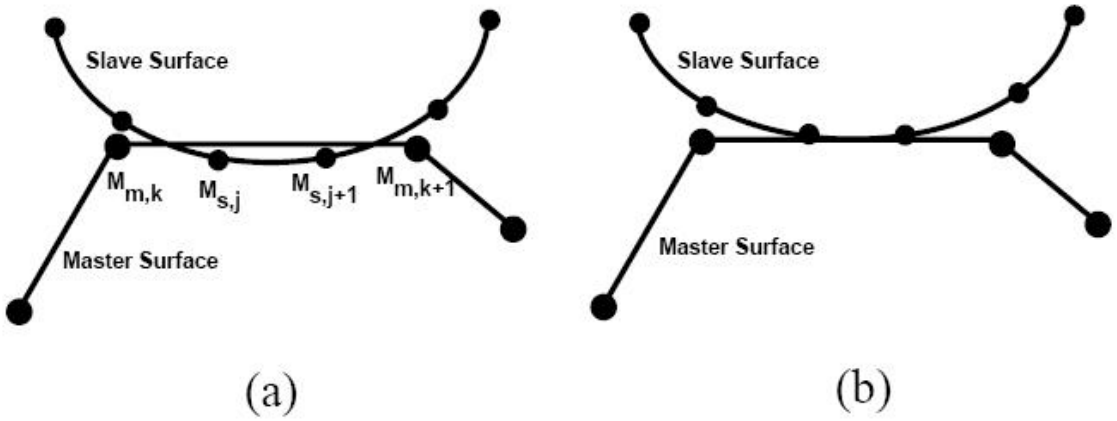

Fig. 5.1 Schematic showing contacting surfaces (a) predictor configuration of surfaces (b) kinematically compatible surfaces [51]

Normal acceleration corrections are calculated to eliminate penetration and to calculate tangential force and sticking force on the slave surface. Coulomb friction model is applied for friction calculations.

5.2 **Element design and adaptive remeshing**

Accuracy of the solution in finite element simulation largely depends on the type and size of element selected. The basic types of elements for 2-dimensional simulation are three noded and six-noded triangular elements and four-noded and eight-noded quadrilateral elements. The most commonly employed elements are the first and second-order isoparametric elements. Six noded, second-order triangular elements are used in *AdvantEdge* for finite deformation formulation and discretization. The element has three corner and three mid-side nodes providing quadratic interpolation of the displacements within the element. The constitutive response of the material is computed at the

integration points consequently, the element provides a linear pressure distribution within the element.

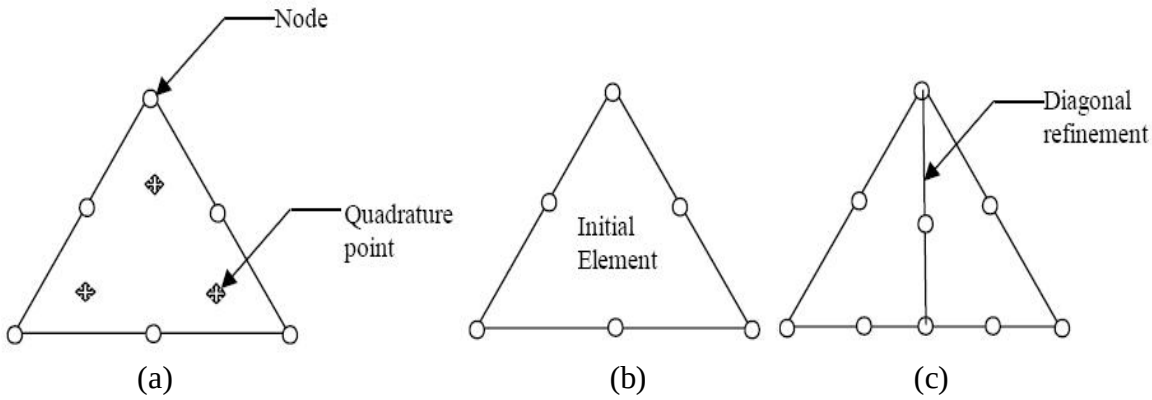

Fig. 5.2 Schematic of six-noded triangular element used for discretization of tool, workpiece and chip system. (a) Basic element shape with six nodes and three quadrature points. (b) Initial shape of element (c) Shape of element after remeshing [50]

Severe mesh distortion of the Lagrangian mesh in metal cutting simulation has been the problem of concern for researchers. Continuous remeshing is the proven way to solve mesh distortion problems. Connectivity of the finite element mesh is redefined at regular intervals for the nodes at their spatial locations. Simple mesh smoothing algorithms are applied to enhance positive effects of adaptive remeshing. The mechanical and thermal boundary layers developed in the contact region and within localized shear bands are smoothed using these algorithms. Refinement of an element is exercised by splitting the diagonal of the element such that a mid-side node becomes a new corner node and new mid-side nodes are then added to both elements formed as shown in Fig. 5.2.

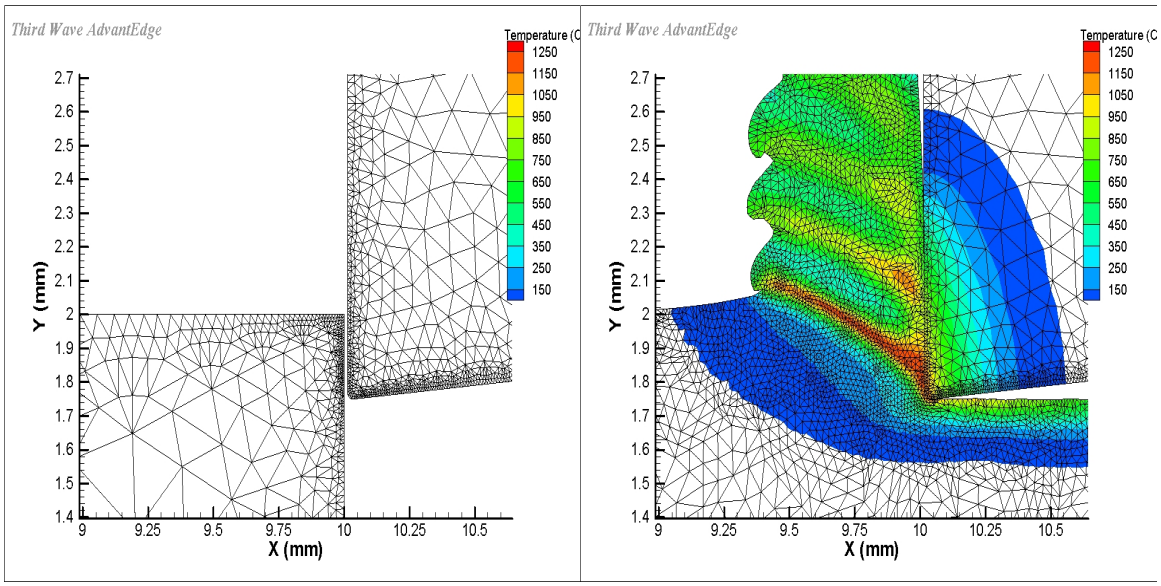

(a) (b)

Fig. 5.3 Mesh in workpiece and tool at (a) initial stage (b) final stage of machining simulation. Refinement of mesh in the deformation zone can be seen in the final stage.

The connectivity of the mesh is defined by a set of corner nodes of the element. An adaptation criterion based on equal distribution of plastic power is used for mesh refinement. Elements exceeding plastic power tolerance are considered for refinement. This criterion leads to refinement in regions of high rate of plastic deformation. The mesh is adapted at regular intervals by adding new corner nodes at the mid-sides of elements targeted for refinement and the element connectivity is then completely redefined. Laplacian smoothing algorithm is applied to overcome residual distortions. A mesh-coarsening algorithm is also used to keep the problem size (number of nodes and elements) within limits for efficient computation. It is applied in the inactive areas of the mesh.

5.3 **Constitutive material model**

Workmaterials are subjected to a broad range of high plastic strains (2-8), strain rates (10^3 to 10^6 s^{-1}), and temperatures (300°-1200° C) in the metal cutting operations. Access of these parameters to establish their relation with strength of deforming material is very much challenging by conventional material tests. Lack of reliable material properties representing influence of these parameters on strength of workmaterial is highlighted in the literature. The material constitutive laws include effect of strain, strain rate, and temperature on flow stress. Most of the material models are developed by fitting regression models to test results. Recently, researchers have used Johnson-Cook material model for metal cutting analyses. It is found to represent dependence of flow stress on strain, strain rate, and temperature satisfactorily, if not perfectly, for many materials. Usually data from Split Hopkinson Pressure Bar (SHPB) test or ballistic impact tests are used for regression analysis to compute Johnson-Cook material model constants.

$$\bar{\sigma} = \left[A + B \left(\bar{\varepsilon}\right)^n \right] \left[1 + C \ln \left(\frac{\dot{\bar{\varepsilon}}}{\dot{\bar{\varepsilon}}_0} \right) \right] \left[1 - \left(\frac{T - T_r}{T_m - T_r} \right)^m \right] \tag{5.4}$$

The designation of material constants in Johnson-Cook material model is as follows:

$\bar{\sigma}$ Flow stress	$\bar{\varepsilon}$ Equivalent plastic strain
A Yield stress constant	$\dot{\bar{\varepsilon}}$ Strain rate
B Strain hardening coefficient	$\dot{\bar{\varepsilon}}_0$ Reference strain rate
n Strain hardening exponent	T Temperature
C Strain rate dependence coefficient	T_r Room temperature
m Temperature dependence coefficient	T_m Melting temperature

The first term in the Equation 5.4 is the strain hardening term indicating strain dependence of flow stress. The second term indicates the strain rate hardening of workmaterial, and the third term represents thermal softening of workmaterial.

Perfectly elastic material model is used for the tool material. Details of material model for tool are not available as material is selected from material library of the software.

5.4 Stress update algorithm

AdvantEdge has user subroutine facility to incorporate user defined material behavior and stress update algorithm in the code. A user subroutine was developed to incorporate Johnson-Cook material model and Recht's thermoplastic shear instability criterion in the code. Tool-workpiece material system is considered as plane strain problem state and large width is assumed in the Z-direction. Strains and deflections in the Z-direction are considered to be negligible. Stress update algorithm is called for each integration point within an element. The material properties and boundary conditions are applied on nodes and are interpolated onto the integration points. The results after stress update are extrapolated on nodes again. General theory for the rate dependent elastic-plastic material model with isotropic hardening is applied to compute stress history from strain history. Total increment in equivalent plastic strain is initialized to zero in every time step.

Elastic modulus and Poisson's ratio for the workmaterial are used from the input data to compute the shear modulus and the Lame's material constant as,

$$\mu = \frac{E}{2\,(1+\nu)} \qquad \lambda = \frac{\nu\, E}{(1-2\,\nu)\,(1+\nu)} \tag{5.5}$$

The elastic trial stresses for the k^{th} time step are computed from velocity strain (strain rate) increments outside the iteration loop. Velocity strain increments are passed into the subroutine as a result from main finite element code. Trace of the strain rate increments is computed as

$$tr\,(d)^{k} = d^{k}{}_{11} + d^{k}{}_{22} + d^{k}{}_{33} \tag{5.6}$$

Elastic trial stress is computed as

$$\sigma_{ij}{}^{k(tr)} = \sigma_{ij}{}^{(k-1)} + \lambda\, tr\,(d)^{k} + 2\,\mu\, d^{k}{}_{ij} \tag{5.7}$$

Iterations for radial return algorithm in the k^{th} time step begin with the computation of deviatoric stress from trial stress state.

Hydrostatic pressure term is deducted from directional stress terms to get deviatoric stress state.

$$P^{i} = \frac{\sigma_{lm}{}^{i(tr)}\,\delta_{lm}}{3} \qquad\qquad \sigma_{lm}{}^{i(div)} = \sigma_{lm}{}^{i(tr)} - P^{i}\delta_{lm} \tag{5.8}$$

Magnitude of the deviatoric trial stress is computed as

$$\sigma_{N}{}^{i(div)} = \sqrt{\sigma_{lm}{}^{i(div)}\,\sigma_{lm}{}^{i(div)}} \tag{5.9}$$

Radial return algorithm [51] is applied as an effective procedure for numerical integration of elastoplastic problem. If the state defined by trial elastic state lies outside the elastic region enclosed by the yield surface, the final state is defined at closest point projection of trial state onto the yield surface. Von Mises yield surface is updated for each iteration using the flow rule given by Johnson-Cook material model. Non-linear

isotropic behavior of the workmaterial is applied in this procedure. Flow stress is computed from previous time step using Johnson-Cook material model as

$$\bar{\sigma}^{k} = \left[A + B \left(\bar{\varepsilon}^{(k-1)} \right)^{n} \right] \left[1 + C \ln \left(\frac{\dot{\bar{\varepsilon}}^{(k-1)}}{\dot{\bar{\varepsilon}}_{0}} \right) \right] \left[1 - \left(\frac{T^{(k-1)} - T_r}{T_m - T_r} \right)^{m} \right] \tag{5.10}$$

Radius of the yield surface for k^{th} time step is computed as

$$R^{k} = \sqrt{2/3}\ \bar{\sigma}^{k} \tag{5.11}$$

Hardening slope depends on the elastic modulus as well as plastic modulus. Plastic modulus is computed as change in flow stress with change in equivalent plastic strain.

$$E^{k}{}_{\mathrm{p}} = \frac{\partial \bar{\sigma}^{k}}{\partial \varepsilon_{pl}{}^{k}} \qquad \& \qquad H^{k} = \frac{E E^{k}{}_{P}}{E - E^{k}{}_{P}} \tag{5.12}$$

Increment in equivalent plastic strain for the i^{th} iteration is computed as

$$\Delta\lambda^{\mathrm{i}} = \frac{\sigma_{N}{}^{i(div)} - R^{k}}{2\mu\left(1 + \frac{H^{k}}{3\mu}\right)} \tag{5.13}$$

If the numerator term in the Equation 5.13 is negative, then stress state lies within the yield surface and there is no further need to separate plastic part from total strain. Stress state is updated and iteration loop is concluded.

But, if the numerator in the Equation 5.13 is positive, it indicates that stress state lies outside the yield surface and separation of plastic stress part is necessary.

Increment in equivalent plastic strain and trial stress are updated as

$$\Delta\lambda_{Total}^{\ i} = \Delta\lambda_{Total}^{\ i-1} + \Delta\lambda^{i} \tag{5.14}$$

$$\sigma_{lm}^{\ (i+1)(tr)} = \sigma_{lm}^{\ (i)(tr)} - 2\,\mu\,\Delta\lambda^{i}\,\frac{\sigma_{lm}^{\ (i)(div)}}{\sigma_{N}^{\ (i)(tr)}} \tag{5.15}$$

Thus the trial stress state for the $(i+1)^{st}$ iteration is computed, total increment in equivalent plastic strain is updated and procedure from the Equation 5.8 is repeated till the trial stress state lies within the yield condition for that time step. On conclusion of the iteration loop, total increment in equivalent plastic strain is added to equivalent plastic strain of the previous time step and strain rate and plastic work rate are updated. Stress history for that particular time step is updated using trial stress state calculated just prior to the conclusion of the iteration loop.

5.5 **Formulation of thermoplastic shear instability criterion**

As discussed in Chapter 4, Recht [16] has developed a criterion for thermoplastic shear instability in metal cutting.

$$0 \le \frac{\dfrac{\partial\tau}{\partial\gamma}}{-\dfrac{\partial\tau}{\partial T}\dfrac{dT}{d\gamma}} \le 1.0 \tag{5.16}$$

Terms in the Equation 5.16 are derived and the formulation is applied to finite element code as the failure criterion. Johnson-Cook material model (Equation 5.4) is used for the derivation of the terms. For using Johnson-Cook material model in Recht's criterion, it is converted to shear stress-shear strain form as

$$\bar{\tau} = \frac{1}{\sqrt{3}}\left[A + B\left(\frac{\bar{\gamma}}{\sqrt{3}}\right)^{n} \right]\left[1 + C\ln\left(\frac{\dot{\bar{\gamma}}}{\dot{\bar{\gamma}}_0}\right)\right]\left[1 - \left(\frac{T - T_r}{T_m - T_r}\right)^{m}\right] \tag{5.17}$$

Equation 5.17 is partially differentiated with respect to shear strain to compute numerator of Recht's criterion as

$$\frac{\partial \bar{\tau}}{\partial \bar{\gamma}} = \left[\frac{\mathrm{n}\,B}{3}\left(\frac{\bar{\gamma}}{\sqrt{3}}\right)^{n-1} \right]\left[1 + C\ln\left(\frac{\dot{\bar{\gamma}}}{\dot{\bar{\gamma}}_0}\right)\right]\left[1 - \left(\frac{T - T_r}{T_m - T_r}\right)^{m}\right] \tag{5.18}$$

Equation 5.17 is partially differentiated with respect to temperature to compute the first denominator term of the Recht's criterion as

$$\frac{\partial \bar{\tau}}{\partial T} = \frac{1}{\sqrt{3}}\left[A + B\left(\frac{\bar{\gamma}}{\sqrt{3}}\right)^{n} \right]\left[1 + C\ln\left(\frac{\dot{\bar{\gamma}}}{\dot{\bar{\gamma}}_0}\right)\right]\left[\frac{-\mathrm{m}}{(\mathrm{T} - \mathrm{T_r})}\left(\frac{T - T_r}{T_m - T_r}\right)^{m}\right] \tag{5.19}$$

Second denominator term of Recht's criterion is rate of change of temperature with strain. Recht developed a model [16] to determine temperature gradient with strain in the catastrophic shear zone.

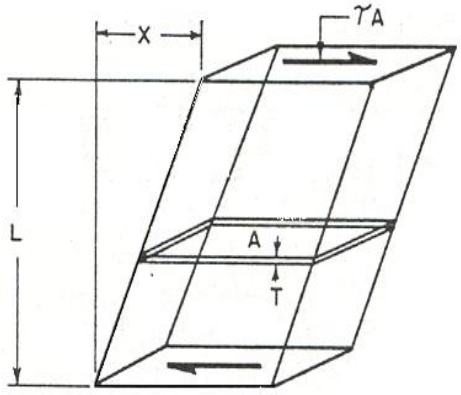

Fig. 5.4 Model used to determine temperature gradient with strain in catastrophic shear zone [16].

The thin zone indicated by area *A* in Fig. 5.4 is of thickness *T* and is considered as the weakest zone within the length *L* of the specimen. It is assumed that this zone will remain thin to achieve catastrophic shear in this zone. A constant rate of average strain x/L is applied on the specimen which is high enough to produce catastrophic shear in area *A*. As zone *A* is very thin, it is assumed to be a plane of uniform heat generation. Plastic deformation is restricted to this zone. Heat generation rate over unit area *A* can be calculated as

$$q = \frac{\tau L}{W} \dot{\gamma} \tag{5.20}$$

Temperature in the area *A* can be calculated as

$$T_A = q \sqrt{\frac{t}{\pi \kappa \rho C}} = \frac{\tau_y L \dot{\gamma}}{W} \sqrt{\frac{t}{\pi \kappa \rho C}} \tag{5.21}$$

For constant strain rate

$$dT_A = \frac{1}{2}\,\frac{\tau_y\, L\,\dot{\gamma}}{W}\sqrt{\frac{1}{\pi\,\kappa\,\rho\, C\, t}}\;\mathrm{d}t \tag{5.22}$$

Substituting Equation 5.23 in Equation 5.22 gives

$$\frac{d\,\gamma}{d\,t} = \dot{\gamma} \qquad \text{and} \qquad \gamma = \dot{\gamma}\; t + \gamma_y \tag{5.23}$$

$$\frac{dT_A}{\mathrm{d}\gamma} = \frac{1}{2}\,\frac{\tau_y\, L}{W}\sqrt{\frac{\dot{\gamma}}{\pi\,\kappa\,\rho\, C\,(\gamma-\gamma_y)}} \tag{5.24}$$

Specimen length L can be considered as feed rate *f* in orthogonal turning operation. Substitution of Equations (5.18), (5.19) and (5.24) in Equation (5.16) gives an equation applicable to finite element simulation for adiabatic thermoplastic shear instability.

$$R = \frac{\left[\;\frac{\mathrm{n}\,B}{3}\left(\bar{\varepsilon}_{pl}\right)^{n-1}\;\right]\left[1-\left(\frac{T-T_r}{T_m-T_r}\right)^{m}\right]}{\frac{1}{\sqrt{3}}\left[\;A\;+\;B\left(\bar{\varepsilon}_{pl}\right)^{n}\;\right]\left[\frac{-\mathrm{m}}{(\mathrm{T}-\mathrm{T_r})}\left(\frac{T-T_r}{T_m-T_r}\right)^{m}\right]\left[\frac{1}{2}\,\frac{\tau_y\,\mathrm{f}}{W}\sqrt{\frac{\dot{\bar{\varepsilon}}_{pl}}{\pi\,\kappa\,\rho\, C\,(\bar{\varepsilon}_{pl}-\varepsilon_y)}}\right]} \tag{5.25}$$

Recht's criterion is applied in the finite element code as a failure criterion for a particular integration point. When the value of *R* is between 0 and 1, stress state of that

integration point is set to zero. When stress state of all integration points in an element gets set to zero, the element is considered to have been failed and is discarded from further calculations.

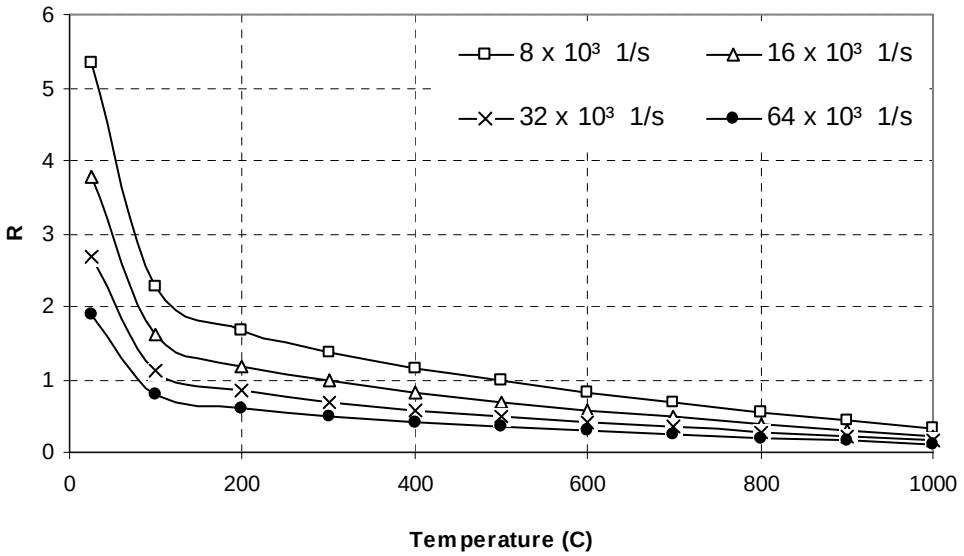

Fig. 5.5 Variation of Recht's expression R with temperature for various strain rates for Inconel 718 with a feed rate of 0.25 mm/rev and at 400 % strain.

Johnson-Cook material model and Recht's catastrophic shear failure criterion in ABAQUS/Explicit (a commercially available FEM software code) were applied in this study. However, simulations with ABAQUS could not deliver results and hence the work is not mentioned in detail. User subroutine was developed for ABAQUS/Explicit but simulations were not successful because of excessive element distortion. Adaptive remeshing of elements could not solve the problem. Calculations were very slow for some unknown reason.

CHAPTER 6

FEM SIMULATIONS OF MACHINING INCONEL 718 UNDER DIFFERENT MACHINING CONDITIONS

6.1 Material properties and simulation approach

Study of chip segmentation process in machining of Inconel 718 is the main objective of this investigation. Some researchers consider “adiabatic shear failure” as the reason for shear instability and chip segmentation [16]. Others suggest “crack initiation and propagation in deformation zone” as the basis of chip segmentation [28]. Experimental study [2] and observations of chip segmentation process [22-27] explained by Komanduri *et al.* are used as guide lines for this study. Adiabatic shear localization is assumed to be the root cause of chip segmentation. Lack of realistic material model and reliable failure criterion for finite element simulation of machining of Inconel 718 is underlined by the literature review for this study. Application and validation of material model and failure criterion is another objective of this study. Recht’s criterion for catastrophic shear failure in the chip is applied to observe chip segmentation procedure. Poor thermal properties of some materials and high strength held at high temperatures are

considered to be the reasons for the shear localization. Variation of thermal properties and strength with temperature are considered in Recht's criterion for failure. Analytical models for flow stress behavior were reviewed, which represent workpiece material strength under the effects of strain, strain rate, and temperature. Johnson-Cook material model is applied to represent effects of various machining conditions on material strength. Material constants for Johnson-Cook material model are listed in Table 6.2 [52]. Strain, strain rate and temperature dependence of Inconel 718 is shown in Fig. 6.1 and Fig. 6.2. Tool material is considered to be perfectly elastic. Observations of deformation or wear of tool are outside the scope of this study. A constant Columbic friction coefficient (0.5) is assumed to govern the friction between the tool and the chip interface.

Table 6.1 Physical Properties of Inconel 718 [1]

Property	**21° C**	**540° C**	**650° C**	**760° C**	**870° C**
Ultimate tensile strength (MPa)	1435	1275	1228	950	340
Yield strength (MPa)	1185	1065	1020	740	330
Elastic modulus (GPa)	200	171	163	154	139
Specific heat capacity (J/Kg.K)	430	560	---	---	645
Thermal conductivity (W/m.K)	11.4	19.6	---	---	24.9
Coefficient of thermal expansion (10^{-6} / K)	---	14.4	---	---	---
Melting range (°C)	1260-1335				
Density (Kg/m^3)	8220				

Table 6.2 Johnson-Cook material model constants for Inconel 718 [52]

A (MPa)	B (MPa)	C	n	m	$\dot{\varepsilon}_0$ (1/s)	Room Temperature (C)	Melting Temperature (C)
450.0	1700.0	0.017	0.65	1.3	0.001	20.0	1297.0

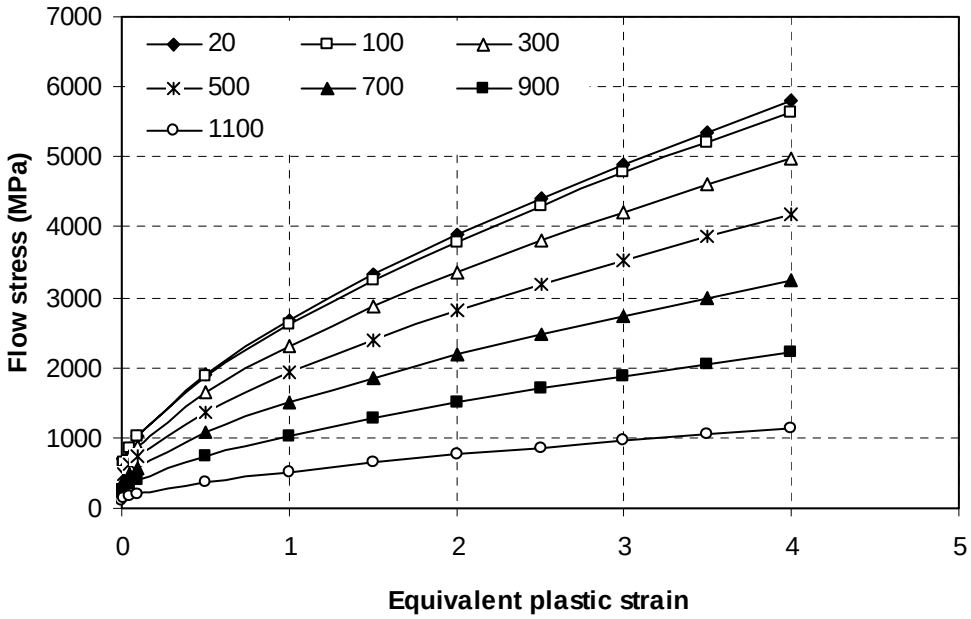

Fig. 6.1 Flow stress variation based on Johnson-Cook material model for Inconel 718 in the temperature range of 20° to 1100° C, and strains in the range of 0.005 to 4.0 at a strain rate of 20 x 10^3 s^{-1}.

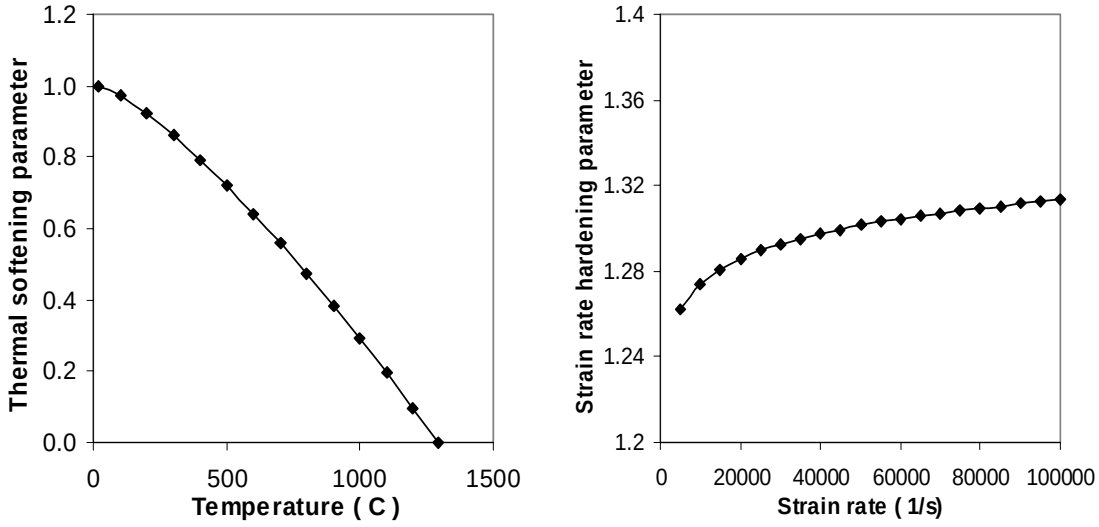

Fig 6.2 Temperature and strain rate dependence of flow stress governing parameters for Johnson-Cook material model of Inconel 718.

Orthogonal machining of Inconel 718 is simulated using AdvantEdge 2D, explicit, Lagrangian formulation finite element code. User subroutine is developed to apply Johnson-Cook material model and Recht's failure criterion in the main code.

Metal cutting is affected by the type of workmaterial, tool material and cutting conditions. The factors affecting chip formation are cutting speed, depth of cut, feed rate and tool normal rake angle. Depth of cut and cutting speed for a particular simulation are assumed to be constant for that run. Adiabatic temperature boundary conditions are assumed. Effect of any cooling material is not investigated in this study. The machining operation is assumed to be performed in air without application of any liquid coolants.

Combination of cutting conditions used for simulations is listed below (for cutting length of 3 mm and depth of cut of 1 mm):

1. Cutting speeds: 30.5, 61.0, 91.5, 122.0, 152.5, 183.5 m/min (each with rake angles of -15°, 0° and 15° at 0.25 mm/rev feed rate) Number of runs : 18
2. Rake angles: -30°, -15°, 0°, 15°, 30°, 45° (each at 61 m/min cutting speed and 0.25 mm/rev feed rate) Number of runs : 6
3. Feed rates: 0.25, 0.5, 0.75, 1.0 mm/rev (each at 61 m/min cutting speed and 0° rake angle) Number of runs : 4

More simulations were run for 50 and 80 m/min cutting speed and with different coefficient of friction (μ = 0.3, 0.5 and 0.7) to compare cutting force and thrust force results with experimental results reported in the literature. Prediction of the onset of chip segmentation under different machining conditions is another objective of this investigation. The effect of different machining conditions on cutting force, thrust force, power consumed during machining, shear zone temperatures and rake face temperatures

are observed by post processing the FEM simulation results. Simulations are run on an Intel Pentium 4 CPU (2.3 GHz) with 1 GB of RAM.

6.2 Comparison of results with experimental data

This investigation involves application of material model which has been used with other failure criteria earlier. It is important to validate the Johnson-Cook material model and Recht's catastrophic shear failure criterion combination used in this study. Results of finite element simulations of machining of Inconel 718 reported in the literature [45, 46] show continuous chip formation under the investigated machining conditions. Experimental results reported along with those studies indicate segmented chip formation. Failure of finite element simulations to predict segmented chip formation was attributed to lack of reliable failure criteria and realistic material properties.

The results of this study are extracted in post processing of FEM simulations run under various machining conditions and compared with experimental results reported in the literature. Kitagawa *et al.* [12] examined performance of silicon nitride (Si_3N_4) with a -5° rake angle in machining Inconel 718 at the feed rate of 0.19 mm/rev and depth of cut of 0.5 mm. Cutting speed was altered from 30 to 500 m/min. A water based coolant diluted with water 50 times was supplied towards the tool edge at a rate of 41 m/min. Relation between local temperatures on the rake and flank face of tool and cutting speed was reported. The temperatures were observed to increase monotonically with increasing cutting speed. Serrations in the chip were observed to become obvious with decrease in chip thickness at increasing cutting speeds. Large plastic flow was observed in the chip at higher cutting speed. The reason for enhanced plastic flow at a specific cutting speed or

cutting temperature was not commented. FEM simulations with similar set of cutting conditions are run for comparison. Cutting conditions used include cutting speeds ranging from 30.5 to 183.5 m/min, feed rate of 0.25 mm/rev, depth of cut of 1.0 mm and rake angle of 0°. Fig. 6.3 shows points on rake face of tool at which temperatures are observed.

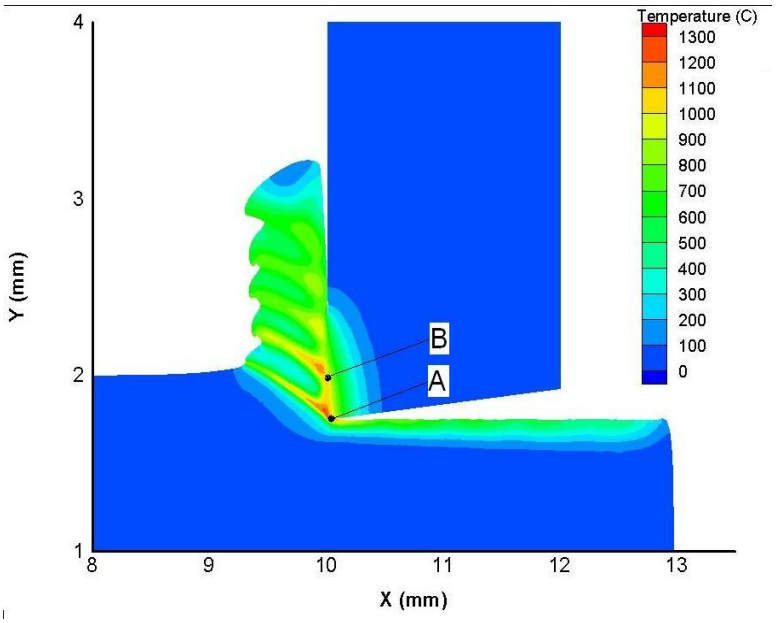

Fig. 6.3 Temperatures are observed at two points (A and B) on the rake face.

Temperature at point A is maximum on the rake face. Localized shear band formation starts at this point. Temperature in the shear band increases continuously until the chip segment reaches point B and then onwards temperature in the shear band is observed to reduce. Average of the temperatures at point A and B is considered for comparison with experimental data and percentage error is reported in Table 6.3. The temperatures in machining depend on cutting speed, feed rate, rake angle, coolant material and friction in tool-chip interface. The difference in the values of temperatures on the rake face observed in the FEM simulation and experiments at various cutting speeds can be attributed to slightly different machining conditions used in two studies.

Coefficient of friction in tool-chip interface used in FEM simulation plays a major role in calculating the rake face temperature. A close match of rake face temperatures in the experimental and FEM simulation study justify the assumption for columbic friction coefficient.

Table 6.3 FEM simulation results at point A, point B and average rake face temperature compared with experimental data and the percentage error.

	Temperature (μ= 0.5)				
Speed (m/min)	**Experimental (C)**	**FEM A (C)**	**FEM B (C)**	**FEM Average (C)**	**Error (%)**
30.5	910	870	720	795	12.6
50.0	1000	1050	840	945	5.5
61.0	1020	1070	920	995	2.5
80.0	1100	1100	960	1030	6.4
91.5	1120	1120	1000	1060	5.4
122.0	1180	1140	1020	1080	8.5
152.5	1220	1150	1045	1097.5	10.0
183.5	1250	1150	1050	1100	12.0

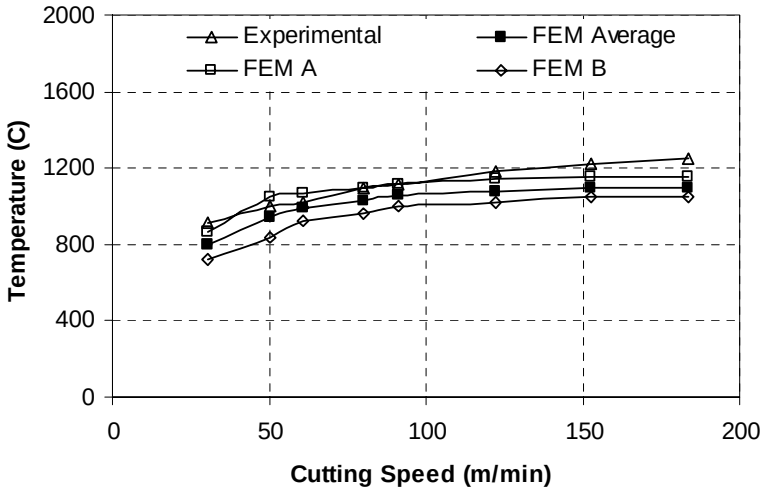

Fig. 6.4 Results of rake face temperature observed at various cutting speeds in FEM simulation and experimental studies [12].

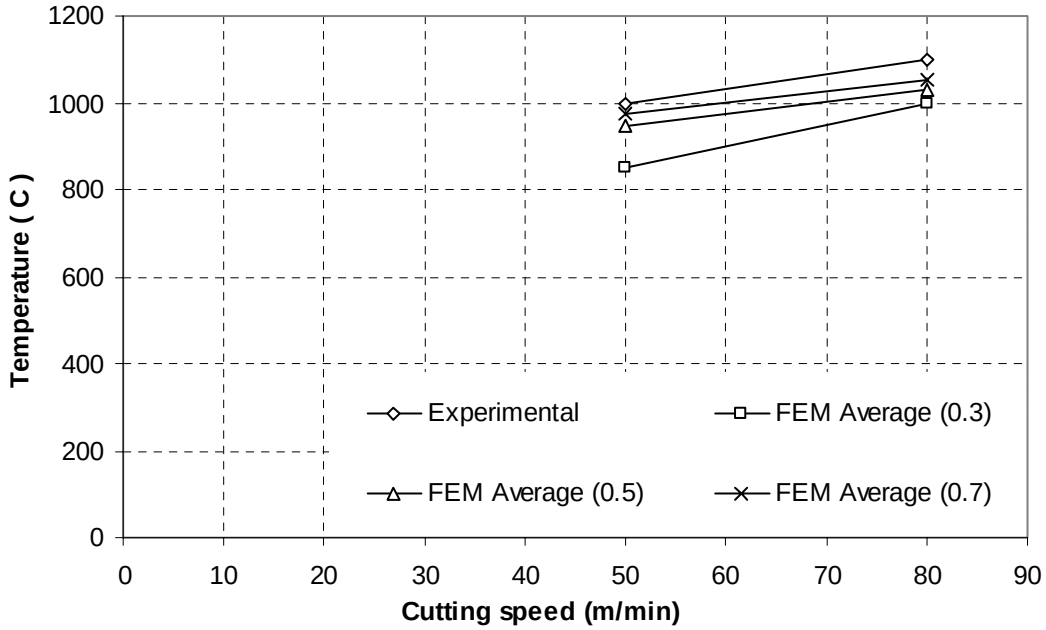

Fig. 6.5 Results of rake face temperature observed at various cutting speeds with different friction coefficients in FEM simulation and compared with experimental data [12].

Fig. 6.5 shows the effect of friction coefficient on the rake face temperature and the results are compared with experimental data. Experimental tests are carried out with a negative rake tool, which generate slightly higher temperature at the tool-chip interface. Observations in FEM simulation are in close agreement with the experimental data. Rake face temperatures in simulations with 0.3 coefficient of friction are observed to be far lower than experimental results, whereas those in case of 0.5 and 0.7 coefficient of friction are observed to be closer to the experimental results. These observations validate selection of moderate coefficient of friction.

Cutting force results obtained from FEM simulations are compared with experimental and analytical results reported in the literature. Soo *et al.* [46] conducted turning experiments on Inconel 718 with a 5° rake angle tool, at 0.2 mm/rev feed rate and 2 mm depth of cut. The cutting speeds used for experiment were 50 and 80 m/min and

cutting force and thrust force readings of the study were reported. Empirical model for cutting force based on experimental data was suggested by Chaudhary *et al.* [53]. The model is expressed as,

$$F = 5938\ V^{-0.1294}\ f^{0.801}\ d^{0.948} \quad \text{.....(6.1)}$$

Here F is cutting force, V is cutting velocity, f is feed rate and d is depth of cut. Cutting force for a set of machining conditions is calculated for comparison with FEM simulation results. The cutting conditions used for comparison include cutting speeds ranging from 30.5 to 183.5 m/min, feed rate of 0.25 mm/rev, depth of cut of 1 mm and rake angle of 0°. Empirical results are not available for comparison of thrust forces.

Cutting forces are observed to reduce with increasing cutting speed in Fig. 6.6. The trend of the curves plotted for cutting force against cutting speed obtained from empirical and FEM study is observed to be similar. Difference in the values for cutting forces can be attributed to different machining conditions and assumptions of two theories, such as friction coefficient. FEM results match closely, if not exactly, with experimental results for cutting and thrust forces. Results with different friction coefficient are reported in Table 6.4. Average cutting forces are reported from FEM simulation data. It is not mentioned in the literature, whether the experimental and empirical results are for average or maximum cutting forces. Discrepancies in the results can be attributed to this fact.

Table 6.4 FEM simulation results compared with experimental data for cutting forces and the percentage error.

Speed (m/min)	Average Cutting Force						
	FEM μ =0.3 (N)	FEM μ =0.5 (N)	FEM μ =0.7 (N)	Empirical (N)	Error μ =0.5 (%)	Experimental (N)	Error μ =0.5 (%)
30.5		950		1256.96	24.4		
50.0	850	950	1000	1179.08	19.4	1125	15.6
61.0		925		1149.13	19.5		
80.0	800	910	950	1109.51	18.0	1130	19.5
91.5		900		1090.39	17.5		
122.0		825		1049.99	21.4		
152.5		800		1020.65	21.6		
183.5		750		996.50	24.7		

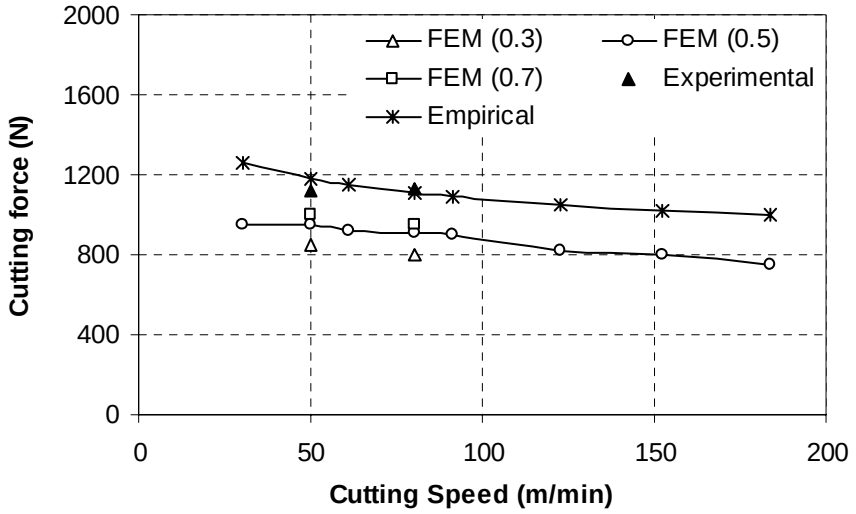

Fig. 6.6 Average cutting forces observed at a range of cutting speeds (30.5 to 183.5 m/min) in FEM simulations, empirical studies [53] and experimental studies [46] of machining Inconel 718.

Thrust forces are also observed to reduce with increase in the cutting speed in Fig. 6.7. In the case of thrust forces, results of simulations with friction coefficient = 0.5 are observed to be in good agreement with experimental results. Thrust forces in simulations

with higher friction coefficient are far higher and those with lower friction coefficient are far lower.

Table 6.5 FEM simulation results compared with experimental data for thrust forces and the percentage error.

Speed (m/min)	Average Thrust Force				
	FEM μ =0.3 (N)	FEM μ =0.5 (N)	FEM μ =0.7 (N)	Experimental (N)	Error μ =0.5 (%)
30.5		450			
50.0	300	450	600	438	2.7
61.0		425			
80.0	250	410	550	412	0.5
91.5		400			
122.0		380			
152.5		350			
183.5		250			

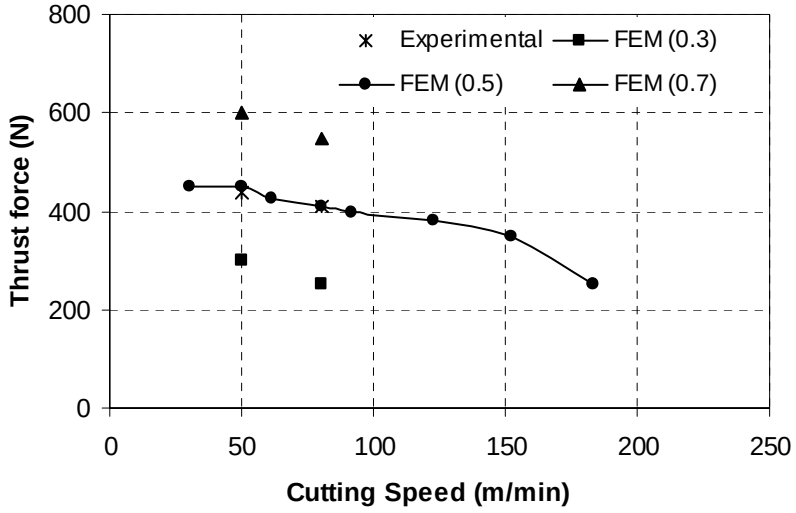

Fig. 6.7 Average thrust forces observed at a range of cutting speeds (30.5 to 183.5 m/min) in FEM simulations and experimental [46] studies of machining Inconel 718.

Close match of the experimental results and FEM simulation results validates the formulation developed in the user subroutine for this study. Application of Johnson-Cook material model to represent material behavior under different strain, strain rate and temperature in machining can be justified by comparison of the results. Recht's catastrophic shear failure criterion can be applied as a successful failure criterion for finite element simulation of machining of Inconel 718.

6.3 Observations of chip formation process

Thermo-mechanical properties play an important role in shear-localization and chip segmentation in the machining of Inconel 718. The superalloy has high strength at elevated temperatures because of the presence of metastable γ" phase. Material looses this strength considerably at temperatures greater than 650° C because of rapid coarsening of the γ" phase. Lower thermal conductivity of Inconel 718 leads to adiabatic shear localization at higher cutting speed. Komanduri and Schroeder [2] observed chip formation in machining of Inconel 718 for a wide range of cutting speeds (15.25 to 213.5 m/min) at 0.2 mm/rev feed rate and 2.5 mm depth of cut. Optical micrographs of the chips formed during machining were examined and analyzed. FEM simulations are run for cutting speeds of 30.5 to 183.5 m/min at 0.25 mm/rev and 1.0 mm depth of cut. Shear localized chips formed with tool of rake angle of -15° in simulation of machining of Inconel are compared with experimental observations in Fig. 6.8. The figure displays strain distribution contours in the chip during FEM simulation of machining.

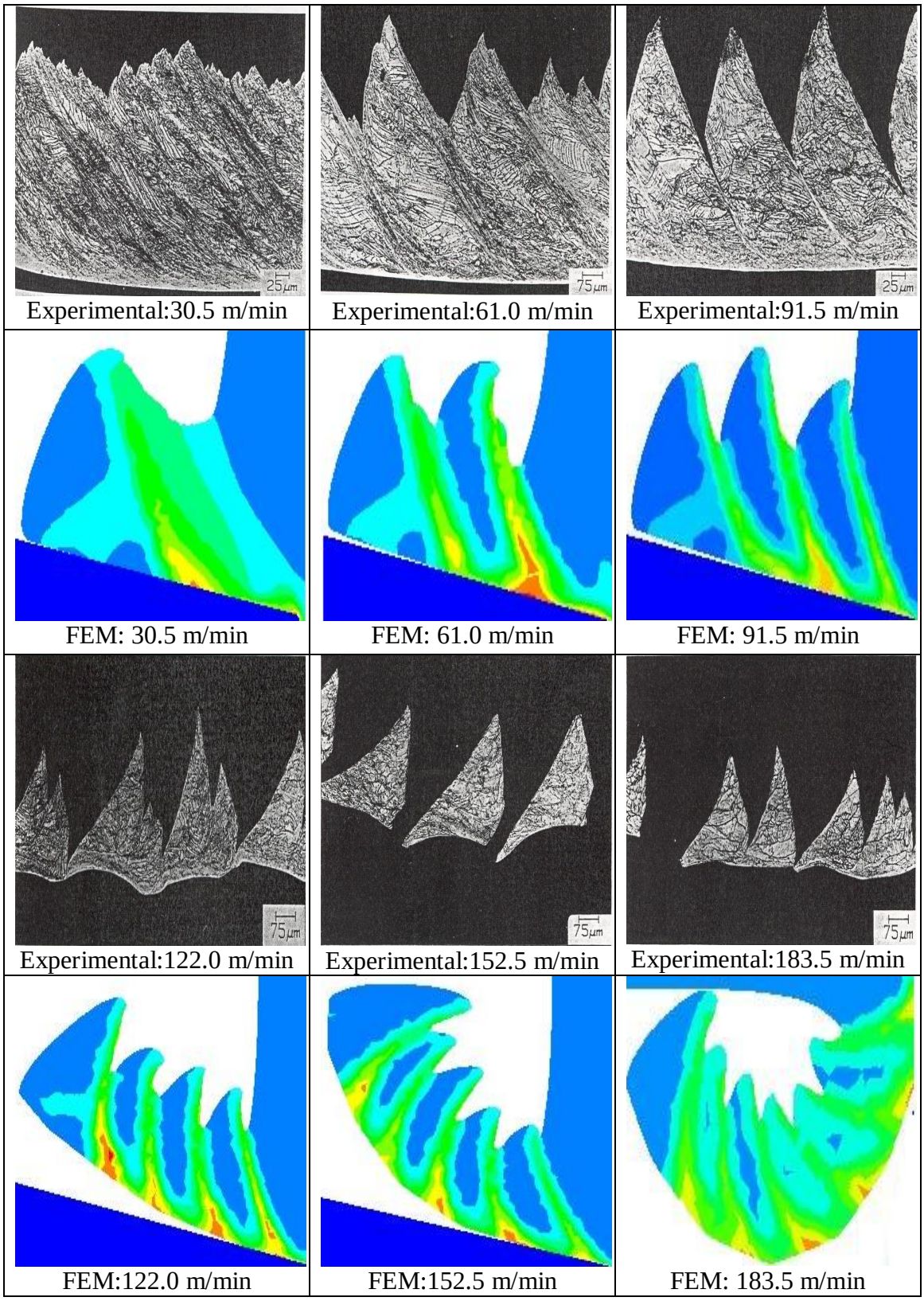

Fig. 6.8 Comparison of optical micrographs of chips formed in the turning of Inconel 718 [2] with the chips formed by FEM simulation of orthogonal machining of Inconel 718.

Continuous chip was observed at lower cutting speed (30 m/min). Strain was observed to be distributed evenly in the chip and there was no sign of shear localization. Shear bands are observed at a cutting speed of 61 m/min with high strain values. Relatively far less strain values are observed in the chip segment between the shear bands. Komanduri and Schroeder [2] reported beginning of chip segmentation at cutting speed of 61 m/min in machining Inconel 718. Observations of FEM simulations regarding the onset of chip segmentation are in agreement with the experimental results reported in the literature. Chip formation in FEM simulation is observed identical to experimental observation at 91.5 m/min speed with sharp shear bands and high strain values. Optical micrographs were observed with short chips with only a few segments joined together at a cutting speed of 152.5 m/min and completely isolated chip segments were formed at higher cutting speeds. FEM simulations could not show complete isolation of chip segments as it requires a failure criterion for the separation of chip segments. No significant change in extent of the contact between chip segments is observed in FEM simulations for total speed range. Mesh is continuously refined in the region of high deformation and elements with high plastic power are considered for refinement. Such an element is divided into two elements to avoid severe mesh distortion. Failure to show complete isolation of chip segments at high cutting speed (above 152.5 m/min) could be considered as side effect of mesh refinement.

Post processing of the FEM simulations is carried out for making some observations of the chip formation process. Mechanism of segmented chip formation is found to be different from continuous chip formation. Komanduri and von Turkovich [24] conducted cutting experiments on titanium alloy and reported certain observations of

chip segmentation procedure. FEM simulations of machining of Inconel 718 at cutting speed of 152 m/min, 0.25 mm/rev feed rate with 0° rake angle tool are studied.

Fig. 6.9 shows concentrated high strain shear bands formed periodically during machining. The chip segments are separated by the high strain shear bands. Strain localization is clearly seen to originate from the tool tip and it moves up along the shear plane toward free surface of the workpiece. No crack initiation is observed in this step. The bulk of the chip segment being formed undergoes upsetting with very less deformation as compared to deformation in shear band.

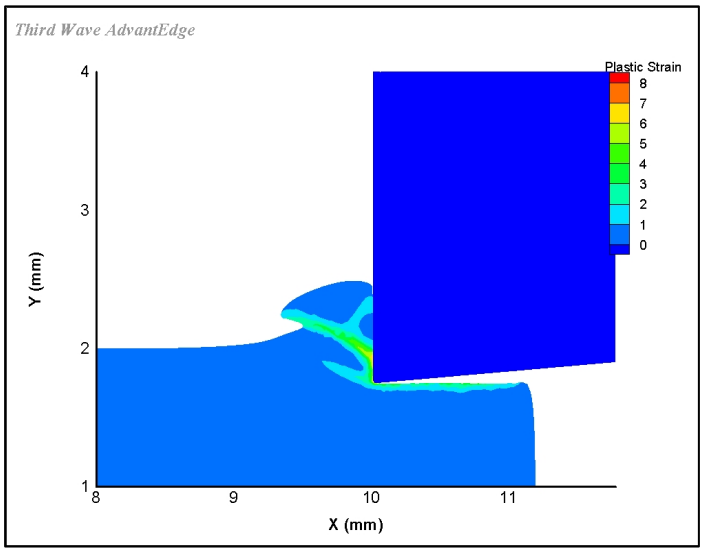

Fig. 6.9 Strain localization along shear plane originating from tool tip during upsetting stage of chip segmentation process.

There is negligible relative motion between the bottom surface of the chip segment and the tool face during the upsetting stage. Chip segment gradually bulges and slowly pushes the earlier segment up on the tool face. Contact between the two chip segments moves gradually from the worksurface towards tool face while the following segment in the upsetting stage. This stage continues till the strain localized band reaches the free surface of the workpiece as in Fig.6.10. As the concentrated shear band reaches

free work surface, catastrophic shear failure takes place. Bulk of the chip segment moves faster in the direction of heavily strained shear band, which is developed during upsetting stage.

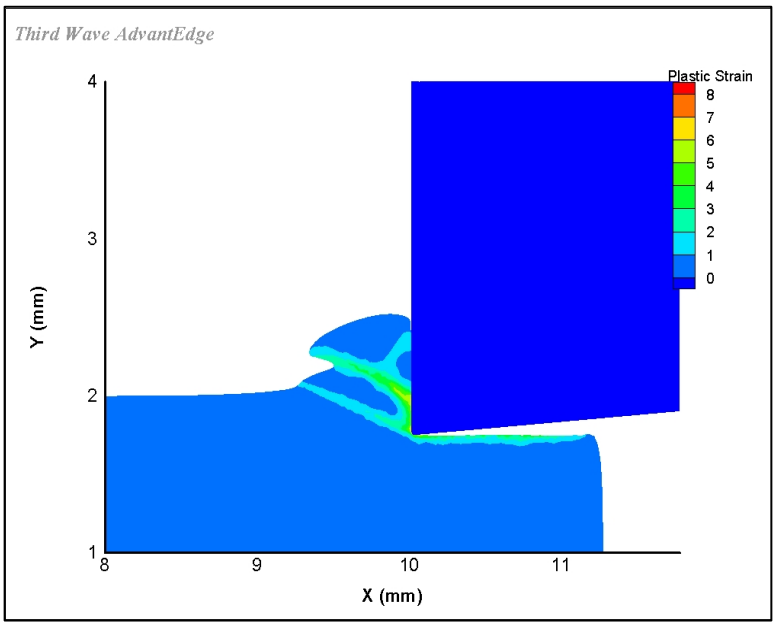

Fig. 6.10 Chip segment being formed at the verge of catastrophic shear failure as the shear band reaches free surface of workpiece.

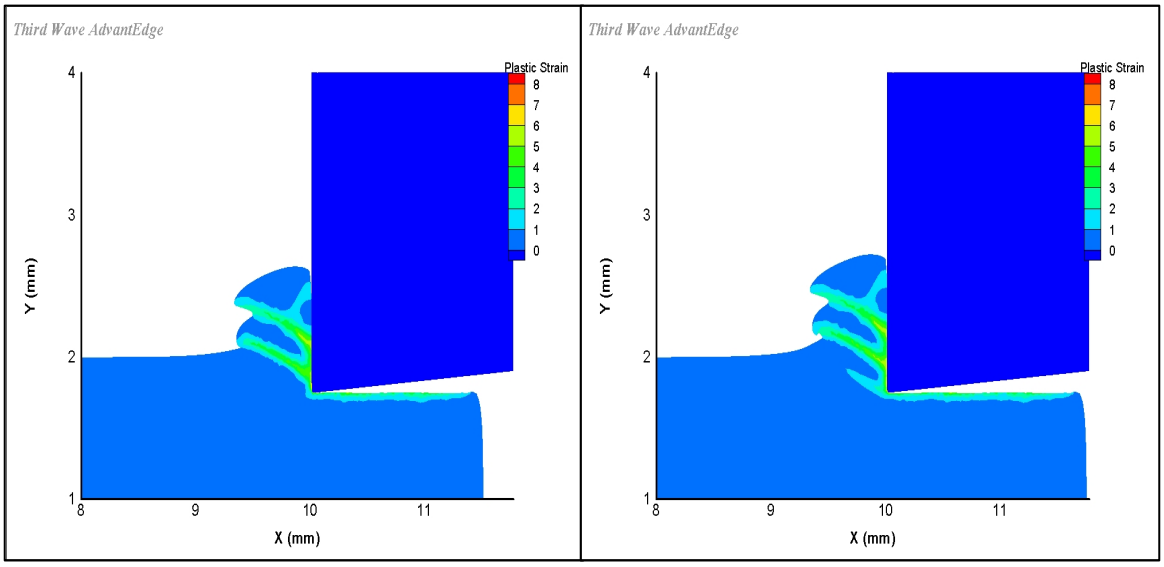

(a) (b)

Fig. 6.11 (a) Completion of chip segment formation process and (b) Beginning of next chip segment formation process.

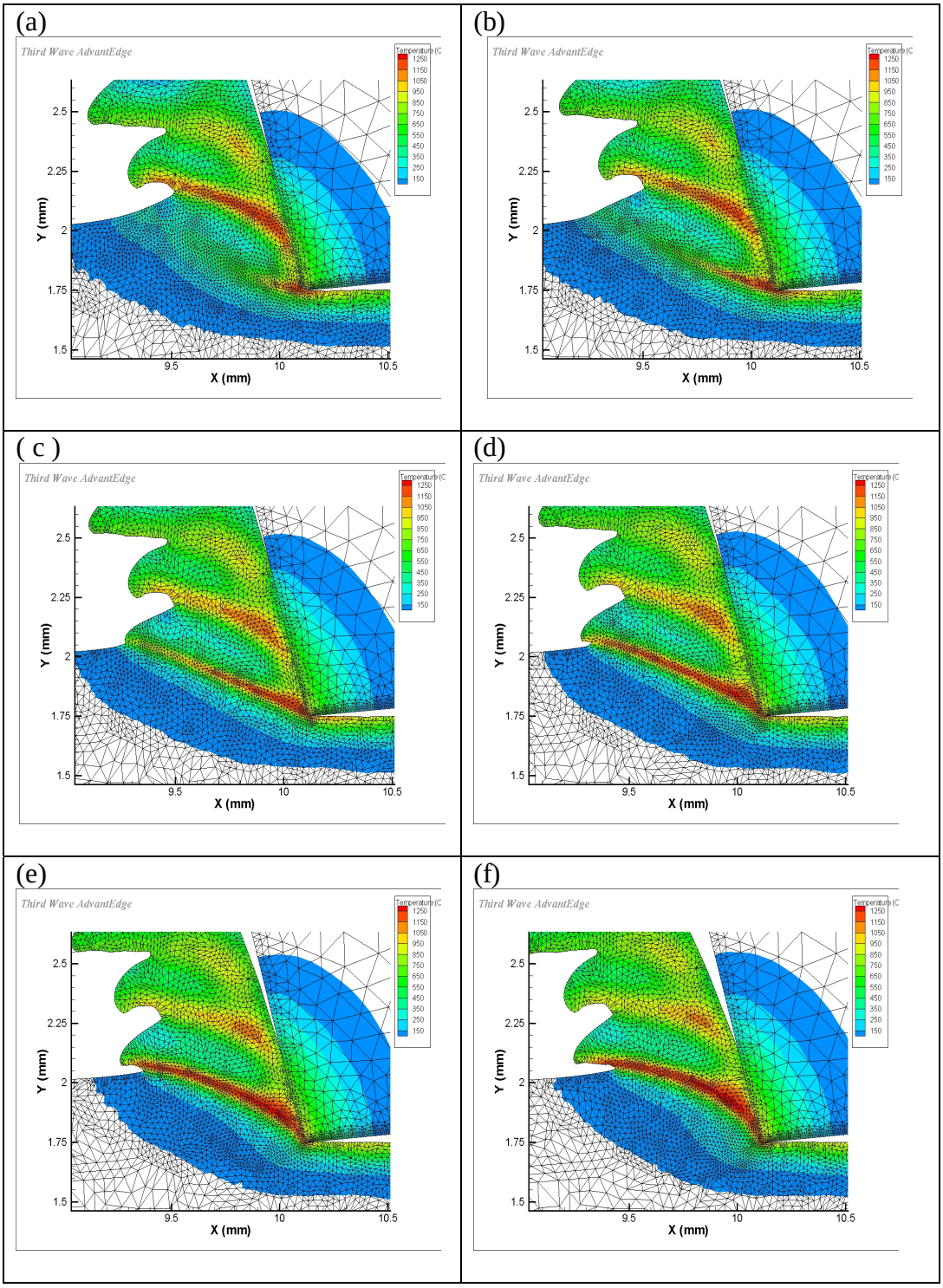
(a)
(b)
(c)
(d)
(e)
(f)
Third Wave AdvantEdge
Temperature (C
1250
1150
1050
950
850
750
650
550
450
350
250
150
Y (mm)
X (mm)
2.5
2.25
2
1.75
1.5
9.5
10
10.5

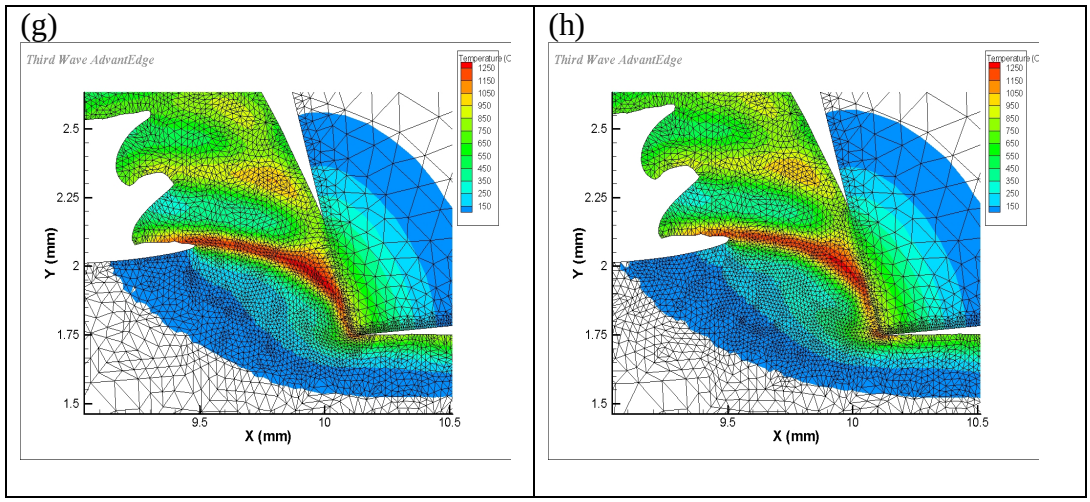

Fig. 6.12 Various stages of chip segment formation in simulation of machining Inconel 718 showing shear bands with localized temperatures at a feed rate of 0.25 mm/rev and a cutting speed of 122.0 m/min with a tool of rake angle of -15°.

Earlier chip segment moves up the tool face rapidly after shear failure. Contact between two chip segments moves rapidly from worksurface toward tool face in this stage. Chip velocity along the tool face fluctuates as the chip segments are formed periodically. The process of chip segment formation seen in Fig.6.12 is similar to the process reported by Komanduri and von Turkovich [24]. Temperature rise in the shear band substantially increases as the localized deformation increases.

Fig. 6.13 shows high temperatures generated in the narrow shear bands. These are due to intense shear concentration and poor thermal properties of the workmaterial. Considerably less heat is dissipated out from the deformation zone rapidly and adiabatic shear bands are formed. Heat generation is moderate during the upsetting stage of the chip segment being formed.

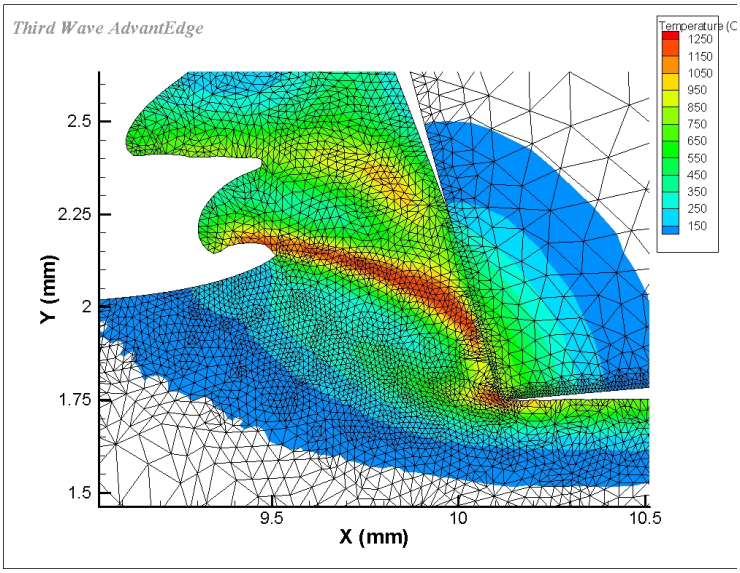

Fig. 6.13 High temperatures are localized in the shear band and relatively lower temperatures are observed in the bulk of the chip segment formed.

Material is strengthened in the shear zone as it undergoes localized heavy deformation in the shear band. At the same time temperature gradients are formed leading to weakening of material in the zone of deformation. As heat is concentrated in the heavily strained zones, temperatures increase rapidly, leading to faster thermal softening of the material. If the thermal softening rate exceeds the rate of increase in strength, due to strain hardening, material continues to deform catastrophically in the shear zone until the higher rate of strain hardening is established again. The observations of FEM simulations further support that adiabatic shear instability as the root cause of chip segmentation in agreement with the findings of Komanduri and co-workers [2, 22-27].

6.4 Effects of cutting speed on machining Inconel 718

Effects of cutting speed on rake face temperature and cutting force are discussed in validation part. Further post processing of the simulation results reveal the effects of cutting speed on shear zone temperatures, equivalent plastic strain in primary and

secondary shear zones and on power consumed during machining. Effects of cutting speed are observed for machining with tool of -15°, 0°, and 15° normal rake angle.

Rake angle : -15°	Rake angle : 0°	Rake angle : 15°
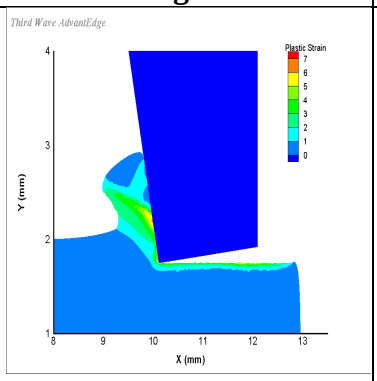	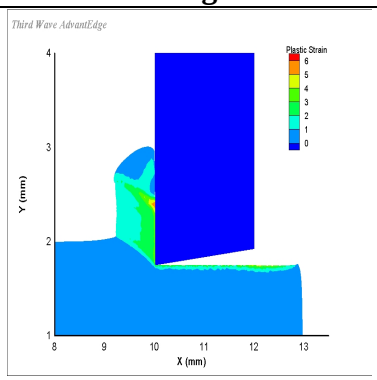	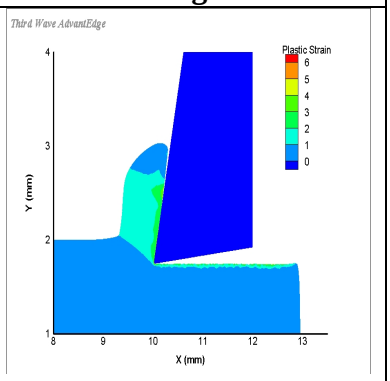
30.5 m/min	30.5 m/min	30.5 m/min
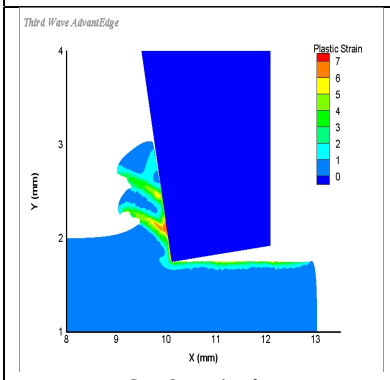	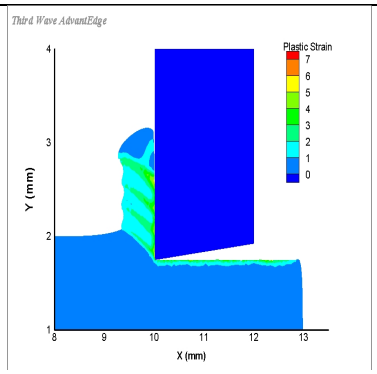	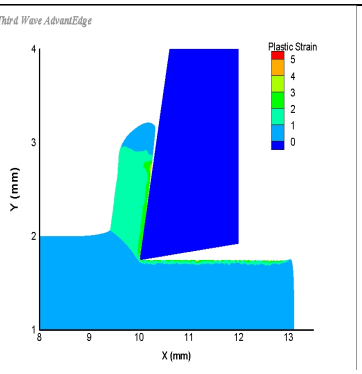
61.0 m/min	61.0 m/min	61.0 m/min
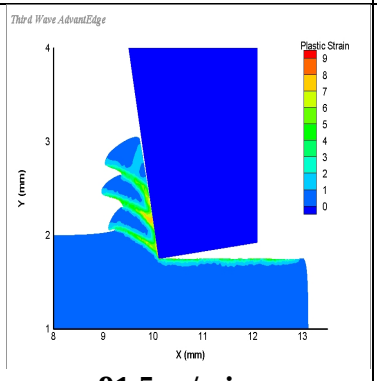	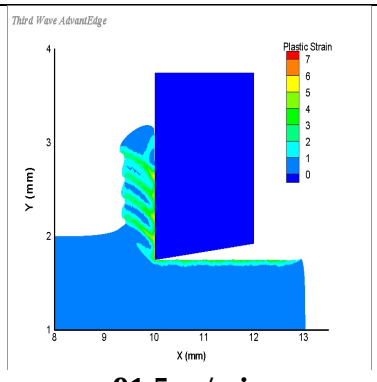	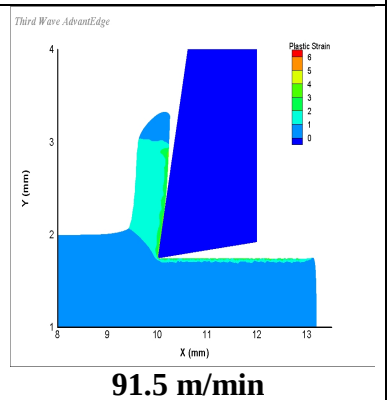
91.5 m/min	91.5 m/min	91.5 m/min

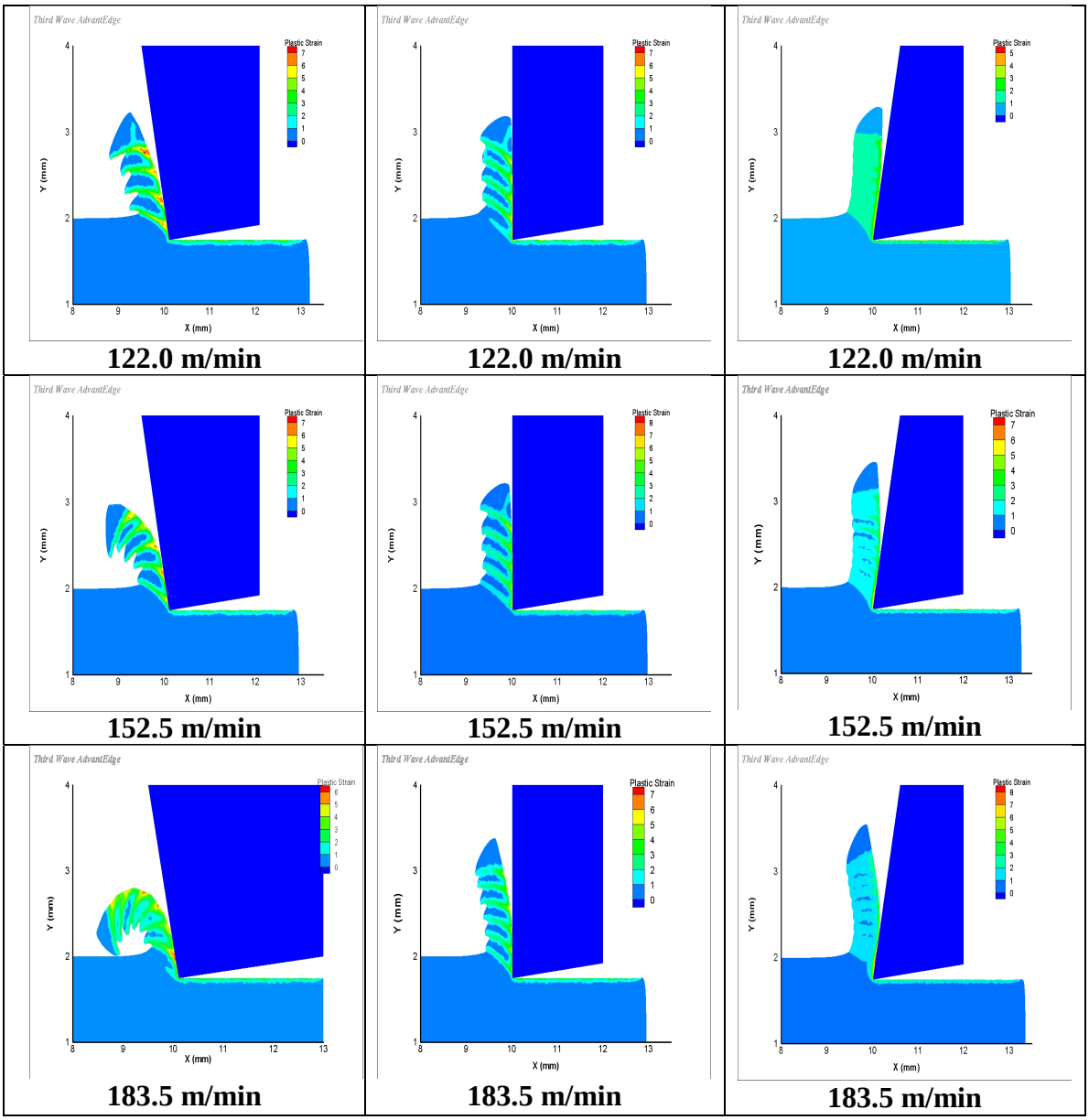

Fig. 6.14 Effect of cutting speed on chip segmentation in simulation of machining Inconel 718 with -15°, 0°, and 15° rake angles at a feed rate of 0.25 mm/rev.

Continuous chip formation is observed in machining at cutting speed of 30.5 m/min with different rake angles. No shear instability is observed in the workmaterial at this speed in machining with tool of any rake angle. Shear instability and chip segmentation are observed for simulations with 0° and -15° rake angle tool at all cutting speeds above 61 m/min. No chip segmentation is observed in the simulations with

positive rake angle tool, although shear instability is observed for machining at cutting speeds of 122 m/min and higher, but it is not enough to produce chip segments. Number of highly strained shear bands and chip segments are observed to increase with increasing cutting speed in simulations of machining with negative rake tools. Number of chip segments is not observed to vary much for simulations with 0° rake tools but intensity of shear localization is observed to increase.

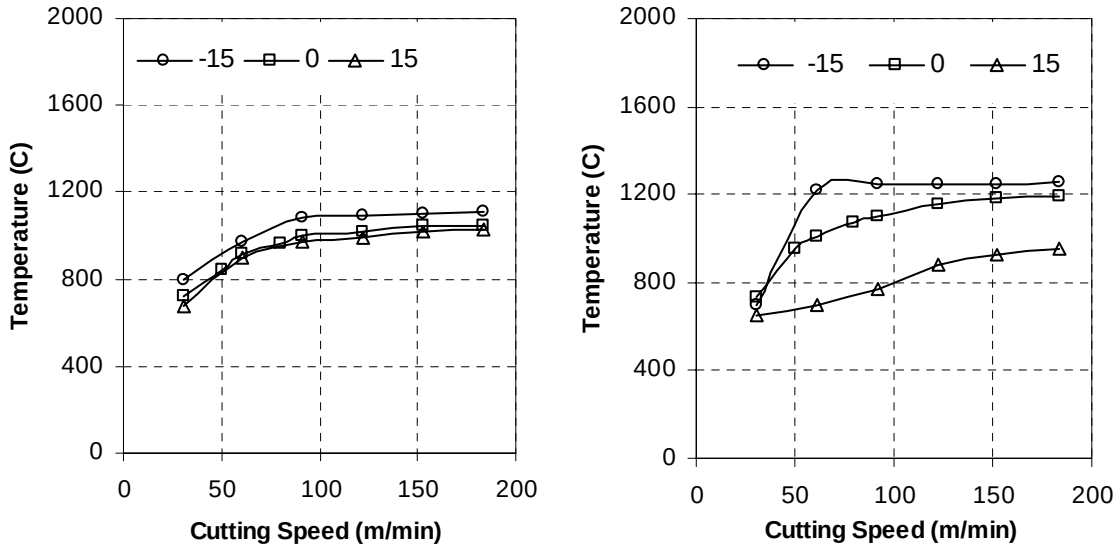

Fig. 6.15 Effect of cutting speed on (a) rake face temperatures and (b) shear zone temperatures in simulation of machining Inconel 718 with -15°, 0°, and 15° rake angles at a feed rate of 0.25 mm/rev.

Fig. 6.15 shows rake face temperatures which increase monotonically with increasing cutting speed. Higher tool temperatures limit the rate of material removal as higher rake face temperatures contribute to tool wear significantly. Not much difference is observed in rake face temperatures for simulations with different rake angles. Rake face temperatures mainly depend on friction coefficient and work done at the tool-chip

interface. The results show no significant change in work done in secondary shear zone during machining with different rake angles.

Shear zone temperatures for machining with 0° rake angle are observed to increase with increasing cutting speed and are constant for cutting speeds more than 122 m/min. For machining with -15° rake angle, temperature in the shear zone is observed to increase for 61 m/min and remains constant there after. Chip segmentation is not observed in simulations at 30 m/min cutting speed in both the cases. Adiabatic shear bands are observed in the shear zone in machining at cutting speed of 61 m/min and at all higher speeds. Results indicate significant amount of work done due to deformation in the shear band in simulation of machining with 0° and -15° rake angles. Deformation is converted into heat but due to poor thermal properties of the material, heat is not dissipated in the work-chip system and catastrophic shear failure is observed.

No chip segmentation is observed for machining with a 15° rake angle tool. Continuous chip is observed in machining for cutting speed up to 91.5 m/min and shear instability is observed for higher cutting speeds, but it is not enough to produce chip segments. Shear zone temperatures are observed to increase with increasing cutting speed. Shear zone temperatures are not as high as in case of simulations with tool of 0° and -15° rake angle. Results indicate not enough deformation taking place in the shear zone to produce chip segments in machining with positive rake angle tool. Most of the heat resulting from the work done on the shear plane is carried away by the chips and a small amount of heat is conducted into the workpiece.

Equivalent plastic strain in the primary and secondary shear zone depends on shear instability in the workmaterial. Equivalent plastic strain is observed to increase

suddenly on the onset of chip segmentation and reduces gradually with increase in cutting speed, as observed in simulations with a -15° rake angle. No significant effect of cutting speed is observed on plastic strain for simulations of machining with tool of 0° and +15° rake angle.

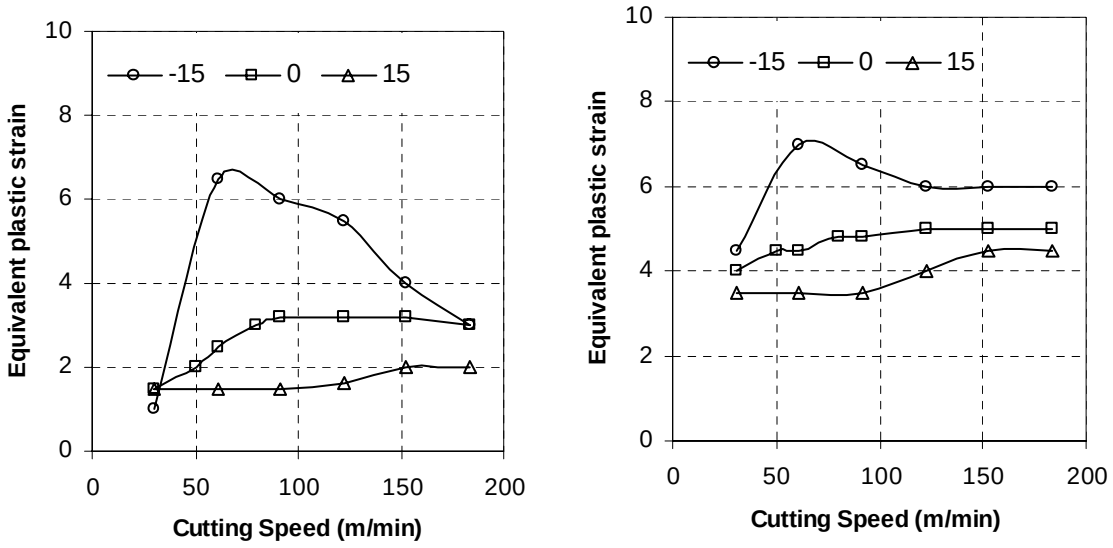

Fig. 6.16 Effect of cutting speed on (a) equivalent plastic strain in primary shear zone and (b) equivalent plastic strain in secondary shear zone in simulation of machining Inconel 718 with -15°, 0°, and 15° rake angles at a feed rate of 0.25 mm/rev.

Fig. 6.16 indicates that average equivalent plastic strain required for chip segmentation is minimum 200% in the primary shear zone. Continuous chip is observed below strain of 200%. Shear instability without chip segmentation is observed at 200% plastic strain. Recht's criterion for catastrophic thermoplastic shear instability and Johnson-Cook material model are based on equivalent plastic strain. Material behavior and shear instability is governed by equivalent plastic strain in the primary shear zone. Observations of plastic strain in the primary shear zone can be helpful in predicting the

onset of chip segmentation in machining Inconel 718 under various machining conditions.

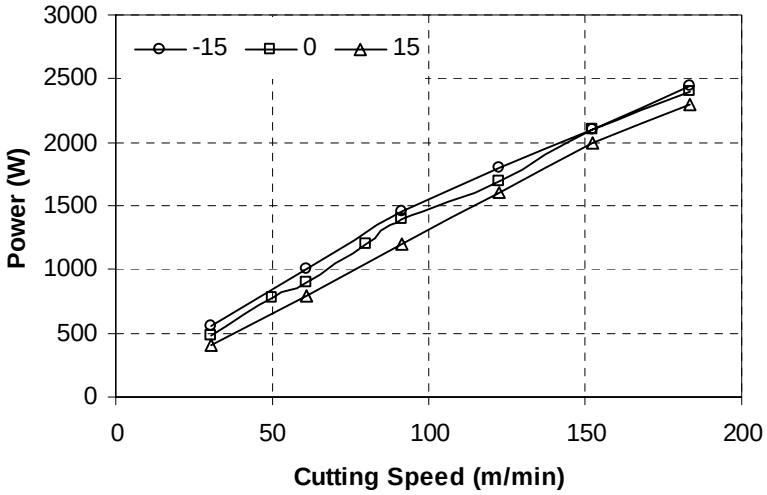

Fig. 6.17 Effect of cutting speed on average power consumed in simulation of machining Inconel 718 with -15°, 0°, and 15° rake angles at a feed rate of 0.25 mm/rev.

Effects of cutting speed on average power consumption and average cutting and thrust forces in the simulation of machining Inconel 718 are shown in Fig. 6.17 and Fig. 6.18. Cutting forces are observed to increase during the upsetting stage of chip segment formation and drop sharply as catastrophic shear failure takes place to form a new chip segment. Power consumption is observed to follow the same pattern of change as that of cutting force for machining at a particular cutting speed. Cutting forces are observed to decrease with increasing cutting speeds. Cutting force in machining depends on chip-tool contact area and shear strength of the material in the primary shear zone.

Chip-tool contact area reduces with increasing cutting speed contributing to a reduction in the cutting force. Workmaterial in the primary shear zone is strengthened in the initial stages of chip segment formation as it undergoes strain hardening. Thermal softening is prominently observed as adiabatic shear band is formed. As temperatures in

the shear zone increase with increasing cutting speeds, it leads to higher rate of thermal softening in the shear zone. Workmaterial is weakened rapidly at higher cutting speeds, which is the reason for lower cutting forces. Power consumption is observed to increase linearly with increasing cutting speed.

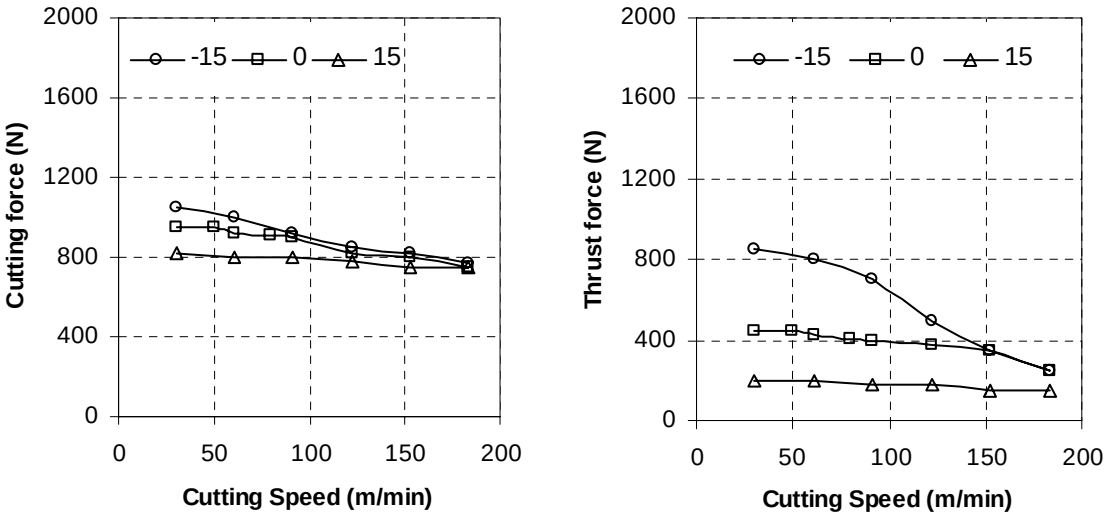

(a) (b)

Fig. 6.18 Effect of cutting speed on (a) average cutting force (b) average thrust force in simulation of machining Inconel 718 with -15°, 0°, and 15° rake angles at a feed rate of 0.25 mm/rev.

6.5 Effects of rake angle on machining Inconel 718

The effects of rake angle on shear zone temperature, rake face temperature, equivalent plastic strain in the primary and secondary shear zone, cutting force, force ratio and power consumed during machining are studied in this investigation. Effects of rake angle are observed for machining with tool of -30° to 45° rake angles at cutting speed of 61 m/min and feed rate of 0.25 mm/rev.

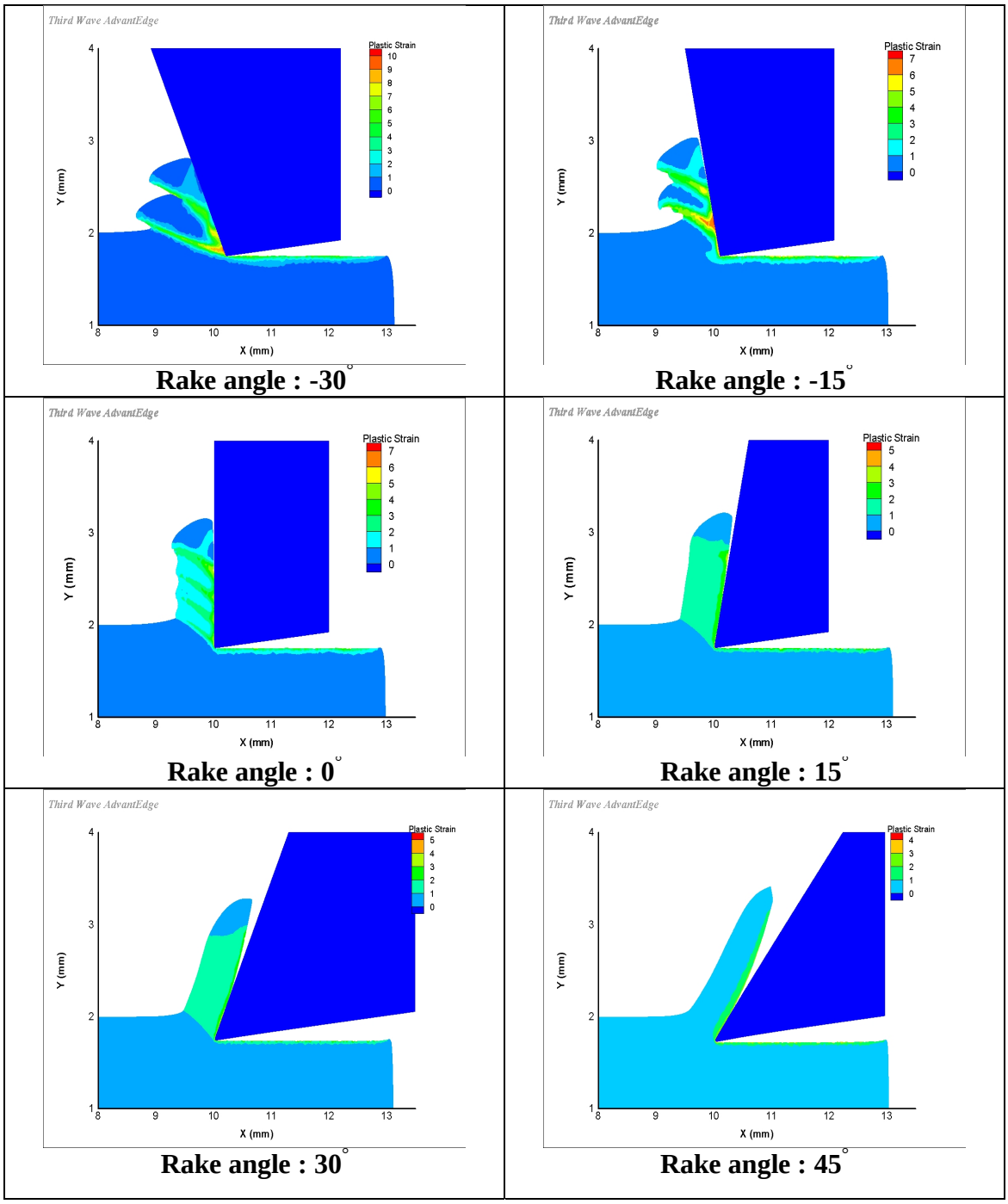

Fig. 6.19 Effect of rake angle on chip formation in simulation of machining Inconel 718 at a cutting speed of 61 m/min and feed rate of 0.25 mm/rev.

Heavily strained shear bands and a much less extent of contact between chip segments are observed in machining with negative rake tools as compared to 0° rake tool. Shear instability is observed for machining with 0° rake tool but no distinct chip segments

are formed. No shear instability is observed in machining with positive rake tools (>15°). Fig. 6.19 shows narrow bands of heavily strained material in machining with negative rake tools. Uniform deformation is observed in simulations of machining with positive rake tool.

Tool forces are influenced by rake angles as tool-chip contact area decreases with increasing rake angles. Fig. 6.20 shows decrease in cutting and thrust forces with increase in rake angles. Strong tool edge is achieved by using negative rake tool but high tool forces are developed which limit its application in machining of intricate parts. Relatively lower tool forces are observed in machining with positive rake tools but it reduces the strength of tool edge and may lead to fracture especially when using brittle ceramic tool.

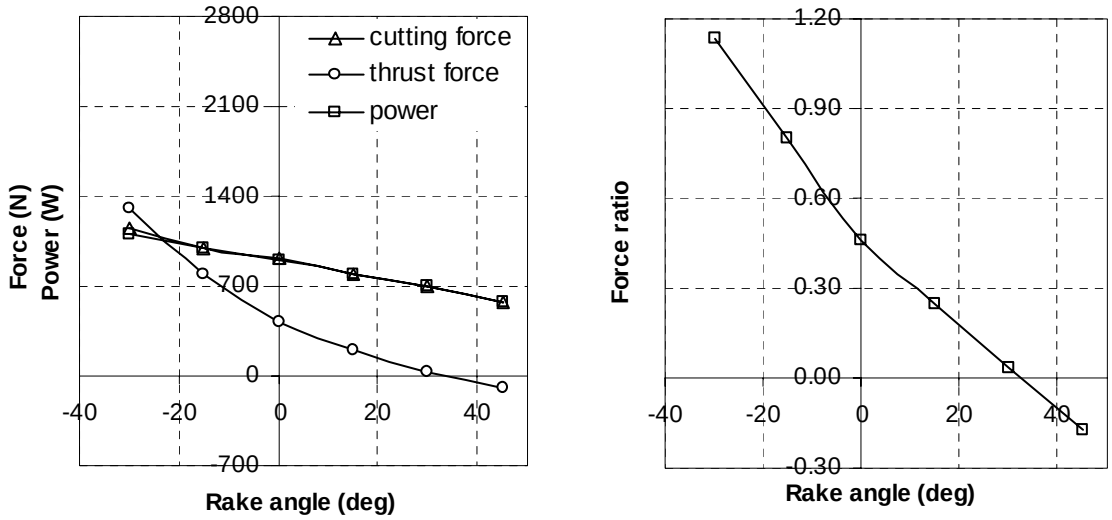

(a) (b)

Fig. 6.20 Effect of rake angle on (a) average power consumed and average cutting and thrust forces (b) force ratio in simulation of machining Inconel 718 with a range of rake angles at a feed rate of 0.25 mm/rev and cutting speed of 61 m/min.

Average cutting and thrust forces and average power consumed are observed to reduce with increase in rake angles as in Fig.6.20. Ratio of thrust force to cutting force, known as force ratio, also drops down as thrust force reduces with increasing rake angle.

Fig. 6.21 shows a sharp reduction in temperatures in the shear zone as rake angle increases from -30° to 45°. Adiabatic shear bands with high temperatures and thermoplastic shear instability are observed in machining with negative rake tools. High temperatures are generated in shear zone due to large amount of work done by deformation of workmaterial in machining with negative rake tools. Machining with positive rake tools forms continuous chips and shear zone temperatures are much less accordingly. Temperatures on the tool rake face reduce with increasing rake angles, but not as significantly as the temperatures in the primary shear zone. Reduced area for frictional contact between tool and chip causes less heat generation at higher rake angles, which leads to lower temperatures on the rake face.

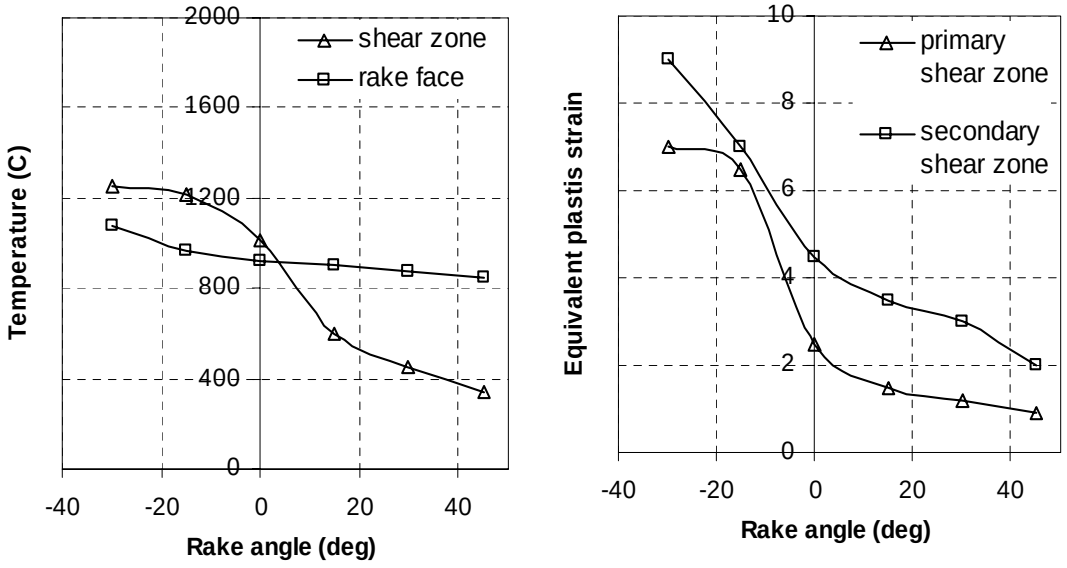

(a) (b)

Fig. 6.21 Effect of rake angle on (a) rake face and shear zone temperature (b) equivalent plastic strain in simulation of machining Inconel 718 with a range of rake angles at a feed rate of 0.25 mm/rev and at a cutting speed of 61 m/min.

Equivalent plastic strain values in the primary and secondary shear zone reduce sharply with increasing rake angles. This indicates reduction in the work done in the

primary and secondary shear zone with increase rake angle. Catastrophic shear failure does not take place at higher rake angles as strain is not localized in primary shear zone and is not of high magnitude.

6.6 Effects of feed rate on machining Inconel 718

The effects of feed rate on shear zone temperatures, rake face temperatures equivalent plastic strain in primary and secondary shear zone, cutting force and on power consumed during machining are observed for machining with feed rates from 0.25 to 1 mm/rev at a cutting speed of 61 m/min with a tool of 0° rake angle.

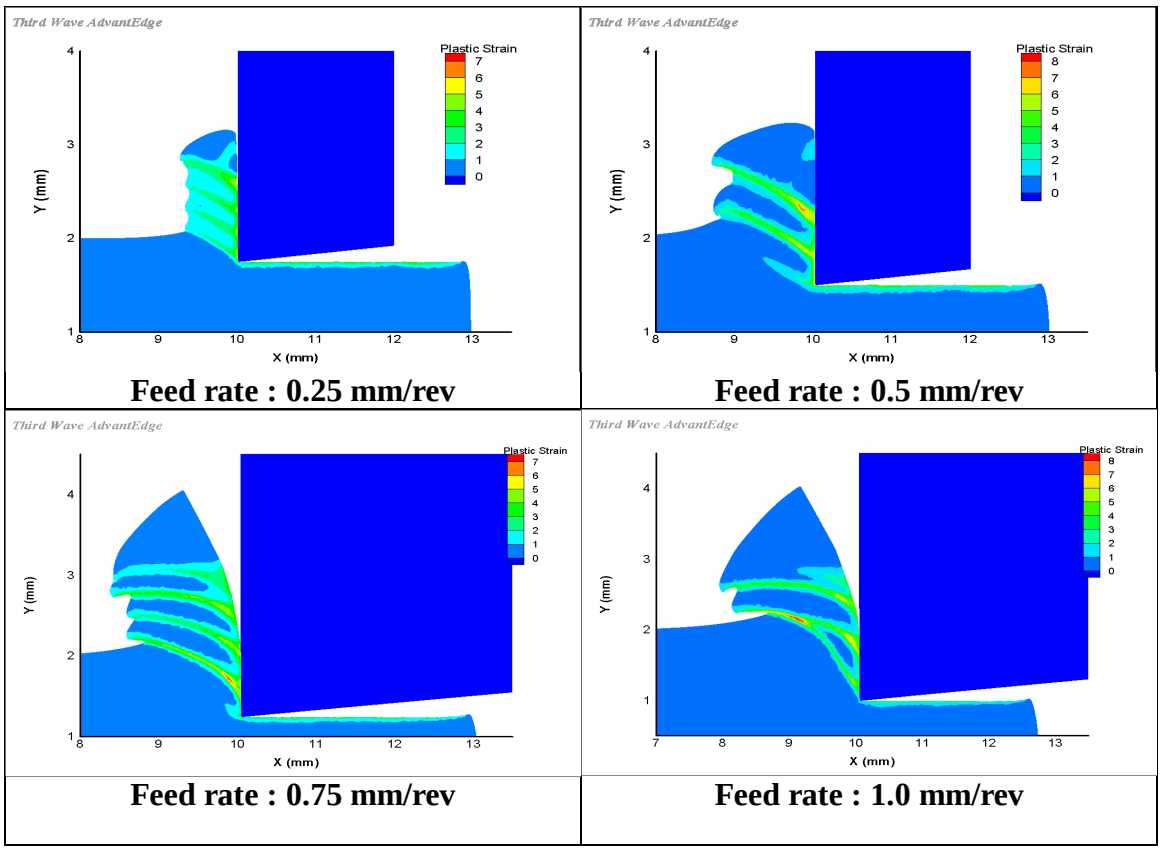

Fig. 6.22 Effect of feed rate on chip formation in simulation of machining Inconel 718 at a cutting speed of 61 m/min with a tool of 0° rake angle.

Shear instability is observed in machining at all feed rates, which indicates no significance of selected range of feed rates in determining onset of chip segmentation although intensity of shear instability increases with increasing feed rate as seen in Fig. 6.22. Chips with sharper chip segments are formed at higher feed rates.

Temperatures in the shear zone and on the rake face are observed to increase monotonically with increasing feed rate as in Fig. 6.23 (a). Plastic strain in the primary shear zone increases sharply as the degree of shear instability increases with increasing feed rate. Plastic strain in the secondary shear zone is not altered significantly by feed rate. Equivalent plastic strain variation is shown in Fig. 6.23 (b).

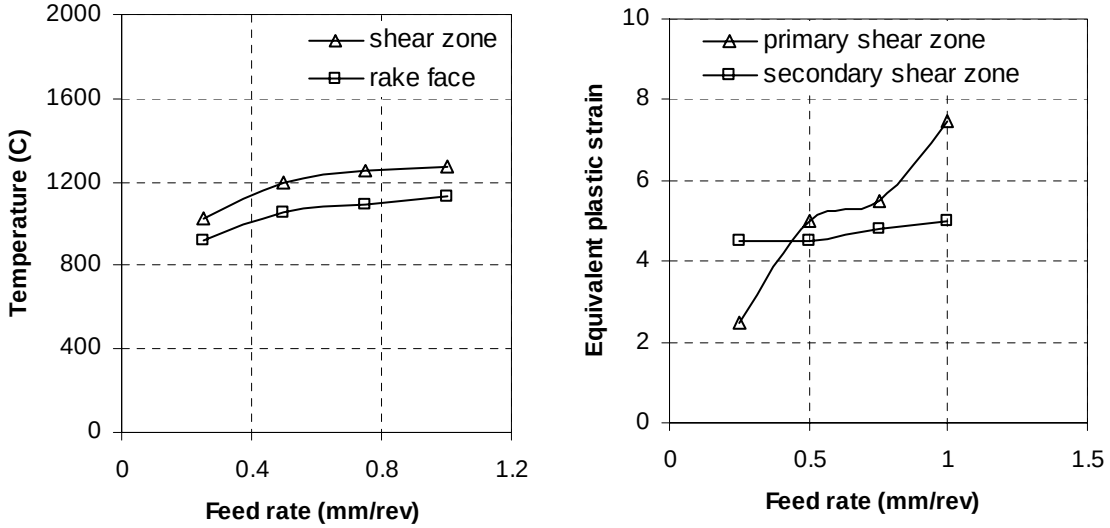

(a) (b)

Fig. 6.23 Effect of rake angle on (a) rake face and shear zone temperature (b) equivalent plastic strain in simulation of machining Inconel 718 with a tool of rake angle of 0° and at a cutting speed of 61 m/min.

Effect of feed rate on average cutting and thrust forces and average power consumed are shown in Fig. 6.24. Cutting force and power consumed are observed to increase significantly with increase in feed rate as material removal rate increases. Larger stock of workmaterial present ahead of cutting tool increases cutting force and power

consumption in machining. Thrust force increases for the feed rate of 0.5 mm/rev but drops down for the feed rate of 0.75 and 1.0 mm/rev.

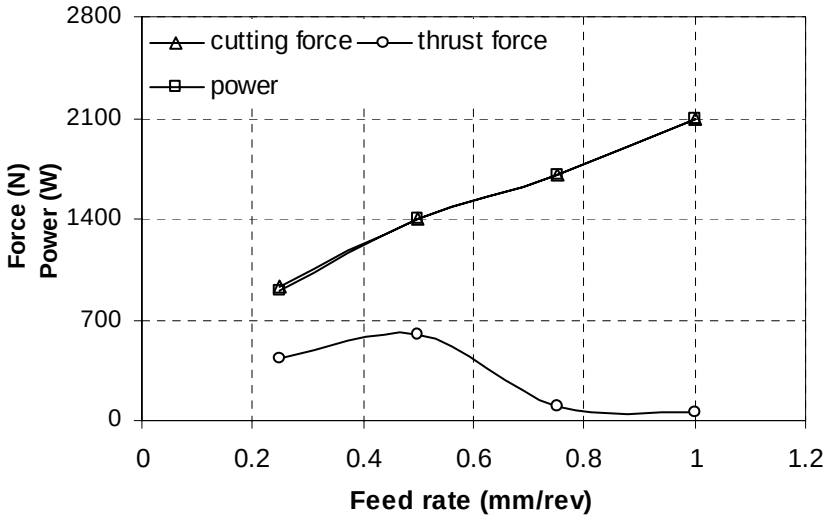

Fig. 6.24 Effect of feed rate on average cutting and thrust forces and average power consumed in simulation of machining Inconel 718 with a tool of rake angle of 0° and at a cutting speed of 61 m/min.

6.7 Possible reasons for tool wear during machining Inconel 718

Freshly formed and extremely hot chip surfaces come in contact with the tool face during the FEM simulations of machining. During the upsetting process there is negligible relative motion between the hot bottom surface of the chip segment formed and the tool face. These surfaces stay in contact for considerable amount of time, which can lead to extensive chemical interactions between the tool material and chip surface. Extensive tool wear because of high temperature chemical reactions between tool material and chip surface could be studied based on observations of this investigation. Thermal softening of workmaterial may also lead to adhesion of workpiece material to the tool. Depth-of-cut line (DCL) notching, nose wear, chipping and abrasion mechanism are other modes of tool failure in machining nickel-based alloys at high speed. The

possible explanation could be given by observation of heavily strain hardened chip surfaces in contact with tool face during chip segmentation at high speeds. No direct observations are possible for tool wear in this investigation as tool material is considered as perfectly elastic and no chemical interactions are considered.

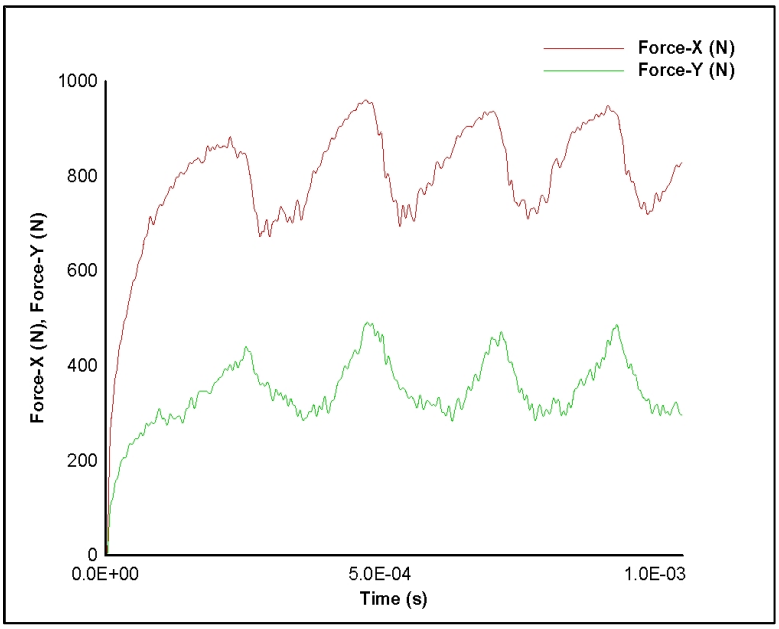

Fig. 6.25 FEM simulation results of cutting force (Force-X) and thrust force (Force-Y) for the time interval of machining Inconel 718 for length of 3 mm at feed rate of 0.25 mm/rev.

Fig. 6.25 shows change in cutting force (Force-X) and thrust force (Force-Y) which affects dynamics of the machining process. Cutting forces are observed to rise gradually during upsetting stage of chip segment formation and drop sharply as catastrophic shear failure takes place. Experimental observations by Komanduri and von Turkovich [24] suggest deflection of tool away from workpiece during the upsetting stage and the tool is allowed to spring back rapidly on the tool after catastrophic shear failure. The repeated process leads to vibrations in the machine tool system and can cause fatigue of the tool.

6.8 Discussions

Thermo-mechanical properties of Inconel 718 give strength at elevated temperatures, which directly translates to difficulties in machining of the material. Poor thermal properties of Inconel 718 limit the cutting speed as high temperatures and fluctuating cutting forces generated during machining are of great importance from tool life and tool wear point of view. Heat generated by deformation is confined to a narrow zone due to poor thermal properties of the material. Inconel 718 holds high strength due to metastable γ" phase up to 650°C and weakens rapidly at higher temperatures. This thermo-mechanical metallurgical characteristic of material is not represented in this investigation. Johnson-Cook material model represents linear weakening of material with increasing temperature. Recht's criterion for thermoplastic shear instability is applied to observe machining of Inconel 718 under different machining conditions. Results indicate shear instability and chip segmentation at all cutting speeds above 61 m/min. Deformation in the shear zone is concentrated in a narrow band and relatively much less deformation is observed in bulk of the chip segment.

Results of the investigation are compared with experimental observations and are found in close agreement. Application of Johnson-Cook material model and Recht's criterion for thermoplastic shear instability is validated by the results. Chip segment formation procedure observed in this investigation is similar to observations reported in the literature. The assumption of thermoplastic shear instability being the root cause of chip segmentation in machining Inconel 718 is supported by the results.

CHAPTER 7

CONCLUSIONS

Chemistry and microstructure of Inconel 718 provide strength at elevated temperatures, which in turn poses machining challenges and limits the cutting speed for the alloy to the range of 15-30 m/min with cemented carbide tools and to 200 m/min with ceramic tools, such as SiAlON, SiC whisker reinforced alumina, and CBN tools. High temperatures, high forces with fluctuating magnitude and hardened chip surface produced during machining Inconel 718 are matters of concern from tool wear and tool life point of view. The foremost goal of this investigation was to study the effect of machining conditions on chip formation, temperatures, and cutting forces. Following are the key features and results of this investigation:

1. Finite element simulation approach is used to study the effect of machining conditions on chip formation, temperatures, equivalent plastic strain and cutting and thrust forces. A commercially available software code (AdvantEdge) is used to accomplish the task. It is a 2-dimensional, explicit, Lagrangian finite element code with adaptive remeshing facility developed by the Third Wave Systems Inc.

2. One objective of this investigation is to present observations on chip segmentation in machining Inconel 718 based on FEM simulation. Adiabatic thermoplastic shear instability is considered as the root cause of chip segmentation in machining Inconel 718. Recht's criterion for catastrophic thermo-plastic shear failure is applied to study chip formation.
3. A need for realistic material model and reliable failure criterion was highlighted based on literature review. An attempt is made in this investigation to alleviate this problem. Johnson-Cook material model is applied to represent material behavior and Recht's shear failure criterion is applied to govern material failure. User subroutine is developed to include material model and failure criterion in the FEM simulation code.
4. Finite element simulations are carried out for a range of cutting speeds from 30.5 to 183.5 m/min at a range of feed rates from 0.25 to 1.0 mm/rev and with a set of tools whose rake angles varied from -30° to $45^{0^{\circ}}$. A constant Columbic friction coefficient (0.5) is assumed to represent friction between the tool and the chip-surface. Simulations are also run with different friction coefficient (0.3 and 0.7) for cutting speeds of 50 and 80 m/min.
5. Chip segmentation is observed in simulations at all cutting speeds above 61.0 m/min and zero or negative rake tools. Chip segmentation is not observed in simulations with tools of positive rake angles. Stages of chip segment formation observed in this study are similar to those observed in experimental study reported in the literature.

6. Results obtained in this investigation are compared with machining test data for validation of subroutine developed to incorporate Johnson-Cook material model and Recht's catastrophic thermo-plastic shear failure criterion. A comparison of the tool rake face temperatures obtained in the FEM simulation found a good match with machining test data with maximum error of 12.6%. Results for cutting force are compared with the experimental and empirical results, and are within an error margin of 19.5% and 24.7%, respectively. Results for thrust force are compared with the experimental results and are within an error margin of 2.7%. The discrepancies observed in the machining simulation data can be attributed to assumptions in FEM, such as coefficient of friction.
7. Close comparison of the results with experimental data and observations of chip segment formation procedure validates assumptions and application of Johnson-Cook material model and Recht's catastrophic thermo-plastic shear failure criterion and formulation of those theories in the user subroutine.
8. Shear localization is not observed in the simulations with positive rake angle tool at the cutting speeds used. Number of highly strained shear bands and chip segments are observed to increase with increasing cutting speed in simulations of machining with negative rake tools. Number of chip segments is not observed to vary much for simulations with 0° rake tools but intensity of shear localization is observed to increase with increasing cutting speed. Chip segments with much narrow shear localized bands are observed in simulations of machining with higher feed rates.

9. Cutting force and thrust force are observed to increase gradually during the upsetting stage of chip formation process and drop sharply as shear failure takes place. Cutting forces and thrust forces are observed to reduce with increasing cutting speed and with increasing rake angles but increase significantly with increasing feed rate. Power consumption follows the same pattern of cutting force in a specific simulation. Power consumption increases with increasing cutting speed and with increasing feed rate but reduces with increasing rake angle.
10. Rake face temperature is observed to increase with increasing cutting speed up to 1050° to 1100° C (depending on rake angle) and then remain constant. Temperature on the rake face and in the shear zone reduces with increasing rake angle and increases with increasing feed rate.
11. Continuous chip is observed below a strain of 200%. Shear instability without chip segmentation is observed at 200% plastic strain. A minimum of 200% average equivalent plastic strain is required for chip segmentation in primary shear zone.

Future Work

1. Having simulated the mechanism of chip segmentation in machining Inconel 718, the set of formulation can be used to apply the material model, such as power law, which can represent rapid drop in strength of the material at temperatures above 650°C.

2. Analytical model for tool wear rate is developed by Usui *et al.* [54]. This model requires input parameters, such as rake face temperature, sliding velocity and normal stress for wear rate predictions. Usui's model can be applied for tool wear

rate predictions in FEM studies as required input parameters can be obtained from FEM simulations without tool wear consideration. Depth-of-cut line notching, abrasive and erosive wear and tool chipping can be studied by using a set of material model and failure criterion for tool material. Although not all types of tool wear can be studied using FEM simulation due to inability of FEM theory to represent chemical interactions between tool and chip surface.

3. Material model and failure criterion can be applied for study of machining titanium alloys and some hardened steels (such as AISI 4340) which exhibit chip segmentation at different machining conditions.

REFERENCES

1. ASM Handbook, Vol.1, 10th edition, (1990) 950-964.
2. Komanduri, R., and Schroeder, T.A., "On shear instability in machining a Nickel-Iron base superalloy," Transactions of ASME, Journal of Engineering for Industry 108 (1986) 93-100.
3. Sims, C., and Hagel, W., "The Superalloys," Wiley, New York, 1972.
4. Metals handbook, Vol. 16, Machining, 9th edition, (1989) 835-845.
5. Ezugwu, E., Wang, Z., and Machado, A., "The machinability of nickel-based alloys: a review," Journal of Materials Processing Technology 86 (1999) 1-16.
6. Mackerle, J., "Finite-element analysis and simulation of machining: a bibliography (1976–1996)," Journal of Materials Processing Technology 86 (1999) 17–44
7. Ng, E., and Aspinwall, D., "Modelling of hard part machining," Journal of Materials Processing Technology 127 (2002) 222–229.
8. Childs, T., Maekawa, K., Obikawa, T., and Yamane, Y., "Metal Machining Theory and Applications," Arnold, London, 2000.
9. Waterman, N., and Ashby, M., The Materials Selector vol. 1, second edition, 579, Chapman & Hall, London, 1997.
10. _ "Advanced machining research program", Technical Information Series Report 84CRD169, July 1984, by G.E. Corporate Research and Development, Schenectady, N.Y.

11. Ezugwu, E., Bonney, J., and Yamane, Y., “An overview of machinability of aeroengine alloys,” Journal of Materials Processing Technology, 134 (2003) 233-253.
12. Kitagawa, T., Kubo, A., and Maekawa, K., “Temperature and wear of cutting tools in high-speed machining of Inconel 718 and Ti-6Al-6V-2Sn,” Wear 202 (1997) 142-148.
13. Choudhury, I., and El-Baradie, M., “Machinability of nickel-based superalloys: a general review,” Journal of Materials Processing Technology 77 (1998) 278-284.
14. Leshock, C., Kim, J., and Shin, Y., “Plasma enhanced machining of Inconel 718: modelling of workpiece temperature with plasma heating and experimental results,” International Journal of Machine Tools and Manufacture 41 (2001) 877-897
15. Hahn, R., contributed the discussion on “Mechanics of formation of discontinuous chip in metal cutting,” by Field, M., and Merchant, M. E., Transactions of ASME 76 (1954) 217.
16. Recht, R., “Catastrophic thermoplastic shear,” Transactions of ASME 31 (1964) 186.
17. Shaw, M. C., “Assessment of machinability,” Machinability, 1 (1967) ISI special report 94, The Iron and Steel Institute (London) U.K.
18. Alberecht, P., “Self-induced vibrations in metal cutting,” Transactions of ASME 84 (1962) 405.
19. Landberg, P., “Vibrations caused by chip formation,” Microtecnic 10 (1956) 219.
20. Rice, W., “The formation of continuous chips in metal cutting,” Engineering Journal, Engineering Institute of Canada 44 (1961) 41.
21. Sharma, C., Rice, W., and Salmon, R., “A relationship between chip-type and shear strain,” Annals of C.I.R.P. 19 (1971) 545.

22. Komanduri, R., and Brown, R., “On mechanics of chip segmentation in machining,” Transactions of ASME, Journal of Engineering for Industry 103 (1981) 33-51
23. Komanduri, R., Schroeder, T., Hazra, J., von Turkovich B., and Flom, D., “On the catastrophic shear instability in high speed machining of an AISI 4340 steel,” Transactions of ASME, Journal of Engineering for Industry 104 (1982) 121.
24. Komanduri, R., and von Turkovich, B., “New observations on the mechanism of chip formation when machining titanium alloys,” Wear 69 (1981) 179-188.
25. Komanduri, R., “Some clarifications on mechanics of chip formation when machining titanium alloys,” Wear 78 (1982) 15-34
26. Komanduri, R., and Hou, Z.B., “On thermoplastic shear instability in machining of titanium alloy (Ti-6Al-4V),” Metallurgical and Materials Transactions 33A (2002) 2995.
27. Komanduri, R., and Hou, Z.B., “Modelling of thermoplastic shear instability in machining,” International Journal of Mechanical Sciences 39 (1997) 1273-1314.
28. Nakayama, K., “The formation of saw-tooth chips,” Proceedings of International Conference on Production Engineering, Tokyo, 1974, 572-577.
29. Vyas, A., and Shaw, M. C., “Mechanics of saw-tooth chip formation in metal cutting,” Transactions of ASME, Journal of Manufacturing Science and Engineering 121 (1999) 163.
30. Usui, E., and Shirakashi, T., “Mechanics of Machining - from ‘descriptive’ to ‘predictive’ theory. In on the Art of Cutting Metals - 75 years later,” Vol. 7, ASME PED, 1982, pp. 13-35.

31. Iwata, K., Osakada, K., and Terasaka, Y., “Process modeling of orthogonal cutting by the rigid-plastic finite element method,” Journal of Engineering Materials Technology 106 (1984) 132-138.
32. Strenkowski, J., and Carroll, J., “A finite element model of orthogonal metal cutting,” Journal of Engineering for Industry 107 (1985) 347-354.
33. Mackerle, J., “Finite-element analysis and simulation of machining: an addendum A bibliography (1996-2002),” International Journal of Machine Tools and Manufacture 43 (2003) 103-114.
34. Maekawa, K., Shirakashi, T., and Obikawa, T., “Recent progress of computer aided simulation of chip flow and tool damage in metal machining,” Journal of Engineering Manufacture (1995) 233-242.
35. Shirakashi, T., and Obikawa, T., “Recent progress and some difficulties in computational modeling of machining,” Machining Science and Technology, 2 (2) (1998) 277-301.
36. Baker, M., Rosler, J., and Siemers, C., “A finite element model of high speed metal cutting with adiabatic shearing,” Computers and Structures 80 (2002) 495-513.
37. Baker, M., Rosler, J., and Siemers, C., “The influence of thermal conductivity on segmented chip formation,” Computational Materials Science 26 (2003) 175-182.
38. Baker, M., “An investigation of the chip segmentation process using finite elements,” Technische Mechanik 23(1) (2003) 1-9.
39. Baker, M., “The influence of plastic properties on chip formation,” Computational Material Science 28 (2003) 556-562.

40. Marusich, T., and Ortiz, M., “Modelling and simulation of high speed machining,” technical report, Third wave systems.
41. Hua, J., and Shivpuri, R., “Influence of crack propagation on chip segmentation in the machining of Ti-6Al-4V,” Advances in Concurrent Engineering, (2002) 357.
42. Shivpuri, R., Hua, J., Mittal, P., and Srivastava, A., “Microstructure-mechanics interactions in modelling chip segmentation during titanium machining,” Timken Company, Canton, USA.
43. Ng, E., and Aspinwall, D., “Modelling of hard part machining,” Journal of Materials Processing Technology 5756 (2002) 1-8
44. Ng, E., El-Wardany, T., Dumitrescu, M., and Elbestawi, M., “Physics based simulation of high speed machining,” Proceedings of 5th CIRP International Workshop on Modeling of Machining Operations, West Lafayette, IN, USA, 2002.
45. Sadat, A., Reddy, M., and Wang, B., “Plastic deformation analysis in machining of Inconel 718 nickel-base superalloy using both experimental and numerical methods,” International Journal of Mechanical Sciences 33 (1991) 829-842.
46. Soo, S., Aspinwall, D., and Dewes, R., “3D FE modelling of the cutting of Inconel 718,” Journal of Materials Processing Technology (2004) article in press.
47. Johnson, G., and Cook, W., “A constitutive model and data for metals subjected to large strain, high strain rate and high temperatures,” Seventh International Symposium on Ballistics, The Hegue, The Netherlands, April 1983.
48. Johnson, G., and Cook, W., “Fracture characteristics of three metals subjected to various strains, strain rates, temperatures and pressures,” Engineering Fracture Mechanics 21 (1985) 31-48.

49. Samiatin, S., and Rao, S., “Shear localization during metal cutting,” Material Science and Engineering 61 (1983) 185-192.
50. -AdvantEdge Theory manual, Third wave systems.
51. Taylor, L., and Flanagan, D., “PRONTO 2D: A Two-Dimensional Transient Solid Dynamics Program," Sandia National Laboratories, SAND86-0594, 1987.
52. Sievert, R., Noack, H.-D., Hamann, A., Löwe, P. Singh, K., Künecke, G., Clos, R., Schreppel, U., Veit, P., Uhlmann, E., and Zettier, R., “Simulation der Spansegmentierung beim Hochgeschwindigkeits-Zerspanen unter Berücksichtigung duktiler Schädigung,” Technische Mechanik Band 23 Heft 2-4 (2003) 216-233.
53. Choudhury, I., and El-Baradie, M., “Machinability assessment of Inconel 718 by factorial design of experiment coupled with response surface methodology,” Journal of Materials Processing Technology 95 (1999) 30-39.
54. Usui, E., Shirakashi, P., and Kitagawa, P., “Analytical prediction of cutting tool wear,” Wear 100 (1984) 129-151.

APPENDIX

User subroutine developed in this study for applying Johnson-Cook material model and Recht's criterion for thermoplastic shear instability.

```
      SUBROUTINE MAT_USER(sig,dtime,temperature,ql,epsl,d,deps)
c
      implicit real*8 (a-h,o-z)
c
c     Defomation tensor * dtime (strain increment)
c     deps(1,1) = Dxx*dtime, deps(1,2)=Dxy*dtime, deps(2,2)=Dyy*dtime
c
c     Material propeties are read from _wp.twm file
c
c     Reserved parameters
c        d(2)           Densitiy (scaled)
c        d(5)           lambda (Lame's constant)
c        d(6)           mu (Lame's constant)
c        d(7)           SIGMA0 (Yield stress)
c        d(24)
c
c     User parameters
c        d(25)          E : Elastic modulud
c        d(26)          xnu : Poisson's ratio
c        d(27)          sigma0 : Initial yield stress
c        d(28)          epsl0 : Initial yield strain
c        d(29)          A : Johnson-Cook material model constant
c        d(30)          B : Johnson-Cook material model constant
c        d(31)          C : Johnson-Cook material model constant
c        d(32)          dn : Johnson-Cook material model constant
c        d(33)          dm : Johnson-Cook material model constant
c        d(34)          epsldot0 : reference plastic strain rate
c        d(35)          epsldotcutoff :cutoff plastic strain rate
c        d(36)          Tm : Melting Temperature
c        d(37)          Tr : Room Temperature
c        d(38)          f : feed rate in meter
c        d(39)          thc : thermal conductivity
c        d(40)          cp : heat capacity
c
c     Reserved parameters
c
c        d(83)          DENSITY
c        d(84)          HEAT CAPACITY
c        d(98)          Conductivity
c        d(100)         Density (thermal)
c*********************************************************************

      real*8 sig(3,3),dtime,epsl(3,3),d(100),ql(15),deps(3,3)

      real*8 temperature
      real*8 sigtr(3,3),sigdiv(3,3),q(3,3)

      parameter ( zero = 0.d0, one = 1.d0, two = 2.d0, three = 3.d0,
     *       third = one / three, half = 0.5d0, twothds = two / three,
     *       op5 = 1.5d0)
```

```
            e           = d(25)
            xnu         = d(26)
            sigma0      = d(27)
            epsl0       = d(28)
            A           = d(29)
            B           = d(30)
            C           = d(31)
            dn          = d(32)
            dm          = d(33)
            epsldot0    = d(34)
            epsldotcutoff = d(35)
            Tm          = d(36)
            Tr          = d(37)
            f           = d(38)
            thc         = d(39)
            cp          = d(40)

          d2mu  = e / ( one + xnu )
          d3mu = 1.5 * d2mu
          dLambda = d2mu * xnu / ( one - two * xnu )

c**********************************************************************

c     Initialize
          ql(3)= 0.0d0

          deltaLamTotal = 0.0d0

c**********************************************************************

c     Elastic stress increment

          tm1 = dLambda*(deps(1,1)+deps(2,2)+deps(3,3))
          sigtr(1,1) = sig(1,1) + d2mu*deps(1,1)+tm1
          sigtr(2,2) = sig(2,2) + d2mu*deps(2,2)+tm1
          sigtr(3,3) = sig(3,3) + d2mu*deps(3,3)+tm1
          sigtr(1,2) = sig(1,2) + d2mu*deps(1,2)
          sigtr(2,1) = sigtr(1,2)

c**********************************************************************

50    continue

c     Calculate Deviatoric stress
          call umat_div_stress(sigtr,sigdiv)
c     Calculate deviatroic stress norm
          sigma_e = umat_sigdiv_norm(sigdiv)


c**********************************************************************
```

```
c      Yield stress: Johnson-Cook material model

       Tstar = (temperature - Tr)/(Tm - Tr)

       sigmaJC= (A+B*ql(1)**dn)*(1-Tstar**dm)*(1+C*dlog(epsldotstar))

c**********************************************************************

c     Strain increment : Radial return method


       ep= (dn*B*ql(1)**(dn-1))*(1-Tstar**dm)*(1+C*dlog(epsldotstar))

       if(ep .ge. e)then
        ep = e - 1
       endif

       dH = ep*e/(e-ep)


       denom = d2mu*(1.0d0+dH/(d3mu))
       deltaLam =(sigma_e-dsqrt(2.0d0/3.0d0)*sigmaJC)/denom

      if (deltaLam.le.0.0d0 .or. deltaLam.lt.1.0e-12) goto 100
c**********************************************************************

c     Case of plasticity

       factor = 1.0d0/sigma_e

       q(1,1)= factor*sigdiv(1,1)
       q(2,2)= factor*sigdiv(2,2)
       q(3,3)= factor*sigdiv(3,3)
       q(1,2)= factor*sigdiv(1,2)
       q(2,1)= factor*sigdiv(1,2)

       deltaLamTotal = deltaLamTotal + deltaLam

c        Updated  stress
c
       sig(1,1) = sigtr(1,1)-deltaLam*d2mu*q(1,1)
       sig(2,2) = sigtr(2,2)-deltaLam*d2mu*q(2,2)
       sig(3,3) = sigtr(3,3)-deltaLam*d2mu*q(3,3)
       sig(1,2) = sigtr(1,2)-deltaLam*d2mu*q(1,2)
       sig(2,1) = sig(1,2)
       sigtr(1,1)=sig(1,1)
       sigtr(2,2)=sig(2,2)
       sigtr(3,3)=sig(3,3)
       sigtr(1,2)=sig(1,2)
       sigtr(2,1)=sig(1,2)
c
        goto 50
c**********************************************************************
```

```
100   continue

c        Plastic strain
        ql(1)=ql(1) + dsqrt(2.0d0/3.0d0)*deltaLamTotal
c
c       Plastic strain rate
        ql(4)= dsqrt(2.0d0/3.0d0)*deltaLamTotal/dtime
c
c
c       Plastic work rate (heat generation)
        ql(3)= dsqrt(2.0d0/3.0d0)*deltaLamTotal * sigmaJC/dtime

c        Updated  stress
        sig(1,1) = sigtr(1,1)
        sig(2,2) = sigtr(2,2)
        sig(3,3) = sigtr(3,3)
        sig(1,2) = sigtr(1,2)
        sig(2,1) = sigtr(1,2)
c
c**********************************************************************

c     for Pure RECHT formulation

        tau = sigma0 / dsqrt(3.0d0)

c     common terms


      constant = 1 / (2 * 4.1868 * dsqrt(3.1428*d(83)*thc*cp))


      DNUM = (dn*B /3)*(ql(1)**(dn-1))*(1- Tstar**dm)


      DENOM1 = (1/dsqrt(3.0d0)) * (A + B * (ql(1)**dn))
     *                 *(- dm/ (temperature - Tr)) * (Tstar**dm)

      DENOM2 = constant * tau * f * dsqrt (ql(4)/(ql(1)- epsl0))


      R = -DNUM / ( DENOM1 * DENOM2 )

      if(R .ge. 0.0d0 .and. R .le. 1.0d0) then
           sig(1,1) = 0.d0
           sig(2,2) = 0.d0
           sig(3,3) = 0.d0
           sig(1,2) = 0.d0
           sig(2,1) = 0.d0
      end if
c**********************************************************************

       END SUBROUTINE

c**********************************************************************
```

```
      double precision function umat_sigdiv_norm(sigdiv)
c
c     Calculate diviatoric stress norm
c
      real*8 sigdiv(3,3)
      real*8 sigma_norm
c
       sigma_norm = sigdiv(1,1)*sigdiv(1,1)
     1             +sigdiv(2,2)*sigdiv(2,2)
     1             +sigdiv(3,3)*sigdiv(3,3)
     1       +2.0d0*sigdiv(1,2)*sigdiv(1,2)

      umat_sigdiv_norm = dsqrt(sigma_norm)
      return
      end
c**********************************************************************


      SUBROUTINE umat_div_stress(sig,sigdiv)

c     Calculate Deviatoric stress

        real*8 sigdiv(3,3),sig(3,3),pressure
        pressure = (sig(1,1)+sig(2,2)+sig(3,3))/3.0d0
        sigdiv(1,1) = sig(1,1)-pressure
        sigdiv(2,2) = sig(2,2)-pressure
        sigdiv(3,3) = sig(3,3)-pressure
        sigdiv(1,2) = sig(1,2)
        sigdiv(2,1) = sig(2,1)

      return
      end
c**********************************************************************
```

VITA

Dhananjay Joshi

Candidate for the Degree of

Master of Science

Thesis: FINITE ELEMENT SIMULATION OF MACHINING A NICKEL-BASED SUPERALLOY- INCONEL 718

Major Field: Mechanical Engineering

Biographical:

Personal data: Born in Akot, India, On September 22, 1978, the son of Ramchandra and Asha Joshi.

Education: Received Bachelor of Engineering degree in Mechanical Engineering from University of Pune, India in June 2000. Completed the requirements for the Master of Science degree with a major in Mechanical and Aerospace Engineering at Oklahoma State University in December 2004.

Experience: Graduate Research Assistant in Mechanical and Aerospace Engineering Department, Oklahoma State University, Stillwater, Oklahoma, August, 2001 - present.

Professional Membership: ASME.

Name: Dhananjay Joshi Date of Degree: December, 2004

Institution: Oklahoma State University Location: Stillwater, Oklahoma

Title of Study: FINITE ELEMENT SIMULATION OF MACHINING A NICKEL-BASED SUPERALLOY- INCONEL 718

Pages in Study: 112 Candidate for the Degree of Master of Science

Major Field: Mechanical Engineering

Scope and Methodology of Study: Inconel 718 is one of the difficult-to-machine materials and is mainly used for aerospace applications. Cutting speed in machining Inconel718 is limited by shear localization observed at cutting speed above 61 m/min. Adiabatic shear failure is considered as root cause for chip segmentation. Johnson-Cook material model is used to represent strain, strain rate, and temperature dependence of strength of Inconel 718. Recht's criterion for catastrophic thermo-plastic shear failure is applied to study shear instability in machining. A commercial finite element software with 2-dimensional explicit code and Lagrangian formulation (AdvantEdge) is used for finite element simulations. A user subroutine is developed to incorporate Johnson-Cook material model and Recht's failure criterion in the main code.

Findings and Conclusions: Finite element simulations are run for a range of cutting speeds from 30.5 to 183.5 m/min. Machining is analyzed at various rake angles (-30^0 to 45^0) and feed rates (0.25-1.0 mm/rev). Results of the simulations are compared with machining test data and are found in close confirmation. Chip formation mechanism is found to be in confirmation with experimental observations reported in the literature. Effects of machining conditions on cutting and thrust forces, shear zone and tool rake face temperatures, and equivalent plastic strain in primary and secondary shear zones are reported.

Adviser's Approval: Dr. Ranga Komanduri